RUNOUT DISTANCE OF DEBRIS FLOWS: EXPERIMENTAL AND NUMERICAL SIMULATIONS

BY

LEO CHIN-PANG CHAN

A Thesis for the Master of Philosophy

Department of Civil and Structural Engineering
The Hong Kong Polytechnic University

January 2001

ABSTRACT of thesis entitled

"Runout Distance of Debris Flows: Experimental and Numerical Simulations"

Submitted by Leo Chin-pang CHAN

for the Degree of Master of Philosophy

at the Hong Kong Polytechnic University in January, 2001

The main objective of this paper is to study the runout distance of debris flow by experimental simulations and to compare the runout distance observed in experiments with numerical predictions.

In the experimental study, we design a new flume for modelling the real scale debris flows, by ensuring the equivalence of three constitutive scaling parameters (Bagnold number, Savage number and friction number) and four geometric scaling factors (velocity factor, flow factor, yield stress factor and viscosity factor) between the model tests and real events. The first three parameters reflect the relative importance of dispersive force, the friction force and the viscous force at the microscopic level, while the latter four factors ensure that the same macroscopic governing equations are applicable to both model and prototype. Debris materials collected by the Geotechnical Engineering Office (GEO) of the Hong Kong Government from the site of the Tsing Shan Debris Flow of 1990 are used in our study. It is found that the seven scaling parameters and factors of experiments are comparable to those of the Tsing Shan Debris Flow. The development of debris fan

and the maximum runout distance of debris flows are investigated as functions of various parameters (including slope gradient, deposition board gradient, granular content and cross section shape of flow channel). For experiments with a flat deposition board, a slope angle increase from 26° to 32° of the flume leads to 84% increase in the runout distance. However, a further 6°increase (from 32° to 38°) in the flume slope only gives a 42% increase in the runout distance. In addition, the runout distance can increase by 59% on average when the flume cross-section is changed from rectangular to triangular for various debris materials with flume slope at 26°and deposition board slope at 0°.

The experimental simulations results are then compared to the predictions of various theoretical models, including the dispersive model (Takahashi and Yoshida, 1979), constant friction slope model (Hungr et al., 1984), sled model (Heim, 1932) and DAN model (Hungr, 1995). The DAN model prediction (Hungr, 1995) is found to be more agreeable to our experimental results than the predictions by other models. In the DAN model simulations, the Voellmy constitutive model is found to yield agreeable results if proper values in friction and turbulence coefficients are employed.

DECLARATION

I hereby declare that this thesis entitled "Runout Distance of Debris Flows: Experimental and Numerical Simulations" has not been, either in whole or in part, previously submitted to any other institution for a degree or other qualifications, and contains no material previously published, except where due reference is made in the text.

Leo Chin-pang CHAN

ACKNOWLEDGMENT

I would like to express my sincere gratitude to my chief-supervisor, Dr. K.T. Chau, for his intensive guidance, encouragement and valuable advice throughout this research study and thesis writing. My supervisor's eager in a broad field of scientific research work has motivated my ambition to be a professional engineer.

I would like to give special thanks to Prof. O. Hungr for generously providing his computer program DAN to us. I am grateful to Dr. Onyx W. H. Wai and Mr. S. T. Luk for their valuable ideas and suggestions. Thanks are also due to Mr. J.P. King of the Geotechnical Engineering Office (GEO) of the Hong Kong Government for generously providing the debris sample to us. Gratitude is extended to Dr. D.O.K. Lo and Dr. Richard Pang of the Special Projects Division of Geotechnical Engineering Office of the Hong Kong Government for helping me to assess relevant reports. I also acknowledge the contribution of Ms. C.W.C. Ho for help in a minor part of the experimental works relating to those tested in the triangular channel.

I thank Mr. M.C. Ng and Mr. K.H. Leung for their help in manufacturing the experimental flume. Special thanks are also due to Mr. K.Y. Lam and Mr. H. Chiu for their technical supports in the Rock and Geology laboratories. I am grateful to Mrs. M. Anson for helping me to check thesis writing. I am also grateful to the Hong Kong Polytechnic University for providing me the RGC research studentship. Last but not the least, I would like to thank Ms. S.Y. Chung and Ms. L.K. Ha for their help and support during the research study.

TABLE OF CONTENT

List of Figures

List of Tables

Chapter 1 Introduction

1.1 Landslide Hazards on Natural Terrain

There are many kinds of natural hazards on natural terrain including fire, rainfall-induced landslides, earthquake-induced landslides and rockfall. Among these dangerous natural hazards, debris flow is known to be one of the most disastrous hazards to natural terrain in most mountainous areas of the world.

Debris flow is a flowing mixture of water, mud, soil, boulders and wood. Debris flow is also known as lahar (in the case of a volcano), debris torrents (in Canada), or mud flow. The geographical appearance of debris flow is extremely widespread. Its grain composition is always nonuniform and ranges from clay to boulders. The blending of these materials produces thick slurries that are normally thoroughly mixed. The flowing slurries resemble wet concrete and is more fluid with increasing water and decreasing solid particles. The majority of debris flows are composed of (1) small shallow landslides, which are commonly termed soil slips, occurred on steep slopes, and (2) those landslide failures developed into channelized debris flow with a long runout distance (Lo and Ho, 1998). An idealized representation of a debris flow failure showing the source area of failure, the flow channel and the deposition fan is shown in Figure 1.1 (Turner, 1996).

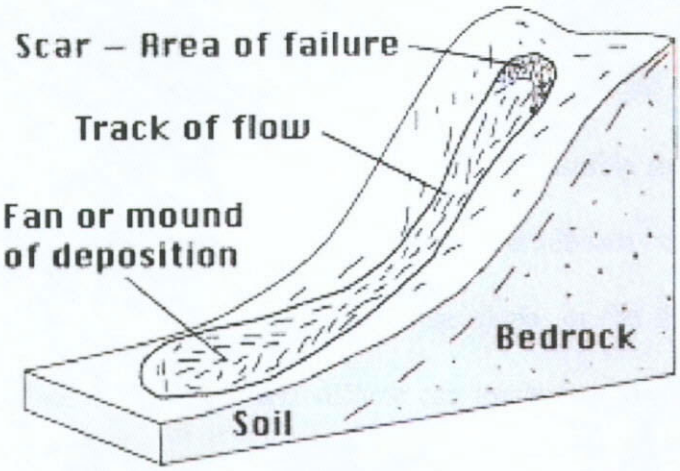

Figure 1.1 Idealised representation of a debris flow failure (Turner, 1996)

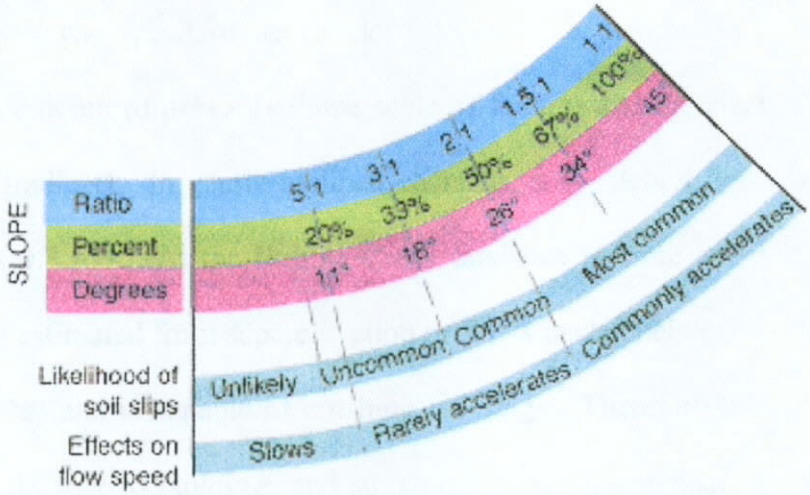

Figure 1.2 Typical description on the likelihood of soil slips and effect on flow speed with slope gradient in Santa Monica, USA (Campbell, 1974)

According to Campbell (1974), debris flow usually begins with soil slips which tend to form on steep slopes. The flowing debris accelerates down to the slope with the gentler gradient. It will then slow down, stop and deposit on the downslope. A typical description on the likelihood (frequency) of soil slips and the effect on flow speed with slope gradient for Santa Monica, USA is shown in Figure 1.2 (Campbell,

1974). Debris flow generated does not tend to accelerate on slopes of less than 26 degrees. Most begin to deposit their material on slope of about 11 degrees.

When a debris flow consisting of loose and unstable rocks and/or soil deposit proceeds down a slope, a canyon or a ravine, materials can be scoured from its flow path. When the flow reaches the base of the slope, or the fan at the mouth of the canyon or ravine, the initial debris volume can increase greatly by the fully saturated sediment scoured from channels along its way. The flow will spread out and deposit. In some cases, the debris flow may slow down and stop if water separates and drains from the debris material, or the flow may spread out and thin if the channel widens abruptly. The speed of debris flow depends on the fluidity (water content), the hydraulic depth of debris (volume scale of failure) and the steepness of the channel (slope gradient). In gently inclined channels, some debris flows move at speeds as slow as 0.3 m/s. At the Rubble Creek landslide (Moore and Mathews, 1978), the velocity estimated from superelevation of flows in channel bends is as large as 20 m/s (72 km/hr) and is capable of crushing buildings. Therefore, debris flows can cause serious damage to buildings and structures in the downstream areas. Debris flow is regarded as one of the most threatening natural hazards in some regions of the world, such as Japan (about 90 lives a year on average were claimed by debris flows, Takahashi, 1981) and China (occurred in almost two-third of mountainous regions in China, Zhang, 1993). The worst debris flow of this century occurred on November 13, 1985 at Nevado del Ruiz volcano in Colombia, which claimed the nearby Armero city, killed 22,000 people, and spread debris of volume 48,000,000m^3 over an area of 30 km^2 (Takahashi, 1991; Garcia and Savage, 1993). On Novermber 5, 1991 about 6,000 peoples were killed by debris flows in Philippines following the torrential rains

from the tropic storm "Thelma" (Day, 1994). Another disastrous event in Thailand which killed 373 lives and cost US$ 280 million in damages was the debris flow between Novermber 19-23, 1988 (Phien-Wej et al., 1993). At a conservative estimate, over 60 countries of the world have been attacked by debris flows, including China, Japan, Canada, USA, Switzerland, New Zealand, U.K., Philippines, Peru, Colombia, Brazil, Sweden, Tanzania, Indonesia, Thailand together with many other countries.

1.2 Landslide Hazards on Natural Terrain in Hong Kong

Hong Kong is not immune to debris flow. The largest debris flow reported in Hong Kong occurred on September 11, 1990 at Tsing Shan and involved the movement of 19,000 m^3 of boulders and soils. The debris was deposited into the "Area 19 Tuen Mun", a designated site for further development (King, 1996a). The total path measured 1,035m in length along a V-shaped gully of slope angle 16-27 degrees. The path of the debris flow narrowly missed a nearby squatter area (San Shek Wan San Tsuen) by less than 200m. Both telephone and electricity services were cut off during the debris flow. On June 13, 1992, another smaller scale debris flow (250m^3) flowed down a nearby gully at Tsing Shan and covered a concrete footpath (King, 1996b). On November 4-5, 1993, over 800 debris flows occurred on Lantau Island (Wong et al., 1996) and many occurred along slopes on the south of the recently-built North Lantau Link which is today playing an important role in connecting the new airport and the urban area of Hong Kong. One of these debris flows covered a road connecting to Tung Chung. An abandoned school located on a mountain side about 1 km west of Lo Wu in Hong Kong was destroyed by debris flow in 1996 (Ayotte and Hungr, 1998).

1.3 Motivation

Natural hillsides cover over 60% of the total area of Hong Kong. In the past 50 years, more than 470 people have been killed by landslides on man-made slopes, including fill slopes, cut slopes and retaining walls, and 4 people are known to have been killed by boulder falls from natural hillsides. There is no known fatality record caused by landslide on natural slopes. Therefore, not much attention has been drawn to the natural slope failures in the past. The Hong Kong Government has given priority to man-made slopes and retaining walls, and a Landslip Preventive Measures (LPM) programme has been conducted to almost all man-made slopes and retaining walls in the past. Landslip preventive works on natural hillsides are expensive, it seems not justified to treat every natural slopes. More recently, a more systemtic investigation against natural terrain landslides has been launched by the Geotechnical Engineering Office of the Hong Kong Government.

However, there were typically more than 300 natural terrain landslides in Hong Kong every year (Lo and Ho, 1998). Although there have been no recorded instance of fatality from natural landslides, the risk of natural slope failure to the community will inevitably increase as the population of Hong Kong grows and the infra-structures and building development continue to spread into areas adjacent to natural hillsides. For example, with the recent development of the new Chek Lap Kok airport and other new satellite towns, such as Tuen Mun and Tung Chung, human habitat and activities have moved into natural terrain which has been prone to debris flows.

Moreover, over the last few years there have been some "near miss" landslides on natural terrain which could have caused very serious damage if existing or planned developments had been presented. These cases remind us of the significance of debris flows, and motivate the present study on debris flows. The outcome of this study should be extremely beneficial to the general public in Hong Kong as well as in mainland China.

1.4 Objectives

In order to minimize the potential hazards associated with landslide failures on natural terrain, a proper prediction to the risk of landslides is necessary. One of the landslide risk assessments is based on the runout distance of landslides because the runout distance of landslides is directly related to their extend of potential destruction. Factors affecting runout distance of debris flows consist of the slope gradient, gradient of deposition ground, granular content, shape of cross section of flow channel, water content, scale of failure, mechanism of failure, and debris entrainment and/or deposition rate.

The main objectives of this study are:

(1) To study experimentally the development of debris fan and the maximum runout distance of debris flow as functions of various parameters (including slope gradient, gradient of deposition ground, granular content and shape of cross section of flow channel) and;

(2) To compare the maximum runout distance of debris flow observed in experiments with those predicted by various theoretical and numerical models.

Chapter 2 Literature Review

2.1 Debris Flows

Debris flows are usually triggered by an unusual presence of water due to intense rainfall or rapid snowmelt and by earthquakes. The initiations of debris flows are usually triggered by rain and earthquake as illustrated in Figure 2.1.

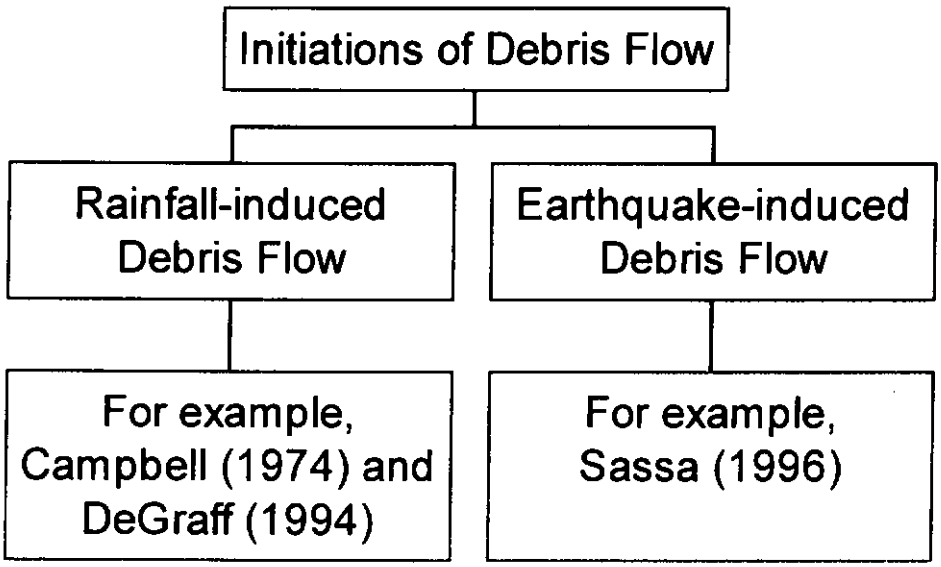

Figure 2.1 Initiations of debris flows

When loose and unstable soil deposits on slope disjoint from a soil mass, the failed landslide mass starts to slip, remould, and incorporate water during the flow. The mobilization of failed mass can be caused by liquefaction of soil due to earthquake and by reduction of soil strength due to the perched water level induced by

heavy rainfall. Debris flow generated during intense rainfall usually causes remoulding of the saturated moving mass into viscous debris flow. Entrainment of boulders or large rock fragments along the transport path of debris flow can also be present. According to the physical properties, debris flows can be categorized into 3 types that are commonly used by Chinese scientists (Table 2.1): mud-rock flow, mud flow and water-rock flow.

Classification	Properties	Zhang (1993)	IGGAS (1982)	Wang (1999)	Chen et al. (1983)
Mud-Rock Flow	ρ ($x10^3$ kg/m^3)	~ 2.17	1.4 – 2.2	/	1.2 – 2.3
	μ (Ns/m^2)	> 1.5	0.1 – 3	/	/
	τ_B (N/m^2)	> 10	0.04 – 3	/	/
	PSD	/	/	Consist of clay (3-5% by weight), silt, sand, gravel and cobble	Consist of clay, silt, sand, gravel and cobble
Mud-Flow	ρ ($x10^3$ kg/m^3)	~ 1.6	>1.4	/	1.6 – 2.2
	μ (Ns/m^2)	> 1.0	0.1 – 2	/	/
	τ_B (N/m^2)	> 5	0.03 – 0.5	/	/
	PSD	/	D_{50} < 1 mm	Mainly consist of clay (>15% by weight) and sand	Consist of clay (d<0.005mm) and silt (d<0.05mm) with little sand and gravel
Water-Rock Flow	ρ ($x10^3$ kg/m^3)	~ 1.2	/	/	1.2 – 1.8
	μ (Ns/m^2)	/	/	/	/
	τ_B (N/m^2)	/	/	/	/
	PSD	/	/	Mainly consist of coarse sand, gravel and boulder	Consist of sand, gravel and cobble with little silt and clay

ρ = Density, μ = Viscosity, τ_B = Yield shear strength, PSD = Particle size distribution

Table 2.1 Physical Properties of Debris Flows (after Wang, 1999)

The above classification is based upon the composition of granular materials in the debris flow. The density of mud-rock flow and mud-flow is generally higher

than that of water-rock flow. The mud-rock flow in general has a higher value in viscosity and yield shear strength than those for mud flow. The mud-rock flow consists of heterogeneous composition of soils while the mud flow is mainly composed of clay and silt with little sand and gravel. In addition, the water-rock flow basically consists of sand, gravel and cobble with little silt and clay content.

2.2 Debris Flow Rheology

There are a number of rheologies used for debris flows. Chen (1987) provided an extensive review of debris flow rheology, and Iverson and Denlinger (1987) gave a concise examination to the physical aspects of rheologies. In this section, we do not intend to include a comprehensive review on the rheological models for debris flows. Instead, we will outline the several rheological models used in the study.

The first rheological model to be discussed is the Bingham model which was put forward by Yano and Daido (1965). In the Bingham model, the shear stress is given as:

$$\tau = \tau_B + \mu \frac{dv}{dh} \tag{1}$$

where τ_B = Bingham yield stress

μ = Bingham viscosity

$\frac{dv}{dh}$ = shear strain rate

The Bingham model behaves as a solid until a yield stress τ_B is exceeded. Subsequently the model exhibits a linear relation between the shear stress and the

shear strain rate (rate of deformation), and flows as a linearly viscous (Newtonian) fluid.

The second rheological model is the dilatant fluid model. The classical work of Bagnold (1954) defined the following relationship.

$$\tau = -p \tan\alpha \qquad (2)$$

where p = inter-particle stress normal to bed surface (dispersive stress)

$\tan\alpha$ = kinematic friction factor and α is an unknown angle affected by collision conditions

B < 40, $\tan\alpha = 0.75$;

B > 40 and $\lambda < 12$, $\tan\alpha = 0.32$;

B > 40 and $\lambda > 12$, $\tan\alpha = 0.4$

The Bagnold number is denoted by B and is defined as $\frac{\dot{\gamma}\rho\delta^2\lambda^{1/2}}{\mu}$, where $\dot{\gamma}$ is the shear strain rate, ρ is the solid mass density, δ is the particle diameter, μ is viscosity and λ is the linear grain concentration that is defined as $\nu^{1/3}/(\nu_*^{1/3} - \nu^{1/3})$. The ν and ν_* are the volume concentration of solid phase and the (close-packed) volume concentration of solid phase respectively. This model is characterized by the concept of dispersive stress of grain flow that was originally introduced by Bagnold (1954). Dispersive stress arises in shear flows of granular solids as adjacent grains collide and exchange momentum as they move past one another.

2.3 Deposition of Debris Flow

2.3.1 Sedimentology

A number of studies attempted to study the sedimentary characteristics of debris flow (Major, 1997; Steijn and Coutard, 1989 and Middleton and Hampton, 1976). Textural features are usually used to identify debris flow deposits which consists of large boulders embedded in a matrix of fine materials. Stratigraphic successions showing details of debris flow deposits sometimes exhibit reverse grading. Reverse grading was also observed at the deposit of the Tsing Shan Debris Flow of 1990 as shown in Figure 2.2, which is based on a photograph taken in March 2000. Dispersive pressure may lead to boulder concentrations at the top of the deposit and form reverse grading. The explanation for reverse grading was originally proposed by Bagnold (1954).

Figure 2.2 Reverse grading of deposits in the Tsing Shan Debris Flow

2.3.2 Runout Prediction

Many landslides with long runout distance are in fluid form, and are normally termed as debris flows. In contrast to the ordinary failure (rotational of man-made slopes), potential destruction of debris flows often cannot be reduced practically and cost effectively by the stabilization of the source triggering areas. Thus, landslide hazard assessments, which include predictions of landslide volume, flow velocity, impact force, thickness and spreading of debris, and runout distance, have been developed and applied to the barrier design. Runout distance is one of the important parameters for hazard assessments. Methods for predicting the runout distance of debris flows can be classified into three main categories (Figure 2.3):

(1) Empirical modeling

(2) Experimental modeling

(3) Mathematical modeling

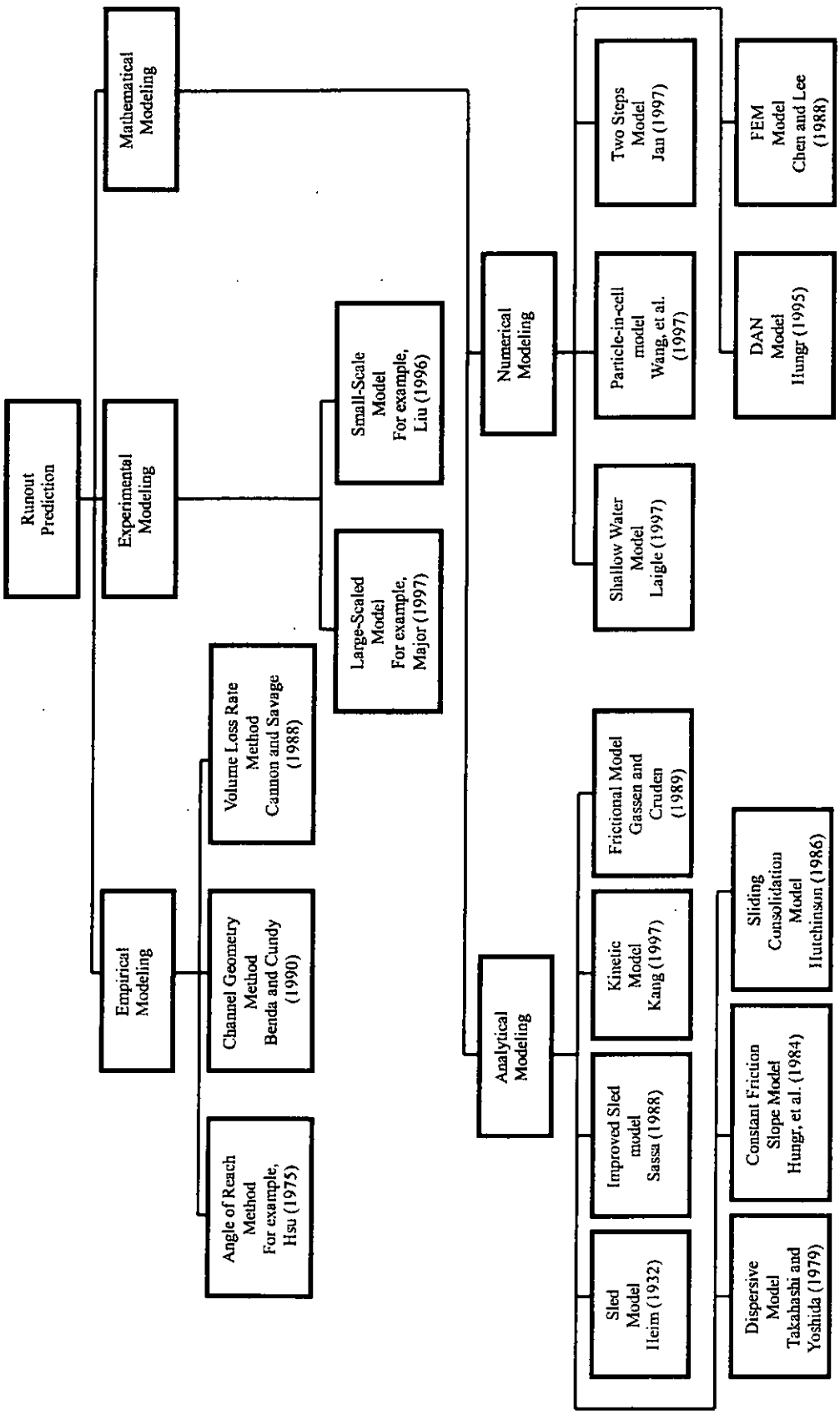

Figure 2.3 Methods for prediction of runout distance of debris flows

2.3.2.1 Empirical Modeling

2.3.2.1.1 Angle of Reach Method

A well known ratio of the height of the highest point of landslide source (i.e. the scar) and the projection of horizontal distance from this point to the distal margin of the displaced mass (i.e. the edge of deposition fan) is defined as the "fahrboschung" or the angle of reach by Heim (1932). In other words, the angle of reach is the angle of the line connecting the head of landslide source to the tip of displaced mass. Shreve (1968) called the tangent of this angle the equivalent friction coefficient. In order to further explain the angle of reach, Scheidegger (1973) asserted that in a frictional model the tangent of the angle of reach is the average friction coefficient of the surface contact between the sliding mass and the slope base. Assuming the sliding mass is a rigid body, Scheidegger's assumption is valid only when the angle of reach is equal to the slope angle of the line connecting the centers of gravity of the landslide source and the displaced mass. In other words, the tangent of the angle of reach is not the friction coefficient but only an approximation for the friction coefficient. The angle of reach of the Elm rockslide (Hsu, 1975), for example, is 17 degrees whereas the line connecting the centers of gravity has an inclination of 23 degrees.

A detailed study to investigate the relationship between the landslide volume and other various factors, and the angle of reach from 204 landslide records was analysed by Corominas (1996). For simplicity, Corominas (1996) categorised the landslide data into 4 classes based upon the movement mechanisms regardless of their initial failure mechanisms. They are (1) rockfalls, (2) translational slides, (3) earthflows and (4) debris flows. Regression equations for each kind of landslides were developed. These equations showed that irrespective of mechanisms of

movement the angle of reach experienced a contiuous reduction with increasing volume. The angle of reach had no sudden change at any specific volume. Most of the reduction of the angle of reach occurred at volumes smaller than 10^6 m^3. As remarked in Lau and Woods (1997), this clear relationship between the landslide volume and the angle of reach was demonstrated by Corominas (1996).

The angle of reach has been adopted in Hong Kong as well for the purpose of studying the relationship between the angle of reach and the landslide volume (Wong and Ho, 1996). The landslide data consists of 250 failures of soil cut slope failures which were triggered by a severe rainstorm on November 5, 1993 on Lantau Island. Based on the failure modes, the landslides were grouped into (1) rain-induced, (2) liquefaction of loose fill and (3) wash-out by convergent water flow. Results showed that the angle of reach for rain-induced landslides generally ranged from 30 to 40 degrees, whereas for landslides caused by liquefaction of loose fill or wash-out action the angle of reach fell within the range from 15 to 30 degrees. As observed from the results of Wong and Ho (1996), the angle of reach reduces with increasing landslide volume. This result is consistent with that of Corominas (1996).

According to the landslides data from Lantau Island of Hong Kong in 1992 and 1993, Lau and Woods (1997) performed a step-wise multivariant regression analysis to establish an equation for calculating the angle of reach. Lau and woods (1997) selected the initial landslide volume, material types, slope morphology, vegetation type, slope angle and rainfall intensity as variables, and obtained the following regression formula.

$$\log\theta = 1.4983 - 0.05384\log V - 0.03626G - 0.01755M + 0.00306C + 0.00493S - 6.7x10^{-5}W \quad (3)$$

where θ = angle of reach (degree)

V = initial landslide volume (m^3)

G = material type (1 = colluvium; 2 = residual soils)

M = slope morphology (1 = planar; 2 = concave; 3 = convex)

C = vegetation type (1 = grass; 2 = scrub; 3 = tree)

S = slope angle (degree)

W = rainfall intensity (mm/24hr)

However, the above method does not account for the physical properties of debris materials, the mechanism of deposition or entrainment of debris material, and the water content of the debris. The analysis also neglects the gradient of the deposition ground.

2.3.2.1.2 Channel Geometry Method

Benda and Cundy (1990) developed an empirical model for predicting the deposition of coarse-textured debris flows in confined mountain channels based on a field measurements of 14 debris flows in the Pacific Northwest of USA. This model was firstly tested by the travel distance of 15 debris flows in the Oregon Coast Range and 6 debris flows in Washington Cascades, and further tested by the travel distance of 44 debris flows in Oregon Coast Range using aerial photos and topographic maps. This model assumed two criteria for deposition: (1) channel slope less than 3.5 degrees and (2) tributary junction angle α greater than 70 degrees (Figure 2.4). The tributary junction angle is defined as the upstream angle between the tangent lines of two intersecting channels. When debris flows encounter a tributary junction of angle greater than 70 degrees, it often collides with the opposite valley wall and starts to deposit. When either one of these criteria is satisfied, the debris flow will deposit.

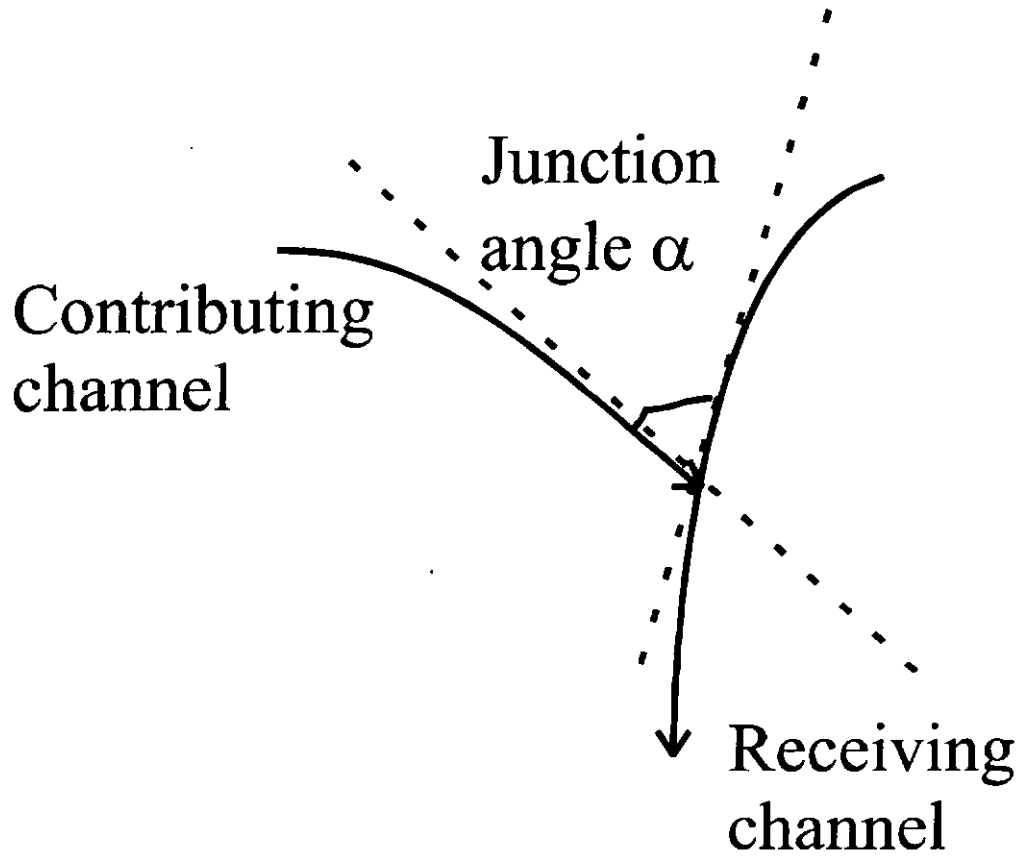

Figure 2.4 Representation of junction angle α (Bendy and Cundy, 1990)

This model consists of a hypothetical channel network (Figure 2.5) including the locations of trigger hollows, first-order channel, second-order channel and so on. When the deposition is predicted based on channel gradient, the predicted travel distance is determined by measuring the map distance from the initial failure to the midpoint of 2.5 to 4.5 degree contours. When the deposition is predicted based on tributary junction angle, the deposition point is at the junction. This model is totally based on the geometry of the channel network, and does not account for the rheological properties, landslide source volume, failure mechanism and channel cross section of the debris flow. This model can only predict the travel distance of debris flow up to the end of the confined channel and cannot be applied to debris fan development. This model can be easily calibrated by using topograhpic maps and aerial photos, but should be field checked prior to its use in other areas.

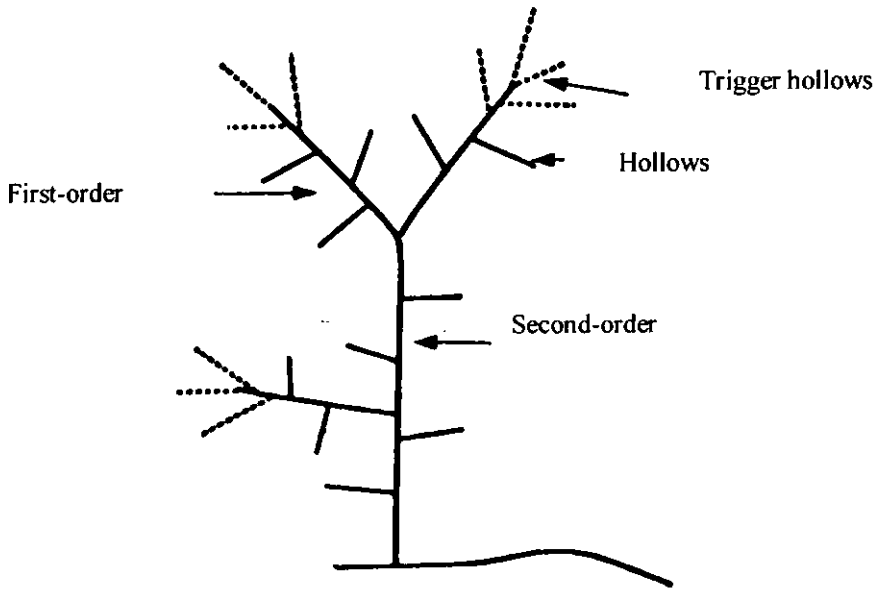

Figure 2.5 Hypothetical channel network showing the location of trigger hollows, hollows, first and second-order channels (Benda andCundy, 1990)

2.3.2.1.3 Volume Loss Rate Method

Field observations of debris flows indicated that debris material can be lost from the flow by deposition in the form of levees or channel fill (Cannon and Savage, 1988). Cannon (1989) and Cannon and Savage (1988) suggested that the potential travel distance of debris flows can be predicted by considering the volume loss behaviour when the flows travel down hillsides. The flow stops when the volume of actively flowing debris becomes negligible.

Cannon (1993) adopted this principle and established an empirical model which can be combined with digital elevation models (DEM) to characterise the travel distance of debris flows. Based on 26 debris flows at the Honolulu district of Oahu, Hawaii, the average volume change over distance (dependent variable) and the variables of slope, confinement and vegetation type (independent variables) were obtained. The average volume change over distance is characterized by dividing the initial scar volume [determined from (1) direct measurement in field or (2) estimation from measurements remotely in field or from aerial photos] by the distance (determined from a 10-m digital elevation grid) traveled down the hillside. The initial scar volume was assumed to decrease linearly with travel distance. This model is applied only to debris flows that have nearly uniform channels, vegetation types and slope angles. A step-wise multiple regression analysis was carried out to evaluate the influence of the independent variables on the average volume change behaviour of debris flows. The regression equation for Honolulu district is represented by the following equation (Figure 2.6):

$$\log[\frac{V_i - V_f}{D}] = 0.14 \log R - 1.40 \log \theta + 2.16 \qquad (4)$$

where V_i = volume of material entering the debris trail (m^3)

V_f= volume of material leaving the debris trail (m^3)

D = length of the debris path along hillside (m)

θ = gradient of path (degrees)

R = transverse radius of curvature of channel in a vertical plane (m)

This volume-loss rate model can be combined with a digital elevation model to predict the runout distance of debris flow. Lau and Woods (1997) also applied this method to predict the runout distance of debris flows in Hong Kong. The main limitation of this model is that it is not capable of taking account of the physical properties of moving debris and the mechanism of debris deposition. It does not allow for the material entrainment or channel erosion, and the debris must stop on the hillslope. This empirical model established for Honolulu should be calibrated prior to use in other areas with different landslide conditions.

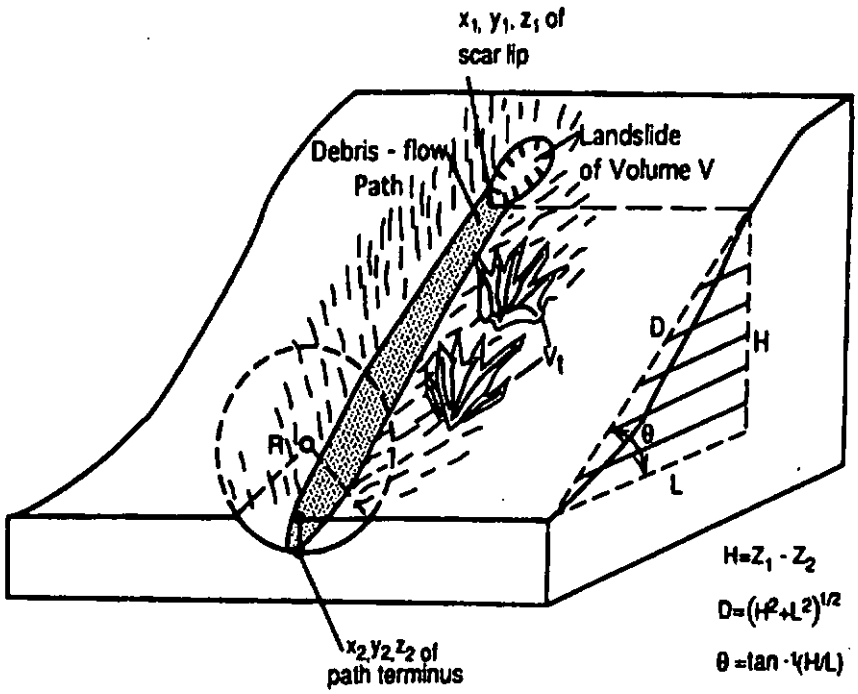

Figure 2.6 Three-dimensional view of debris flow (Cannon, 1993). Here H is the vertical drop of path (m); L is the map length of path measured from scar lip to terminus of deposits (m); D is the length of path along hillside (m); θ is the gradient of path (degree); R is the transverse radius of curvature of channel (m) and V_t is the vegetation type

2.3.2.2 Experimental Modeling

2.3.2.2.1 Large-Scaled Model

Large-scaled laboratory models permit systematic experimental study on the behaviour and runout distance of debris flow from initiation to deposition (Mizuyama and Uehara, 1983; Iverson and LaHusen, 1993; Iverson et al., 1992; Iverson, 1997 and Major, 1997). In 1991, the U.S. Geological Survey constructed a large flume for conducting controlled experiments on debris flows. The flume is located about 45 miles east of Eugene, Oregon and near the headquarters of the H.J. Andrews Experimental Forest, Blue River Ranger District, Willamette National Forest. This flume is a reinforced concrete channel 95 m long, 2 m wide and 1.2 m deep. The smoothly bedded flume slopes 31 degrees along the upper 88 m and flattens gradually to 3 degrees over the last 7 m. The sediment comes down the flume and deposits on a flat runout surface at the flume base. As much as 20 cubic meters of sediment which is saturated with water from subsurface channels and surface sprinklers can be loaded behind a steel gate at the head of flume. As debris flow is initiated, removable glass windows built in the side of flume allows the passing flow to be observed and photographed.

Iverson and LaHusen (1993) also introduced three dimensionless parameters (Bagnold number, Savage number and friction number) to ensure compatibility of the constitutive behaviour of the tested materials and the real debris. These three dimensionless parameters have also been adopted in the experimental study in this thesis and will be discussed in details in chapter 3. The flow depth and flow velocity as well as the runout distance of debris flows have been compared with the model

prediction of Savage and Hutter (1989, 1991). Major (1997) also used this flume and studied the deposition mechanisms, in relation to the sedimentology of field deposits and estimation of rheological properties of debris flows. The advantages of this model are that the experiments can use realistic geological debris ranging in composition from fine-grained silty-clay slurry to coarse-grained cobble-boulder material. The effect of stresses and pore water pressure on the flowing debris can also be measured.

Another 20 cm wide and 25 m long flume (jointed by five 5 m long segments) was used to investigate deposition process and runout distance of debris flows in channels with abruptly change in width and gradient (Mizuyama and Uehara, 1983). The first segment of flume is at 25 degrees, and each subsequent segment of flume slope decreases by 5 degrees (from 25 to 5 degrees). A layer of sand with constant thickness of 10 cm is placed at the flume base and constant discharge of water was supplied from the top of the flume to start the flow.

Since almost all debris flows occur under adverse conditions of severe rainstorm and/or earthquake, very few field observations have been made on debris flow. The large-scaled model can provide a reasonable and reliable way to study debris flow dynamics and physical phenomena under well-designed conditions. These observations can be used in assessing both theoretical and numerical debris flow models.

2.3.2.2.2 Small-Scaled Model

A series of model experiments using samples collected from Jiangjia Creek at Yunnan, China were conducted to study the deposition and runout distance of debris flow (Liu, 1996). These model experiments studied the influence of debris deposition on the channel slope, deposition board slope, unit weight of debris samples and the initial debris flow volume. The physical model consisted of a 150cm length channel (16cm width and 18cm depth) and a 150cm width and 200cm length deposition board. As the channel and the deposition board are adjustable from 10 to 34 degrees and 1 to 10 degrees respectively, thus enabling the runout distance of debris flow to be simulated according to different parameters. This physical model provides a direct means to assess the effect of different parameters to the runout distance of debris flow in a reasonable manner. But the limitation of this miniature experiment is its inadequate geometrical and constitutive similitude to the real debris flow cases, due to arbitrary selection of channel dimension and unlikeness to use actual physical properties of debris material.

Another experimental model has been used to study the total initial debris flow volume to the maximum values of the fan length, fan width and fan depth (Shieh and Tsai, 1997). The advantage of this method is that it relates the initial volume of debris to the maximum fan length, maximum fan width and maximum fan depth by an empirical coefficient. As the shape of the debris fan is assumed to be half ellipse, this method is unsuitable for landslides with a very long runout distance.

2.3.2.3 Mathematical Modeling

2.3.2.3.1 Analytical Modeling

2.5.2.3.1.1 Sled Model

The sled model was originally proposed by Heim (1932). This model assumes that all energy loss during motion is caused by friction only. But the nature of friction during motion is not clear, many reseachers tried to interpret this landslide motion by an apparent friction angle ϕ_a. For example, Shreve (1968) proposed the use of equivalent friction coefficient and Scheidegger (1973) proposed the use of average friction coefficient. When a debris flow has a potential head h, the energy line being divided by mg is shown in Figure 2.7. This line represents the total energy head (the kinetic energy head + the potential energy head). The kinetic energy head ($v^2/2g$) is shown by the height between the energy line and the center of the moving mass. When the debris mass having potential energy head h moves by a horizontal distance x along the sliding path as shown in Figure 2.7, the energy loss due to friction (E_f) is:

$$E_f = \int_0^x (mg\cos\theta)\tan\phi_a\left(\frac{dx}{\cos\theta}\right) = mgx\tan\phi_a \qquad (5)$$

where ϕ_a = apparent friction angle

m = mass of debris

g = gravitational acceleration

θ = slope gradient

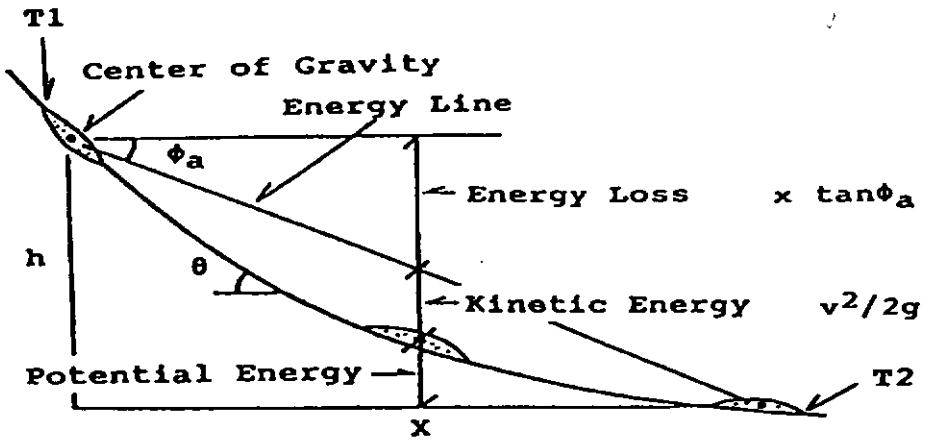

Figure 2.7 Sled model for the motion of landslides (Sassa, 1988)

By considering the conservation of momentum and assuming debris mass is constant, we have :

$$m\frac{dv}{dt} = mg\sin\theta - (mg\cos\theta)\tan\phi_a \tag{6}$$

$$\text{then, } \frac{dv}{dt} = g\sin\theta - (g\cos\theta)\tan\phi_a = g\cos\theta(\tan\theta - \tan\phi_a) \tag{7}$$

where v is the velocity.

For simplicity, Lo and Ho (1998) gave a formula for the determination of the runout distance of debris flow from the initial point of deposition. Based on the assumption that the slope gradient is constant and the velocity decreases linearly, the formula for a runout distance can be obtained. Integrating both sides of equation (7) where v_u is the entry velocity (the entry point at which initial deposition occurs), we have:

$$\int_{v_u}^{0} dv = \int_{0}^{t} g\cos\theta(\tan\theta - \tan\phi_a)dt \tag{8}$$

$$V_u = g\cos\theta(\tan\phi_a - \tan\theta)t = g\cos\theta(\tan\phi_a - \tan\theta)\frac{2X_L}{V_u} \quad (9)$$

$$\text{so, } X_L = \frac{V_u^2}{2g\cos\theta(\tan\phi_a - \tan\theta)} \quad (10)$$

where X_L = runout distance of debris flow

The above method can provide an effective means to predict the runout distance of debris flows. However, the apparent friction angle ϕ_a is usually estimated from past failure events (for example, correlation between landslide volume and apparent friction angle, Sassa 1988) such that it is sometimes difficult to determine the apparent friction angle precisely and specifically for each prediction. This model assumes the debris mass as a single point (lump mass model), and it is unable to take account for the internal deformation and to simulate the motion of the flow surge. It also overlooks the effects of channel cross section and the constitutive relationship of the debris mass.

2.3.2.3.1.2 Improved Sled Model

Sassa (1988) assumed that the apparent friction angle ϕ_a can be approximately (as an estimation because causes of energy loss during motion is not solely due to friction but other causes such as energy loss due to collision) expressed as a combination of the internal friction angle during motion and the pore pressure as:

$$\tan\phi_a = \frac{\sigma - u}{\sigma}\tan\phi_m \quad (11)$$

where ϕ_a = apparent friction angle

ϕ_m = internal friction angle during motion

σ = normal stress

u = pore pressure

Sassa (1984) developed a new ring shear apparatus to measure the internal friction angle during motion. However, it is difficult to estimate the pore pressure during motion, Sassa (1988) classified pore pressure generation mechanism into three cases. (Case A): A landslide mass is moving on a ground without generation or dissipation of pore pressure (for example, flow on concrete channel); (Case B): A landslide mass is moving on a saturated or partially saturated ground, and high pore pressure will be generated by undrained loading; and (Case C): A landslide mass is moving on a relatively dry and permeable ground, and pore pressure from moving mass is dissipated to the ground. Adopting the pore pressure parameters (B_D and A_D) proposed by Skempton (1954) and expressing B_D in terms of the compressibility of soil and pore liquid (Lambe and Whitman, 1979), Sassa et al. (1985) formulated a new equation for case B to estimate the pore pressure during motion:

$$B_D = \frac{1}{1 + \frac{n}{C_{c3}}\{\frac{S_r}{100}C_w + \frac{100 - S_r(1 + \alpha B_D \Delta\sigma_3)}{100}\frac{1}{u_0 + B_D\Delta\sigma_3}\}} \tag{12}$$

where n = porosity

C_{c3} = three dimensional compressibility of soils

S_r = degree of saturation (in %)

u_0 = initial pore pressure including atmospheric pressure

C_w = compressibility of water

$\Delta\sigma_3$ = confining pressure increment

α = constant for absorption of air into water

The pore pressure A_D for fully saturated debris can be determined from measurement of pore water pressure during application of principal stress difference under undrained conditions in a triaxial test. For simplicity, Sassa (1988) simplified equation (11) and expressed the apparent friction angle in terms of ϕ_m, B_D and A_D by equation (13).

$$\tan\phi_a = \frac{(1 - B_D)\tan\phi_m}{1 + B_D A_D \tan\phi_m} \tag{13}$$

By the use of the apparent friction angle estimated by laboratory testings, Sassa (1988) called the conventional sled model as the improved sled model. The improved sled model can determinate ϕ_a for each part of the expected travel distance by laboratory testings, for instance, a low ϕ_a for a saturated and less permeable ground, and a high ϕ_a for a relatively dry and permeable ground. The improved sled model can overcome the limitation of the conventional sled model which is limited to estimate a single ϕ_a for the whole travel distance by introducing different ϕ_a for each part of the travel distance. Nevertheless, the improved sled model suffers the same limitations as the sled model because it simulates the debris flows to be a lump mass model.

2.3.2.3.1.3 Kinetic Model

Kang (1997) assumed the movement of viscous debris flow can change from grain shearing collision to grain shearing slide after reaching the deposition section or alluvial fan. When debris mass (assumed as saturated mixture with slurry filled in between the coarse grains) moves at a steep slope, the weight of coarse grains in debris flow is transmitted to the channel bed through inter-particle collisions and the

flow is considered similar to the fluid movement (grain shearing collision). As the channel slope becomes milder, the debris flow starts to decelerate and deposits. The debris flow can be considered as solid movement (grain shearing slide). Kang (1997) expressed the deceleration and deposition location in terms of dynamic friction angle of grains and bed slope of alluvial fan. For a debris flow reaches an alluvial fan where $\phi_m > \theta$, its deceleration is:

$$a = g\cos\theta(\tan\theta - \tan\phi_m) \tag{14}$$

where a = deceleration

θ = bed slope angle of alluvial fan

ϕ_m = dynamic friction angle of grain

g = gravitational acceleration

Denoting V_0 as the velocity of debris flow in the conveyance section (similar to the entry velocity in the sled model), the velocity and runout distance of debris flow after time t of deceleration are:

$$V_t = V_0 + gt\cos\theta(\tan\theta - \tan\phi_m) \tag{15}$$

$$S_t = V_0 t + \frac{1}{2}gt^2\cos\theta(\tan\theta - \tan\phi_m) \tag{16}$$

When $V_t = 0$ (stoppage of debris flow), $t = -\dfrac{V_0}{g\cos\theta(\tan\theta - \tan\phi_m)}$ and the runout distance of debris flow is

$$S_t = -\frac{V_0^2}{2g\cos\theta(\tan\theta - \tan\phi_m)} \tag{17}$$

The above model is simple and provides a theoretical prediction for deceleration, velocity and runout distance of debris flow. The deceleration of debris flow can also be applied to estimate its impact force to adjacent structures. But this model takes no

account of the channel morphology, mechanism of movement, and deposition or entrainment of debris mass.

2.3.2.3.1.4 Frictional Model

When a layer of loose, dry and purely frictional material slides down an inclined surface and enters its accumulation zone with a given velocity V_0, VanGassen and Cruden (1989) derived that the runout distance of rock avalanches depends on the momentum transfer within the slide mass. According to the Newton's second law, the change of momentum of the system is equal to the resultant of external forces acting on the system:

$$F = \frac{d(MV)}{dt} \tag{18}$$

where F = resultant of external forces

M = mass

V = velocity

Assuming the resistance against movement of sliding mass along a slope of angle θ is caused by friction only, we have (by chain rule, $V = \frac{dS}{dt}$)

$$F = M\frac{dV}{dt} + V\frac{dM}{dt} = MV\frac{dV}{dS} + V^2\frac{dM}{dS} = \frac{M}{2}\frac{d(V^2)}{dS} + V^2\frac{dM}{dS} \tag{19}$$

$$\frac{M}{2}\frac{d(V^2)}{dS} + V^2\frac{dM}{dS} = Mg\sin\theta - Mg\mu\cos\theta \tag{20}$$

where θ = slope angle

μ = coefficient of friction

dS = incremental distance along the slope

Gassen and Cruden (1989) developed three models for the prediction of runout distance: (1) constant mass model or sliding block, (2) linear mass-change model, and

(3) exponential mass-change model. For a constant mass model, we can set $dM/dS = 0$ into equation (20) and obtain

$$\frac{d(V^2)}{dS} = 2g(\sin\theta - \mu\cos\theta) \tag{21}$$

Integrating both sides of equation (21), where V_0 is the initial velocity and L the runout distance,

$$L = \frac{-V_0^2}{2g(\sin\theta - \mu\cos\theta)} \tag{22}$$

This equation is identical to equation (17) if we set $\mu = \tan\phi_m$

If the slide mass is changing linearly with distance, we have

$$M = M_0 \frac{S_f - S}{S_f} \tag{23}$$

Where M_0 = initial mass

S_f = distance at which velocity and mass become zero.

Equation (20) becomes $\frac{d(V^2)}{dS} - \frac{2V^2}{S_f - S} = 2g(\sin\theta - \mu\cos\theta)$ (24)

and can be solved as

$$V^2(S - S_f)^2 = \{V_0^2 + \frac{2}{3}g(\sin\theta - \mu\cos\theta)S_f\}S_f^2 + \frac{2}{3}g(\sin\theta - \mu\cos\theta)(S - S_f)^3 \tag{25}$$

When $V = 0$, $S = S_f$ (boundary condition for deposition zone)

$$S_f = -\frac{1.5V_0^2}{g(\sin\theta - \mu\cos\theta)} \tag{26}$$

By assuming a rectangular deposition profile with a center of gravity at midpoint, the runout distance L becomes

$$L = \frac{S_f}{2} = -\frac{1.5V_0^2}{2g(\sin\theta - \mu\cos\theta)} \tag{27}$$

If the slide mass is changing exponentially with distance,

$$M = M_0 e^{\frac{-S}{L_0}} \tag{28}$$

where L_0 = travel distance of the center of gravity for the exponential deposition profile. Gassen and Cruden (1989) assumed that the exponential deposition profile can be truncated at $S = 5L_0$ and the sliding mass beyond $S > 5L_0$ is negligible. For the truncated profile at $S = 5L_0$, the center of gravity is at $L = 0.966L_0$. Similarly, when $V = V_0$ at $S = 0$ and $V = 0$ at $S = 5L_0$, we have,

$$L = -\frac{1.93V_0^2}{2g(\sin\theta - \mu\cos\theta)} \tag{29}$$

A comparison of equations (22), (27) and (29) show that the runout distance of the sliding mass depends on the rate of deposition along the slope. This result indicates if a slide with a changing mass is assumed to be a sliding block with a constant mass, the runout distance of slide would have been underestimated. Accordingly, it also indicates that the runout distance predicted by a lump mass model would be underestimated if the rate of deposition is not zero.

However, there is strong objection against this model. More specifically, equation (18) which is the foundation of this model is for a rocket with an implicit assumption U = 0 or $U_{rel} = -V$ (Hungr, 1990a,b; Erlichson, 1991):

$$M\frac{dV}{dt} + V\frac{dM}{dt} - U\frac{dM}{dt} = F \tag{30}$$

or

$$M\frac{dV}{dt} - U_{rel}\frac{dM}{dt} = F \tag{31}$$

where V = absolute velocity of rocket

U = absolute velocity of the gases expelled from the rocket engine

U_{rel} = velocity of the gas relative to the rocket

M = changing mass of rocket

F = resultant of external forces acting on the system

Analogous to the rocket equation, Cannon and Savage (1988) and Gassen and Cruden (1989) attempted to apply the rocket equation to the deposition of a sliding mass. Unfortunately, the application of rocket equation to the deposition of the sliding mass is not justified (Hungr, 1990a,b; Erlichson, 1991). For a rocket, it is obvious that the exhausted gas is ejected from the rocket. This process assumes the action-reaction of forces to be internal in the rocket system. But, for the deposition system of a sliding mass, the depositing mass just separates from the flow, drops down on adjacent land and is decelerated from flow speed to zero speed by the friction of adjacent land. This process involves momentum change to the adjacent land that is external to the deposition system of a sliding mass. In other words, the depositing mass is not ejected or spurted at a velocity $U_{rel} = -V$ by the sliding mass itself, but it is brought to rest by the adjacent land. To further elaborate this, Erlichson (1991) supposes a man is sitting at the rear of the sliding mass and this man is considered as a part of the flow. Supposing this man throws a rock from the flow in the backward direction with a speed equal to the flow speed. The speed of the rock is zero relative to the ground and the rock simply drops to the ground behind the sliding mass. If this is the case, the rocket equation can be applied to the deposition system of sliding mass. But, it is not.

2.3.2.3.1.5 Dispersive Model

For a steadily moving debris flow traveling abruptly from a steep channel to a lower channel of gentler slope, Takahashi and Yoshida (1979) formulated an equation for its stoppage based on the principles of momentum conservation and continuity equations. For simplicity, Takahashi and Yoshida (1979) made the following assumptions: (1) shape of longitudinal profile is assumed to be trapezoidal (Figure 2.8); (2) all parts of flow proceed at the same velocity u; (3) concentration of granular phase c_u is constant throughout the process and (4) slope of channel abruptly level out without expansion in width.

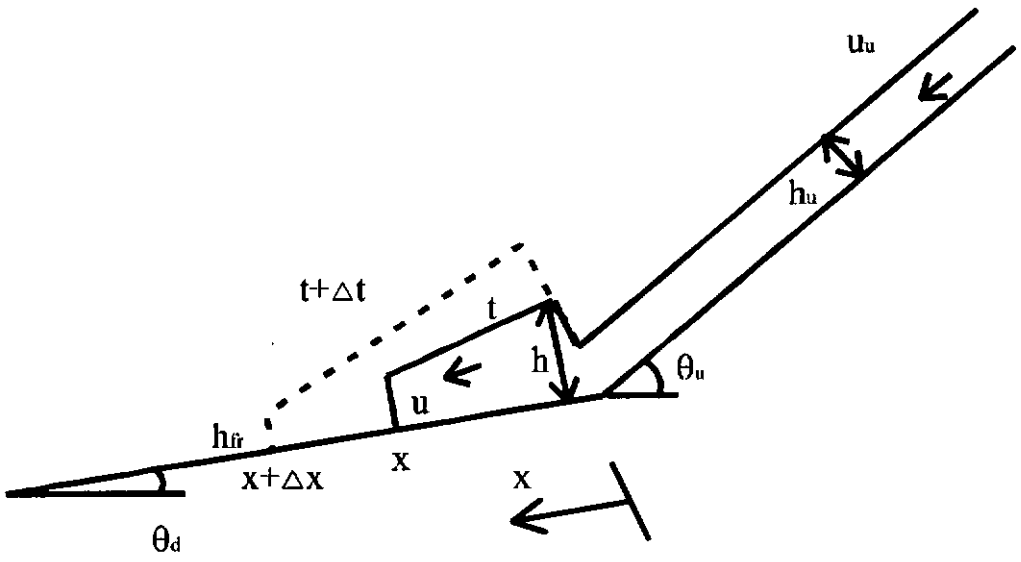

Figure 2.8 Process of stoppage of debris flow (Takahashi and Yoshida, 1979)

Where u_u = upstream velocity

h_u = upstream flow depth

θ_u = slope of upstream channel

θ_d = slope of downstream channel

t = time

x = distance

For momentum conservation, we have

$$\frac{d}{dt}\{\frac{1}{2}(h+h_{fr})x\rho_t u\} = \frac{1}{2}(h+h_{fr})x\rho_t g\sin\theta_d + \rho_t q_t u_u \cos(\theta_u - \theta_d) + \frac{1}{2}gh_u^2\cos\theta_u\cos(\theta_u-\theta_d)\{(\sigma-\rho_m)c_u k_a + \rho_m\} - F \quad (32)$$

where ρ_m = density of interstitial fluid

ρ_t = apparent density of debris flow = $(\sigma-\rho_m)c_u + \rho_m$

k_a = coefficient similar to active earth pressure coefficient

σ = density of particle

g = gravitational acceleration

F = friction force at the bed surface

c_u = volume concentration of solid phase

q_t = discharge

Where the left term expresses the temporal momentum change, the first term on the right expresses force due to gravity, the second term momentum flux from upstream, the third term the forces due to hydrostatic and earth pressure and the fourth term the friction force at the bed surface.

The shear stress at the bed surface τ_0 is the sum of granular shear stress τ_1 and shear stress τ_2 produced by turbulence and by viscosity of the interstitial fluid. τ_2 is normally considered negligible. Bagnold (1954) found the following relationship.

$$\tau_1 = -p\tan\alpha \quad (33)$$

where p = inter-particle stress normal to bed surface (dispersive stress)

$\tan\alpha$ = kinematic friction factor and α is an unknown angle affected by collision conditions

B < 40, $\tan\alpha$ = 0.75;

B > 40 and $\lambda < 12$, $\tan\alpha$ =0.32;

B > 40 and $\lambda > 12$, $\tan\alpha$ =0.4

B = Bagnold number (see definition given in Section 2.2)

Takahashi (1978) assumed that

$$p = -(\sigma - \rho)cgh\cos\theta \tag{34}$$

and, thus, the friction force can be approximated by

$$F = \frac{1}{2}(\sigma - \rho_m)gc_u(h_{fr} + h)x\cos\theta_d \tan\alpha \tag{35}$$

From continuity equation, we also have

$$\frac{1}{2}(h + h_{fr})x = h_u u_u t \tag{36}$$

Substituting equations (35) and (36) into equation (32), and simplifying the results, we obtain

$$\frac{du}{dt} + \frac{u}{t} = \{g\sin\theta_d - \frac{(\sigma - \rho_m)gc_u\cos\theta_d\tan\alpha}{(\sigma - \rho_m)c_u + \rho_m}\} + \frac{1}{t}u_u\cos(\theta_u - \theta_d)\{1 + \frac{[(\sigma - \rho_m)c_u k_a + \rho_m]\cos\theta_u gh_u}{2[(\sigma - \rho_m)c_u + \rho_m]u_u^2}\} \tag{37}$$

$$\text{or } \frac{du}{dt} + \frac{u}{t} = \frac{U}{t} - G \tag{38}$$

where $U = u_u\cos(\theta_u - \theta_d)\{1 + \frac{[(\sigma - \rho_m)c_u k_a + \rho_m]\cos\theta_u gh_u}{2[(\sigma - \rho_m)c_u + \rho_m]u_u^2}\}$

$$G = -\{g\sin\theta_d - \frac{(\sigma - \rho_m)gc_u\cos\theta_d\tan\alpha}{(\sigma - \rho_m)c_u + \rho_m}\}$$

To solve equation (38) and take $e^{\int \frac{1}{t}dt}$ as integrating factor, we have

$$e^{\int \frac{1}{t}dt}\frac{du}{dt} + e^{\int \frac{1}{t}dt}\frac{u}{t} = e^{\int \frac{1}{t}dt}(\frac{U}{t} - G) \tag{39}$$

$$\frac{d}{dt}(e^{\int \frac{1}{t}dt}u) = e^{\int \frac{1}{t}dt}(\frac{U}{t} - G) \tag{40}$$

Integrating equation (40) by parts,

$$e^{\int \frac{1}{t}dt}u = \int e^{\frac{1}{t}dt}(\frac{U}{t} - G)dt = \int (U - Gt)de^{\int \frac{1}{t}dt} = (U - Gt)e^{\int \frac{1}{t}dt} - \int e^{\int \frac{1}{t}dt}d(U - Gt) \quad (41)$$

$$e^{\int \frac{1}{t}dt}u = (U - Gt)e^{\int \frac{1}{t}dt} + G\int e^{\int \frac{1}{t}dt}dt \quad (42)$$

where

$$\begin{aligned}\int e^{\int \frac{1}{t}dt}dt &= e^{\int \frac{1}{t}dt}t - \int td(e^{\int \frac{1}{t}dt}) = e^{\int \frac{1}{t}dt}t - \int te^{\int \frac{1}{t}dt}d(\int \frac{1}{t}dt) \\ &= e^{\int \frac{1}{t}dt}t - \int te^{\int \frac{1}{t}dt}\frac{1}{t}dt = e^{\int \frac{1}{t}dt}t - \int e^{\int \frac{1}{t}dt}dt\end{aligned} \quad (43)$$

so, $\int e^{\int \frac{1}{t}dt}dt = \frac{1}{2}e^{\int \frac{1}{t}dt}t$ (44)

Substitution of equation (44) into equation (42),

$$e^{\int \frac{1}{t}dt}u = (U - Gt)e^{\int \frac{1}{t}dt} + G\frac{1}{2}e^{\int \frac{1}{t}dt}t \quad (45)$$

$$u = (U - Gt) + \frac{Gt}{2} \quad (46)$$

$$u = -\frac{Gt}{2} + U \quad (47)$$

Under the initial condition t = 0, x = 0,

$$x = -\frac{Gt^2}{4} + Ut \quad (48)$$

When u = 0 the debris flow stops,

$$t_{stop} = \frac{2U}{G} \quad (49)$$

We have $x = \frac{U^2}{G}$ (50)

The above method provides a simple analytical prediction of the runout distance of debris flows. But the limitation is that the width of gentler slopes cannot be abruptly changed and is the same as the width of steeper slopes.

2.3.2.3.1.6 Constant friction slope model

Hungr et al. (1984) simplified the above model and combined the model with the concept of a constant friction slope (Takahashi, 1978).

$$\tau_1 = \{(\sigma - \rho)c + \rho\} gh \sin\theta \tag{51}$$

where σ = particle density

ρ = density of interstitial fluid

θ = slope angle

h = flow depth

c = volume concentration of solid phase

g = gravitational acceleration

$$S_f = \frac{(\sigma - \rho)c}{(\sigma - \rho)c + \rho} \tan\alpha \tag{52}$$

Substitution of equation (52) into equation (32) and assuming $k_a = 1$ as for fluid like flowing and simplifying, we have

$$\frac{d(tu)}{dt} = u_u \cos(\theta_u - \theta_d)\{1 + \frac{gh_u \cos\theta_u}{2u_u^2}\} - t(S_f g \cos\theta_d - g \sin\theta_d) \tag{53}$$

$$\text{or } \frac{d(tu)}{dt} = V - Gt \tag{54}$$

$$\text{where } V = u_u \cos(\theta_u - \theta_d)\{1 + \frac{gh_u \cos\theta_u}{2u_u^2}\} \tag{55}$$

$$G = g(S_f \cos\theta_d - \sin\theta_d) \tag{56}$$

Solving equation (54) similar to equation (38), we have

$$x = \frac{V^2}{G} \tag{57}$$

For simplicity, if we neglect the term $\cos(\theta_u - \theta_d)\{1 + \frac{gh_u \cos\theta_u}{2u_u^2}\}$, the result is simplified to:

$$x = \frac{u_u^2}{g(S_f \cos\theta_d - \sin\theta_d)} \tag{58}$$

Equation (58) is similar to equations derived by Gassen and Cruden (1989) as both equations are based on the principle of momentum conservation. The difference is that Gassen and Cruden (1989) attempted to incorporate the mass change function. When comparing equation (22) (for constant mass) and equation (58), runout calculated from equation (22) is 2 times less than that from equation (58), because the term $\cos(\theta_u - \theta_d)\{1 + \frac{gh_u \cos\theta_u}{2u_u^2}\}$ is neglected in equation (58). Thus, equation (58) is more conservative.

However, from the principle of energy conservation (i.e. total work done is equal to the summation of kinetic energy loss and potential energy loss), we can simply obtain an expression which is very similar to equation (58).

Work done = change in K.E. + change in P.E.

$$mgx(\sin\theta - \mu\cos\theta) = -\frac{1}{2}mu_u^2 - mgx\sin\theta \tag{59}$$

where m = mass of slide

μ = coefficient of friction

u_u = entry velocity

g = gravitational acceleration

x = runout distance

θ = slope of deposition ground

$$\text{therefore, } x = -\frac{u_u^{\,2}}{2g(2\sin\theta - \mu\cos\theta)} \tag{60}$$

If we neglect the potential energy change (Hungr, 1990a), we have

$$x = -\frac{u_u^{\,2}}{2g(\sin\theta - \mu\cos\theta)} \tag{61}$$

which is the same as equation (22) given earlier.

2.3.2.3.1.7 Sliding Consolidation Model

A sliding consolidation model in loose, cohesionless materials is proposed for the behaviour of flow slides (Hutchinson, 1986). Excess pore water pressure is generated by undrained loading caused by collapse of flow slide source. When the flow slide travels on an impermeable and unerodible ground (Figure 2.9), the excess pore water pressure decays gradually due to consolidation to a value that brings the slide to rest, while at the same time the friction during motion increases accordingly. The resulting flow slide travels until the degree of consolidation approaches close to unity for the moving mass to freeze.

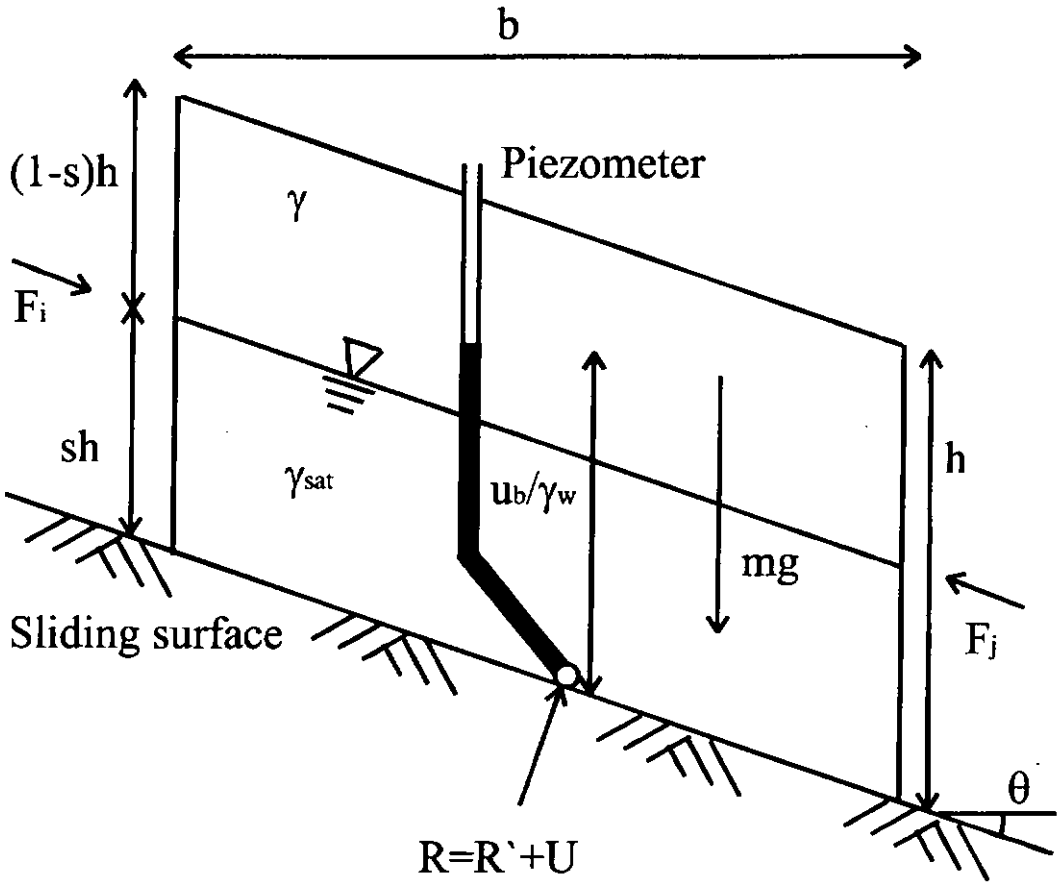

Figure 2.9 Forces on an element of the flow slide (Hutchinson, 1986)

Where F_i = total interslice force (assumed =F_j)

m = mass of slide

b = length of slide

h = flow depth of slide (s = fractional number)

R = total normal force on base

R' = effective normal force ($= mg\cos\theta$)

U = force due to pore water pressure ($= u_b b \sec\theta$)

γ = unit weight of flow slide

γ_{sat} = unit weight of saturated flow slide

u_b = basal pore pressure

It is assumed the flow slide consolidates by means of a single upward one-dimensional consolidation. The forces acting on an element of flow slide is shown in Figure 2.9. Assuming the basal resistance to be purely frictional, we have

$$ma = mg\sin\theta - (mg\cos\theta - u_b b\sec\theta)\tan\phi \tag{62}$$

where ϕ = undrained friction angle

$mg = bh\{(1-s)\gamma + s\gamma_{sat}\}$

a = acceleration

Hence,

$$a = g\{\sin\theta - (\cos\theta - \frac{u_b}{h\cos\theta[(1-s)\gamma + s\gamma_{sat}]})\tan\phi\} \tag{63}$$

Assuming the flow velocity decreases from initial velocity v_0 to zero linearly, one obtains

$$v = at + v_0 \tag{64}$$

and

$$x = \frac{at^2}{2} + v_0 t \tag{65}$$

where t = time required for basal excess pore water pressure to decay from u_{bo} to u_b

$$t = \frac{Td^2}{c_v} \tag{66}$$

T = time factor for degree of dissipation of basal excess pore water pressure

$$= 1 - \frac{u_b}{u_{b0}} \tag{67}$$

u_{b0} = pore pressure at t = 0 and is assumed to be

$$= [(1-s)\gamma + s\gamma_{sat}]h\cos^2\theta \tag{68}$$

d = average length of drainage path $= sh\cos\theta$ (69)

c_v = coefficient of consolidation of material

Using the above relationship the acceleration and velocity, and runout of flow slide can be calculated. The main limitation of model is that it is difficult to determine the thickness ratio (s) of the saturated flow slide and the average thickness of flow slide.

2.3.2.3.2 Numerical modeling

2.3.2.3.2.1 Shallow Water Model

Laigle (1997) treated debris flows as movements of a continuum flow based on the 2 dimensional shallow water equations.

$$\frac{\partial h}{\partial t}+\frac{\partial}{\partial x}(\bar{u}_x h)+\frac{\partial}{\partial y}(\bar{u}_y h)=0 \tag{70}$$

Equation (70) is the continuity equation for 2-D shallow water equation,

where h = flow depth

$\bar{u}_x$ *and* $\bar{u}_y$ = mean velocity in x and y direction respectively

Laigle adopted the Herschel-Bulkley rheological model and the equation of conservation of momentum in x direction as,

$$\frac{\partial(h\bar{u}_x)}{\partial t}+\frac{\partial(h\delta\bar{u}_x^{\,2}+\frac{1}{2}gh^2)}{\partial x}+\frac{\partial(h\delta\bar{u}_x\bar{u}_y)}{\partial y}=g\sin\theta_x h-\frac{\bar{u}_x}{\sqrt{\bar{u}_x^{\,2}+\bar{u}_y^{\,2}}}\frac{\tau_p}{\rho} \tag{71}$$

Similarly in y direction,

$$\frac{\partial(h\bar{u}_y)}{\partial t}+\frac{\partial(h\delta\bar{u}_y^{\,2}+\frac{1}{2}gh^2)}{\partial y}+\frac{\partial(h\delta\bar{u}_x\bar{u}_y)}{\partial x}=g\sin\theta_y h-\frac{\bar{u}_y}{\sqrt{\bar{u}_x^{\,2}+\bar{u}_y^{\,2}}}\frac{\tau_p}{\rho} \tag{72}$$

where g = gravitational acceleration

ρ = density of debris flow

θ_x *and* θ_y = slope angle in x and y direction respectively

$\tau_p = \tau_c\{1+1.93[\frac{\tau_c}{K}(\frac{h}{\sqrt{\bar{u}_x^{\,2}+\bar{u}_y^{\,2}}})^{\frac{1}{3}}]^{-0.9}\}$ (Herschel-Bulkley rheological model)

τ_p = yield strength

K = a parameter of the fluid

On the basis of the governing equations (70), (71) and (72), the model is solved by the simplified Godunov type explicit scheme. However, the limitation of this model is that the propagation time, during the stoppage stage, varies largely especially when flow velocities are low. The flow height near the front also varies rapidly. In addition, O'Brien et al. (1993) applied a finite difference method to solve the 2-dimensional shallow water equations and to simulate clear debris flow on alluvial fan and urban floodplains. But the main limitation is that detailed boundary conditions on the alluvial fan should be specified.

2.3.2.3.2.2 Particle-in-cell model

The formation of an alluvial fan was simulated by using a particle-in-cell model (Wang et al., 1997). Wang et al. (1997) assumed the debris medium to be an assembly of a large number of debris particles. According to the two-phase theory, each particle is composed of water, fine and coarse solid grains. The liquid phase consists of water and fine grains while the solid phase is composed of coarse grain only. The particle-in-cell model is represented by a fixed-and-moving grid (2-dimensional and squared). The debris flow depth and topographic elevation is represented at each fixed grid point.

With regard to the two-phase theory, the friction of debris flow S_{fd} is due to the friction of solid phase S_{fs} and the friction of liquid phase S_{fl}: That is

$$S_{fd} = S_{fs} + S_{fl} \tag{73}$$

This model takes account of the gravity term due to topographical elevation and the friction term related to the flow rheology, but neglects the pressure gradient of the flow.

However, it should be noted that as the individual particles are discrete points and cannot behave as a continuum flow, a long distance translation of particles during a time interval may lead to discontinuities or numerical instability. Thus the maximum translation distance of particles during time increment must be constrained. The boundary conditions (flow discharge at the entrance of the alluvial fan and its time duration) required for this model are also difficult to determine.

2.3.2.3.2.3 Two steps model

Jan (1997) simply treated debris flows as movements of a continuum which follows the continuity and conservation of momentum equations. For a 2-D incompressible and unsteady debris flow in a wide channel (shallow water), the governing equations are:

$$\frac{\partial h}{\partial t}+\frac{\partial Q_x}{\partial x}+\frac{\partial Q_y}{\partial y}=0 \tag{74}$$

$$\frac{\partial Q_x}{\partial t}+\frac{\partial}{\partial x}(\beta\frac{Q_x^{\,2}}{h})+\frac{\partial}{\partial y}(\beta\frac{Q_xQ_y}{h})=-gh\frac{\partial h}{\partial x}+ghS_x-\frac{\tau_{bx}}{\rho_m} \tag{75}$$

$$\frac{\partial Q_y}{\partial t}+\frac{\partial}{\partial x}(\beta\frac{Q_xQ_y}{h})+\frac{\partial}{\partial y}(\beta\frac{Q_y^{\,2}}{h})=-gh\frac{\partial h}{\partial y}+ghS_y-\frac{\tau_{by}}{\rho_m} \tag{76}$$

where h = flow depth

Q_x, Q_y = flow discharge in x and y direction respectively

S_x, S_y = bed slopes in x and y direction respectively

g = gravitational acceleration

ρ_m = density of debris flow

β = momentum correction factor

τ_{bx}, τ_{by} = bed shear stress components

The Bingham model is used to express the rheological behavior of debris flows and the assumed the bed stress shears are :

$$\tau_{bx} = \frac{\tau_0 U}{\sqrt{U^2 + V^2}} + \frac{\mu_B U}{H[\frac{1}{2} - \frac{H}{6h}]} \tag{77}$$

$$\tau_{by} = \frac{\tau_0 V}{\sqrt{U^2 + V^2}} + \frac{\mu_B V}{H[\frac{1}{2} - \frac{H}{6h}]} \tag{78}$$

where τ_0 = Bingham yield stress

μ_B = Bingham viscosity

U, V = flow velocities ($U = Q_x / h$ *and* $V = Q_y / h$)

$H = h - \delta_0$

$\delta_0 = \frac{\tau_0}{\rho_m g S}$ = *plug thickness*

$S = \sqrt{S_x^{\ 2} + S_y^{\ 2}}$

The above model was used to simulate debris flow in inclined channels having constant bottom slope and gradually varying slope with reasonable results, but comprehensive verification with experimental or field data for this model is necessary.

2.3.2.3.2.4 FEM model

Chen and Lee (1998) developed a three dimensional model for unsteady gravity-driven debris flows based on the Galerkin finite element method to simulate the flow along the longitudinal direction and the spread in the transverse direction. This method uses Lagrangian scheme in space and explicit Eulerian framework in time. This model has been applied to simulate a disastrous landslide in Hong Kong

(Shum Wan Road landslide) and gives reasonable results in comparison with the field observation.

2.3.2.3.2.5 DAN model

Because the conventional lump mass model is unable to take account of internal deformation and simulates the motion of flow front, Hungr (1995) developed a "Dynamic Analysis" model. The abbreviation of this model is "DAN" model. The DAN model simulates a slide mass as a number of blocks in contact with each other, free to deform and retaining fixed volumes of material (Figure 2.10). This model is basically an extension of the conventional lump mass model.

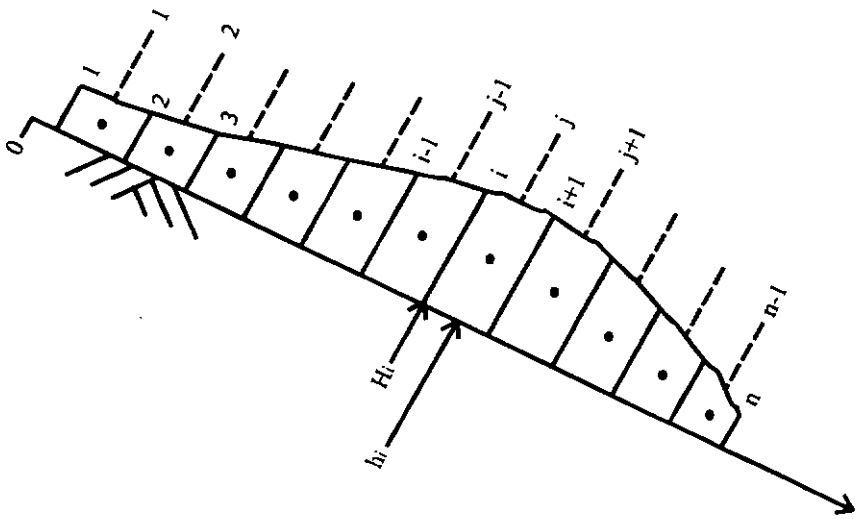

(a)

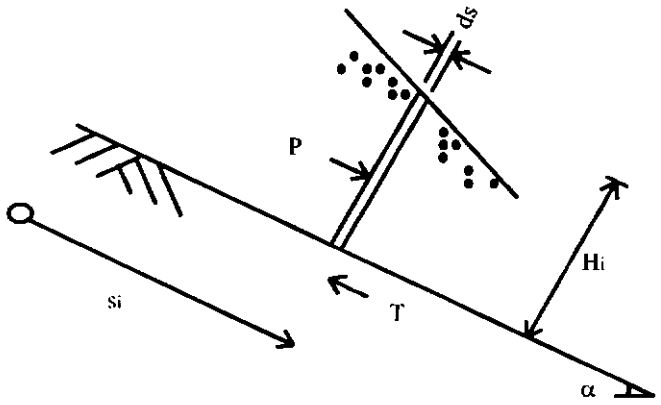

(b)

Figure 2.10 (a) Flow is represented in curvilinear coordinates where boundary blocks (i = 1 to n) and mass blocks (j = 1 to n-1). (b) Forces acting on boundary block (except the self weight)(Hungr, 1995).

Perhaps most existing models are associated with one distinct rheological material, the DAN model is designed to allow selection of a variety of material rheologies, which can vary along slide path or within slide mass. In this model, an equivalent fluid, whose properties will approximate the prototype behavior, is proposed to replace the real heterogeneous moving slide mass. Thus, the constitutive properties of the equivalent fluid must be obtained by back analysis. In order to facilitate such back analysis, the model must be flexible to account for major characteristics of landslide motion. That is why the DAN model is designed to allow selection of a variety of material rheologies. The model is referenced to curvilinear coordinates and a moving mesh, as illustrated in Figure 2.10. The momentum equation is applied to boundary blocks numbered i = 1 to n. The continuity equation is then applied to the mass blocks of fixed volume numbered j = 1 to n–1. There are 2n–1 unknowns for longitudinal displacements of boundary blocks and average normal depths in mass block. The available motion equations for boundary blocks and continuity equations for mass blocks are also 2n–1, therefore the problem is determinate. The solution is explicit and occurs in time steps. As shown in Figure 2.10(b), for a boundary block, the net driving force (F) acting on the boundary block is equal to the sum of tangential component of weight, the tangential internal pressure (P) and the basal resisting force (T).

$$F = \gamma H_i B_i ds \sin\alpha + P - T \tag{79}$$

where γ = unit weight of debris flow

H_i = height of boundary block i

B_i = width of boundary block i

α = slope angle

The new velocity v_i of boundary block at the end of a time step is obtained from the velocity v_i' at the previous time step.

$$v_i = v_i' + \frac{g(F\Delta t - M)}{\gamma H_i B_i ds} \tag{80}$$

where g = gravitational acceleration

Δt = time step interval

M = momentum flux resulting from erosion of material

The new displacement S_i of boundary block at the end of a time step is obtained from the displacement S_i' at the previous time step.

$$S_i = S_i' + \frac{\Delta t}{2}(v_i - v_i') \tag{81}$$

The new average depth of flow in mass block with constant volume v_j is now determined as:

$$h_j = \frac{2v_j}{(S_{i+1} - S_i)(B_{i+1} + B_i)} \tag{82}$$

The new height of boundary block is obtained as the mean depth of adjacent mass blocks:

$$H_i = \frac{h_{j-1} + h_j}{2} \tag{83}$$

while the end mass blocks are assumed to be triangular so that $H_1 = \frac{h_1}{2}, H_n = \frac{h_{n-1}}{2}$

The lateral pressure coefficient k at the boundary block is evaluated as

$$k_i \frac{dH}{ds} = \frac{1}{2}\left[\frac{k_j(h_j - H_i)}{s_j - S_i} + \frac{k_{j-1}(H_i - h_{j-1})}{S_i - s_{j-1}}\right] \tag{84}$$

This coefficient is determined both for the boundary blocks and mass blocks. The incremental tangential strain in mass block is calculated from displacements of adjacent boundary blocks.

$$\Delta\varepsilon_j = \frac{(S_{i+1} - S_i) - (S'_{i+1} - S'_i)}{S'_{i+1} - S'_i} \tag{85}$$

The tangential internal pressure (P) is obtained based on the assumption that the flow line is approximately parallel to the bed surface and that the pressure increases linearly with depth:

$$P = -\gamma\, k\frac{dh}{ds}(1 + \frac{a_c}{g})H_i B_i \cos\alpha\, ds \tag{86}$$

where $k\frac{dh}{ds}$ is obtained by equation (84). The value k_j is based on tangential strain at mass block and expressed as:

$$k_j = k'_j + S_c\Delta\varepsilon_j \tag{87}$$

where S_c = stiffness coefficient. For compression, $S_c=(k_a-k_p)/0.05$, or for unloading $S_c=(k_a-k_p)/0.025$. The maximum and minimum value of k_j can be estimated corresponding to the active and passive states.

The basal resisting force (T) depends on the rheology of material. Seven rheological models have been incorporated into the computer program DAN.

(1) Plastic flow: This flow occurs under constant shear strength, c, of liquefied material. $T = cA_i$ (88)

where $A_i = B_i ds$

(2) Friction flow: The resisting force of this flow is a function of the effective normal stress on the flow base and the centrifugal acceleration.

$$T = A_i \gamma H_i (\cos\alpha + \frac{a_c}{g})(1 - r_u)\tan\phi \tag{89}$$

where $a_c = v_i^2 / R$ = centrifugal acceleration, dependent on the vertical curvature radius of the path R, r_u = pore pressure coefficient (ratio of pore pressure to total normal stress at base of block), γ = unit weight of debris flow, α = slope angle and ϕ = friction angle.

(3) Newtonian laminar flow: The resisting force of this flow is a linear function of flow depth and velocity with dynamic viscosity μ.

$$T = \frac{3A_i v_i \mu}{H_i} \tag{90}$$

(4) Turbulent flow: The resisting force of this flow is a function of velocity v squared and flow depth H. The Manning roughness coefficient n is used.

$$T = A_i \gamma v_i^2 n^2 H_i^{\frac{-1}{3}} \tag{91}$$

(5) Bingham flow: The resisting force of this flow is a function of flow depth, velocity, constant Bingham yield strength τ and Bingham viscosity μ. The resisting force T requires the solution of the cubic equation (92).

$$v_i = \frac{H_i}{6\mu}(\frac{2T}{A_i} - 3\tau + \frac{\tau^3 A_i^2}{T^2}) \tag{92}$$

(6) Coulomb viscous flow: When the Bingham yield strength in equation (92) is not constant and is dependent on the normal stress, the Coulomb viscous flow occurs.

$$\tau = \gamma H_i (\cos\alpha + \frac{a_c}{g})(1 - r_u)\tan\phi \tag{93}$$

Substitution of equations (93) into equation (92) leads to a cubic equation for the resisting force T.

(7) Voellmy fluid: Voellmy (1955) introduced this model, which contains a friction term and a turbulent term, for snow avalanches.

$$T = A_i[\gamma H_i(\cos\alpha + \frac{a_c}{g})\tan\phi + \gamma\frac{v_i^2}{\xi}] \quad (94)$$

where ξ = turbulence coefficient (m/s^2). The laboratory results of Bagnold (1954) suggested a physical justification for this relationship. Bagnold (1954) found the strength of a granular material rapidly sheared under constant volume conditions will increase with the square of the shear strain rate. For a landslide moving on a thin and partially liquefied undrained basal layer, the landslide starts movement with a low frictional resistance and increases with the square of velocity at higher speed. Implicitly the turbulence coefficient ξ included the thickness of the basal layer.

The above model has been compared favorably with results of controlled laboratory experiments. The runout of coal mine flow slides in the southeast part of British Columbia has been predicted satisfactorily through back analysis by this model. It is also found to be able to predict the observed runout distance of debris flows in Hong Kong (Ayotte and Hungr, 1999). It is simple and can incorporate a number of rheological models. However, this model approximates the complex and heterogeneous 3-D problem into a simple 1-D formulation. It will be used later in chapter 5 to compare with the experimental observations obtained in this study.

Chapter 3 A New Design For Debris Flow Flume

3.1 Introduction

Efforts have been made in assessing the potential hazards for debris flow prone areas in mountainous regions. One of the way to express debris flow hazards is the use of its runout distance. One way to contain debris flow is to build a catchment basin in restraining the extent of the deposition fan and to control the maximum runout distance. Before designing the catchment basin, a good understanding of the mechanisms of debris flow deposition is required. However, since most debris flows occur unexpectedly under adverse conditions of severe rainstorm and/or earthquake, except in some designated areas, such as Mt. Yakedake in Japan (Okuda et al., 1981; Takahashi, 1991), Jiangjia Ravine in Yunnan, China (Wu et al., 1990), and Mount St. Helens in USA (Pierson, 1995), very few field observations have been made on debris flows. One alternative to study debris flow dynamics is the use of experiments under well-designed conditions in laboratories. However, to date all previous experiments on debris flow has been done in a rather ad-hoc manner (except those by Iverson and LaHusen, 1993), to the best of our knowledge no complete dimensionless analysis has been proposed and used in flume design. Thus, scaling problems may lead to the observed phenomena in laboratories differing from the real debris flows in the field.

In view of this deficiency in the experimental approach, we propose to design an appropriate flume for modeling the real scale debris flows, by ensuring the equivalence of three constitutive scaling parameters (the Bagnold number B, Savage number S, friction number F) and four geometric scaling factors (velocity factor π_V, flow factor π_Q, shear strength factor π_τ, and viscosity factor π_μ) between the model tests and real events. The next section presents a new flume and material design in simulating debris flows in laboratory according to dimensionless analysis.

3.2 Basic Properties of Debris Materials

On September 1990, the largest debris flow reported in Hong Kong occurred on September 11, 1990 at Tsing Shan. This Tsing Shan debris flow involved the movement of 19,000 m^3 of boulders and soils. The debris was deposited into the "Area 19 Tuen Mun" which was a designated site for further development at that time (Figure 3.1 and 3.2). A detailed study of the Tsing Shan Debris Flow was conducted by the Geotechnical Engineering Office of the Hong Kong Government (King, 1996a). In March 2000, a visit was made to the site of the Tsing Shan Debris Flow. The site has not been developed yet and the debris flow scar is still clearly visible on the upper valley (Figure 3.3). However, most of the deposits and surface soils have been washed away by rain.

In this study, the experimental samples that are provided by the Geotechnical Engineering Office (GEO) of the Hong Kong Government are the debris materials obtained from the Tsing Shan Debris Flow site.

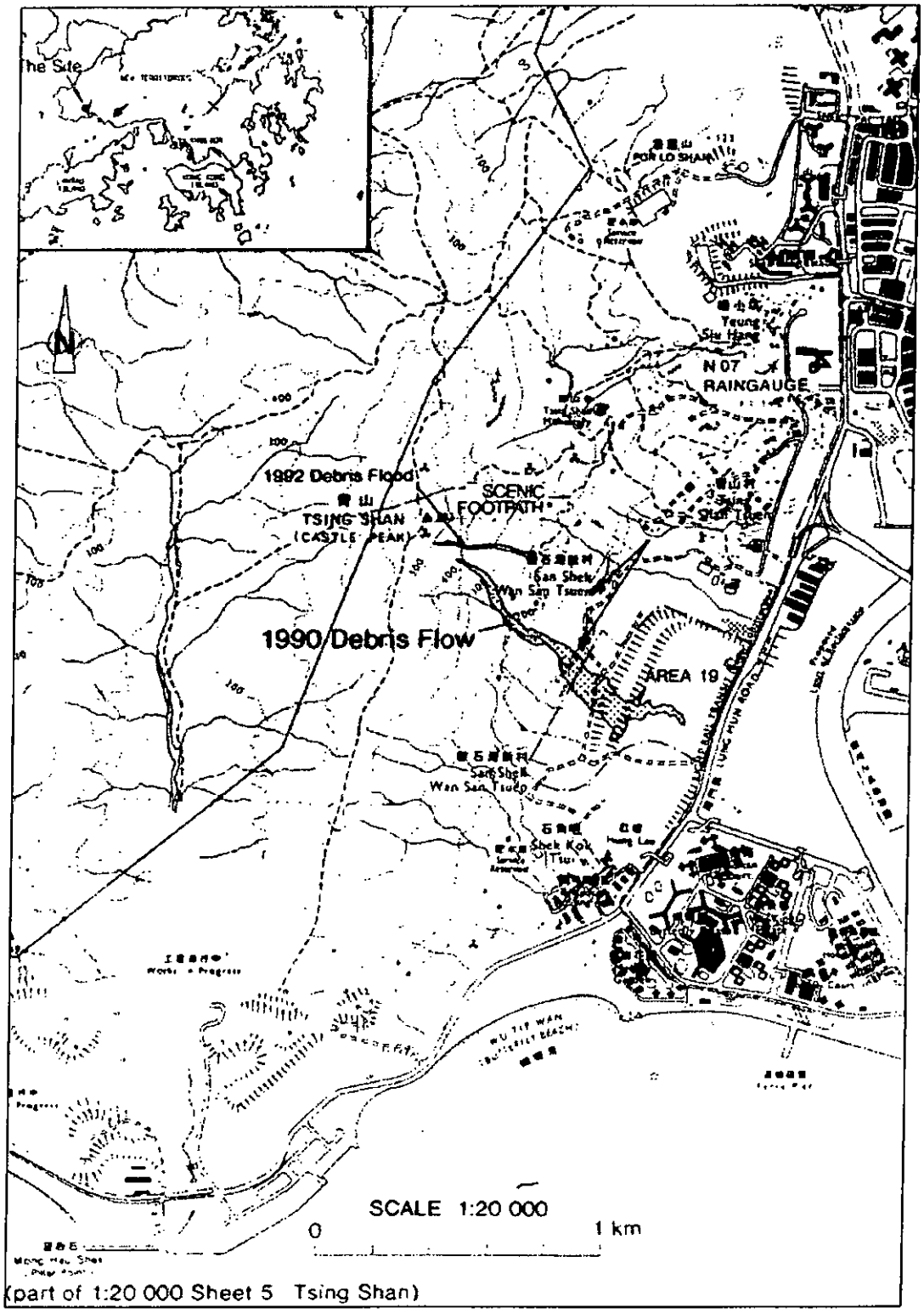

Figure 3.1 Site location of the Tsing Shan Debris Flow (King, 1996a)

Figure 3.2 A photograph for the Tsing Shan Debris Flow in September 14, 1990 (King, 1996a)

Figure 3.3 A photograph for the Tsing Shan Debris Flow in March 2000

3.2.1 Granular Content

Three granular materials with different particle size distributions (PSD) plotted in Figure 3.4 were used in our study. The standard dry sieving analysis was performed according to BS 1377 (part 2). The material m1 consists of 50% fine gravel and 50% sand by weight while the material m2 is composed of 20% fine gravel and 80% sand by weight. The material m3 used is somewhere between the PSD curves of material m1 and material m2. Except for the removal of particles of size larger than 5mm (i.e. medium gravel or larger), the fine grain PSD should closely resemble that of the debris of the actual event at Tsing Shan (see Figure A1 and A2 of King, 1996a).

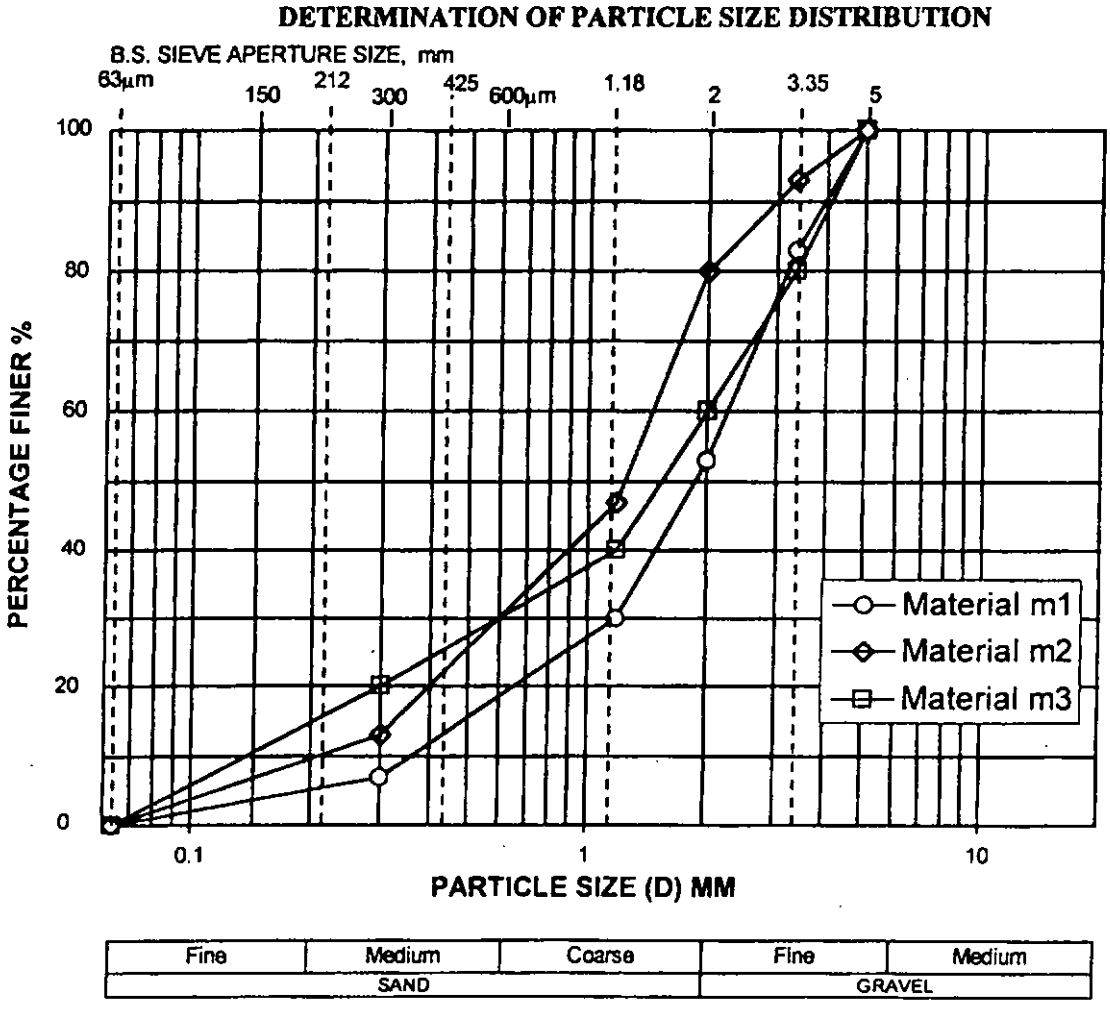

Figure 3.4 Particle size distribution of debris materials used in our study

3.2.2 Compaction

The optimum water content of debris materials as shown in Figure 3.5 were assessed by Proctor test (BS1377, Part4) so that ν_* can be determined. This result will be used to determine the linear grain concentration λ of the debris materials (Bagnold, 1954) which depends on ν and ν_*, where ν and ν_* are the volume fraction of solid phase and maximum (closed-packed) volume fraction of solid phase of debris materials. In particular, we have the following equation:

$$\lambda = \frac{\nu^{1/3}}{\nu_*^{1/3} - \nu^{1/3}} \tag{95}$$

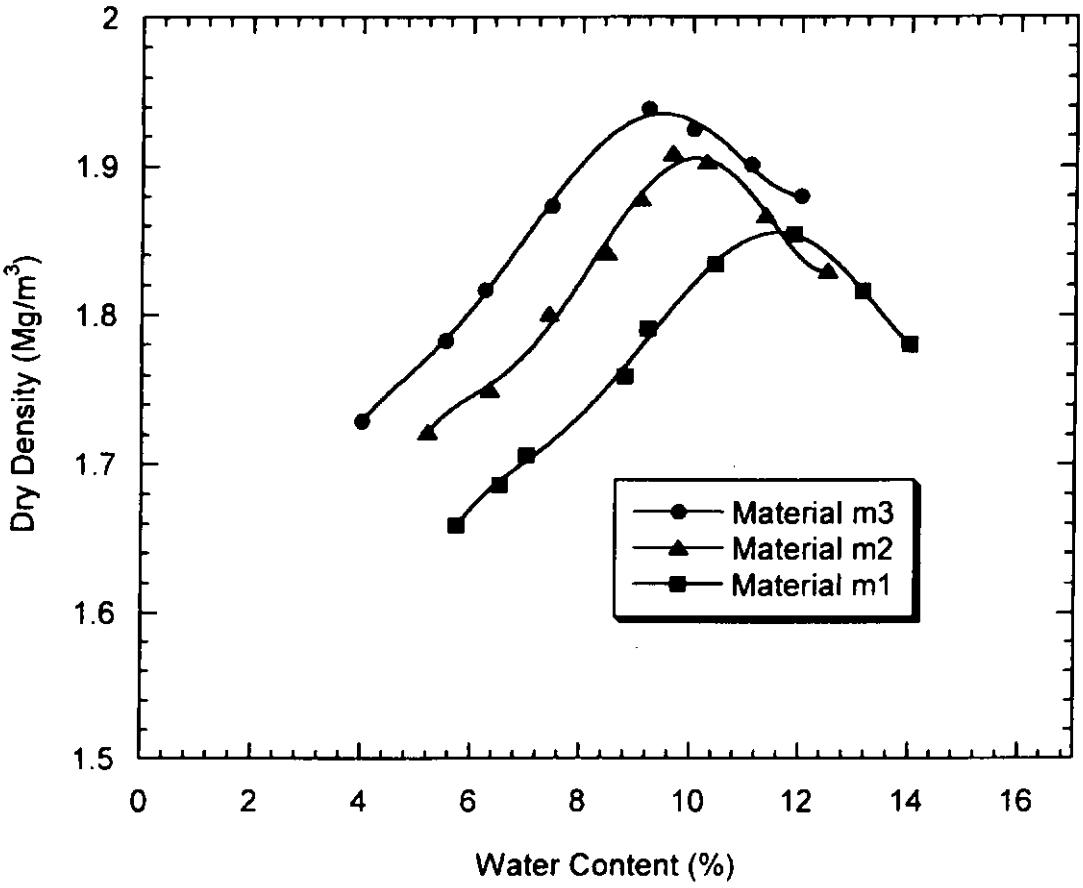

Figure 3.5 Relationship of dry density and water content of debris materials

3.2.3 Viscosity

As debris material is a complex material consisting of various compositions of granular materials and water, many rheological models for debris flows have been developed empirically and theoretically under idealized flow conditions (Wan and Wang, 1994; Bagnold, 1954; Chen, 1988 and Johnson and Rodine, 1984). In our study, the well-known Bingham model was adopted to characterize the constitutive flow behavior :

$$\tau = \tau_B + \mu \frac{dv}{dh} \tag{96}$$

where τ is the shear stress, τ_B is the shear strength, μ is the viscosity and dv/dh is the shear strain rate. The viscosity of debris material is defined as the slope of the shear stress-shear strain rate curve, and the shear strength of debris material is defined as the shear stress required to initiate the movement of debris flow. These rheological properties of debris materials were measured by a variable speed-type viscometer (Figure 3.6), that is made by Brookfield Engineering Laboratories Inc. By adjusting the rotational speed of the viscometer from 20 to 200 revolutions per minute (rpm), the obtained peak-torque values can be used to determine the shear stress and shear strain rate in each experiment (equations for shear stress and shear strain are summarised briefly in Appendix 1). The shear stress - shear strain rate curves of debris materials m1, m2 and m3 used in this study are shown in Figure 3.7. Then, τ_B and μ of equation (96) can be determined from the intercepts and line slopes shown in Figure 3.7. Table 3.1 summarizes the basic physical properties of the debris materials used. It should be noted that we have taken out all large particles (i.e. sand and gravel content) when we applied the viscometer test. In terms of the yield stress, Fei and Yang (1985) showed that the yield stress is independent of whether the coarse

particles were taken out or not. But, in terms of the viscosity, Shen and Xie (1985) suggested that the measurement of viscosity may depend on the amount of coarse particles taken out. They also gave an empirical relation for correcting the measured value if the viscometer test was done without the coarse particles. However, the full details of their experimental procedure in obtaining this correction formula is not given, and such correction has not attained a wide acceptance yet. We, therefore, will not attempt to make such correction in this study. Nevertheless, further experiments are still needed to examine this.

Figure 3.6 A rotational viscometer with variable speeds

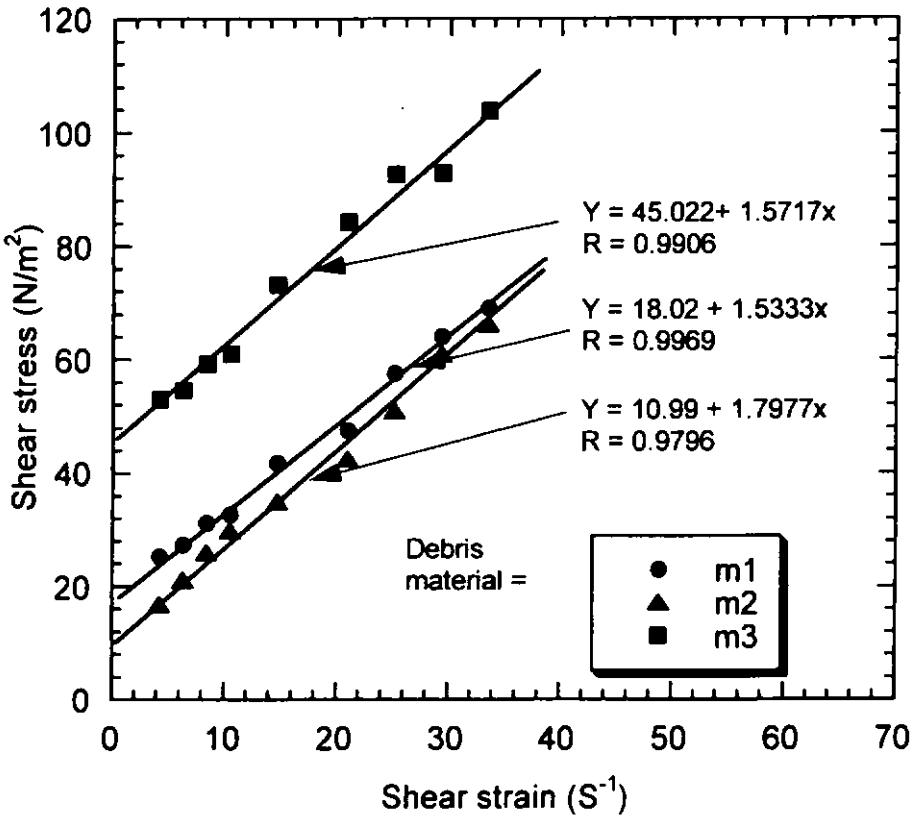

Figure 3.7 Rheological properties of debris materials

Materials		m1	m2	m3
Particle Density (kg/m^3)		2620	2620	2620
Max. volume concentration of solid		0.7669	0.7924	0.8024
Yield strength (N/m^2)		18.02	10.99	45.02
Viscosity (Ns/m^2)		1.53	1.80	1.57
Particle Size	d_{50} (mm)	1.90	1.35	1.50
	$d_{30}^2/d_{60}d_{10}$	1.68	1.13	1.20
	d_{60}/d_{10}	6.39	7.08	13.33
	Gravel	50%	20%	40%
	Sand	50%	80%	60%

Table 3.1 Physical properties of debris materials used in our study

3.3 Dimensionless Analysis for Debris Flow Modeling

3.3.1 Determination of Field Parameters

In choosing the parameters for the flume design, we focus on the debris flow episode occurred at Tsing Shan on September 11, 1990, although it is noted that many of the flow parameters were not recorded accurately during the flow. But, following the discussions by Johnson and Rodine (1984), all flow parameters can in fact be estimated by interpreting properly the field observations after the debris flow event.

King (1996a) has estimated some of the flow parameters. Other parameters have not been calculated by King (1996a) were also estimated here by using the following equations (Johnson and Rodine, 1984).

Radius of plug $$R_k = \frac{2\tau_B}{\gamma \sin\psi} \tag{96}$$

Flow rate $$Q = \frac{1}{\mu}\frac{\pi}{48}\gamma R^4 \sin\psi[(\frac{R_k}{R})^4 - 4(\frac{R_k}{R}) + 3] \tag{97}$$

Viscosity $$\mu = \frac{\tau_B w_p}{4v_{max}}(\frac{w}{w_p} - 1)^2 \tag{98}$$

Shear strength $$\tau_B = \frac{w_p}{4}\gamma \sin\delta \tag{99}$$

Where τ_B is the yield shear strength of debris material, γ is the unit weight of the reconstituted debris, v is the velocity (by assuming $v_{max} = 2v$, where v is the average flow velocity), w is the channel width, w_p is the plug width, ψ is the slope angle of the upper and lower surfaces of deposit, μ is the viscosity of debris materials and R is the equivalent channel radius. The properties of the Tsing Shan Debris Flow are tabulated in Table 3.2.

	Properties of the Tsing Shan Debris Flow	
King (1996a)	Channel length (m)	330
	Channel width W(m)	20
	Flow depth (m)	3 – 5
	Mean velocity (m/s)	12.5
	Shear strain rate (s^{-1})	2.50 – 4.17
	Typical grain diameter (i.e. d_{50})	200
	Density of reconstituted debris (kg/m^3)	1877
Present study	Slope angle of upper and lower surfaces of deposit ψ	10°
	Width of Plug W_p (m)	5
	Radius of channel R (m)	8
	Mean volume fraction of granular phase	0.56
	Radius of plug R_k (m)	2.5
	Flow rate Q (m^3/s)	839
	Viscosity μ (Ns/m^2)	1877
	Shear strength τ_B (N/m^2)	4171

Table 3.2 Properties of the Tsing Shan Debris Flow

3.3.2 Constitutive Scaling Parameters

In this study, three constitutive scaling parameters proposed by Iverson and LaHusen (1993) were adopted in controlling the constitutive behavior of the debris materials.

Iverson and LaHusen (1993) speculated that solid friction, liquid viscosity and particle collisions may play important roles in determining the mechanisms of debris flow, and thus proposed the following three dimensionless numbers (i.e. Bagnold number B, Savage number S and friction number F). These dimensionless numbers were adopted for modeling debris flows in this study. They are defined as

$$B = \frac{\dot{\gamma}\rho\delta^2\lambda^{1/2}}{\mu} \tag{100}$$

$$S = \frac{\dot{\gamma}^2\delta^2}{\upsilon g h} \tag{101}$$

$$F = \frac{\rho\upsilon g h}{\dot{\gamma}\mu} \tag{102}$$

where $\dot{\gamma}$ is the typical shear-strain rate, ρ is the debris density, δ is the typical grain diameter, μ is the viscosity, h is the typical flow depth and g is the gravitational acceleration. The definitions of λ and ν are the same as those given in section 3.2.2. The definitions of B and S were obtained by Bagnold (1954) and Savage (1984) respectively, and F was defined as $\lambda^{1/2}B/S$ by Iverson and LaHusen (1993). They represent different ratios of the characteristic shear stresses due to grain collisions, liquid viscosity and solid friction as shown in Figure 3.8. In particular, we have:

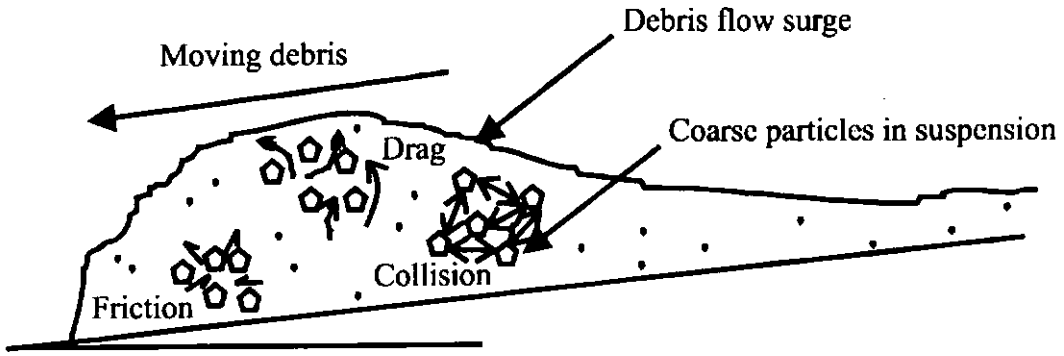

Figure 3.8 Theoretical representation of the mechanism of debris flow

$$B \propto \frac{stress\ due\ to\ grain\ collision}{stress\ due\ to\ liquid\ viscosity}$$

$$S \propto \frac{stress\ due\ to\ grain\ collision}{stress\ due\ to\ solid\ friction}$$

$$F \propto \frac{stress\ due\ to\ solid\ friction}{stress\ due\ to\ liquid\ viscosity}$$

where $\dot{\gamma}^2 \rho\delta^2$ is the grain collision term, $\dot{\gamma}\mu$ is the liquid viscosity term and $\nu\rho gh$ is the solid friction term. Experiments by Bagnold (1954) demonstrated that the stresses due to the grain collision dominate the viscous stresses if B > 450, or vice versa if B < 40. Savage and Hutter (1989) concluded that if S > 0.1 the grain collision dominates the grain friction, while if F > 1400, the grain friction dominates the viscosity (Iverson and LaHusen, 1993).

The use of these constitutive dimensionless numbers has been adopted in designing the debris material for the 95m long and 2m wide flume located in Eugene, Oregon USA (Iverson and LaHusen, 1993). However, due to financial and space limitations, this kind of full-scale flume is not feasible and practical in our laboratory. Thus the four geometric scaling factors proposed by Hua (1989) have been adopted in this study and are discussed next.

3.3.3 Geometric Scaling Factors

Hua (1989) proposed to use four dimensionless scaling factors for velocity V, flow rate Q, yield strength τ, and viscosity μ :

$$\pi_V = \frac{V}{V_m} = (\frac{L}{L_m})^{1/2} \tag{103}$$

$$\pi_Q = \frac{Q}{Q_m} = (\frac{L}{L_m})^{5/2} \tag{104}$$

$$\pi_\tau = \frac{\tau}{\tau_m} = (\frac{\rho}{\rho_m})(\frac{L}{L_m}) \tag{105}$$

$$\pi_\mu = \frac{\mu}{\mu_m} = (\frac{\rho}{\rho_m})(\frac{L}{L_m})^{3/2} \tag{106}$$

where L and ρ are the length and density of the debris in the prototype, and those for model is denoted by the subscript "m". In essence, the debris flow phenomena occurring in the model and the prototype are both governed by the same Navier-Stokes equations of fluid flow and the same Bingham constitutive model. The derivation of these scaling factors is briefly summarised in Appendix 2. Equations (103 - 106) show that the ratios of velocity, flow rate, shear strength and viscosity can be expressed in terms of the ratio of the length scale and the ratio of density. The required scaling parameters and factors shown in Table 3.3 are obtained from using the physical parameters obtained for the Tsing Shan Debris Flow given in Table 3.2. Therefore, the proposed experiments are expected to yield phenomena that are observable in debris flow events comparable to those of the Tsing Shan event. In short, microscopically the three constitutive scaling parameters can reflect the importance of the grain collisions, liquid viscosity and solid friction while macroscopically the characteristics of the debris flow can be reflected by the Bingham

fluid (the four geometric scaling factors). The application of the seven scaling parameters and factors are expected to be able to simulate the debris flows in the field.

Required Dimensionless Scaling Parameters			
Hua (1991)		Iverson and LaHusen (1993)	
$\pi_v = V/V_m = (L/L_m)^{0.5}$	10.5	$B = (\gamma * \rho * \delta^2 * \lambda^{1/2})/\mu$	0.3163 - 0.5271
$\pi_Q = Q/Q_m = (L/L_m)^{2.5}$	126905.9	$S = (\gamma^2 * \delta^2)/(\upsilon * g * H)$	$9.10 \times 10^{-3} - 4.21 \times 10^{-2}$
$\pi_\tau = \tau/\tau_m = (\rho/\rho_m) * (L/L_m)$	104.7	$F = (\rho * \upsilon * g * H)/(\gamma * \mu)$	3.9551 – 10.9864
$\pi_\mu = \mu/\mu_m = (\rho/\rho_m) * (L/L_m)^{1.5}$	1098.1		

Table 3.3 Required scaling parameters for dimensionless analysis

3.4 Flume Design

3.4.1 Experimental Setup

By examining the requirements in Table 3.3, a flume for debris flow simulation was constructed in the Department of Civil and Structural Engineering of the Hong Kong Polytechnic University (Figure 3.9). The schematic configuration of the debris flow flume is shown in Figure 3.10. The dimension of the flume is 300x20x30cm with adjustable slope angles ranging from 10° to 40°. The main flume can also be decomposed into three sub-sections, each 1 meter long enabling the topography of the flume to be adjusted. Two different cross sections of the flume have been constructed: one rectangular and the another triangular. Markers are placed along the lower part of the channel. The sidewall of the channel is made from transparent plastic board so that the movement of the debris flows can be viewed and measured from the side. The deposition board at the flume toe can also be adjusted from 0° to 10°. A supply tank for storing the debris (maximum volume of 60,000 cm^3) is inclined at 40° and placed at the upper end of the flume. Although, in general, the channel base can be erodible, the experiments in this study have been done on a rigid bed. That is the effect of an erodible bed is ignored. A rough surface of the channel base is simulated by gluing particles of 2.68mm mean diameter onto the base of the flume. The front of the supply tank is equipped with a hinged opening gate. Two digital video cameras were used to capture the transient motion of the debris flows in the low channel and at the deposition board.

Figure 3.9 A photograph for the new flume

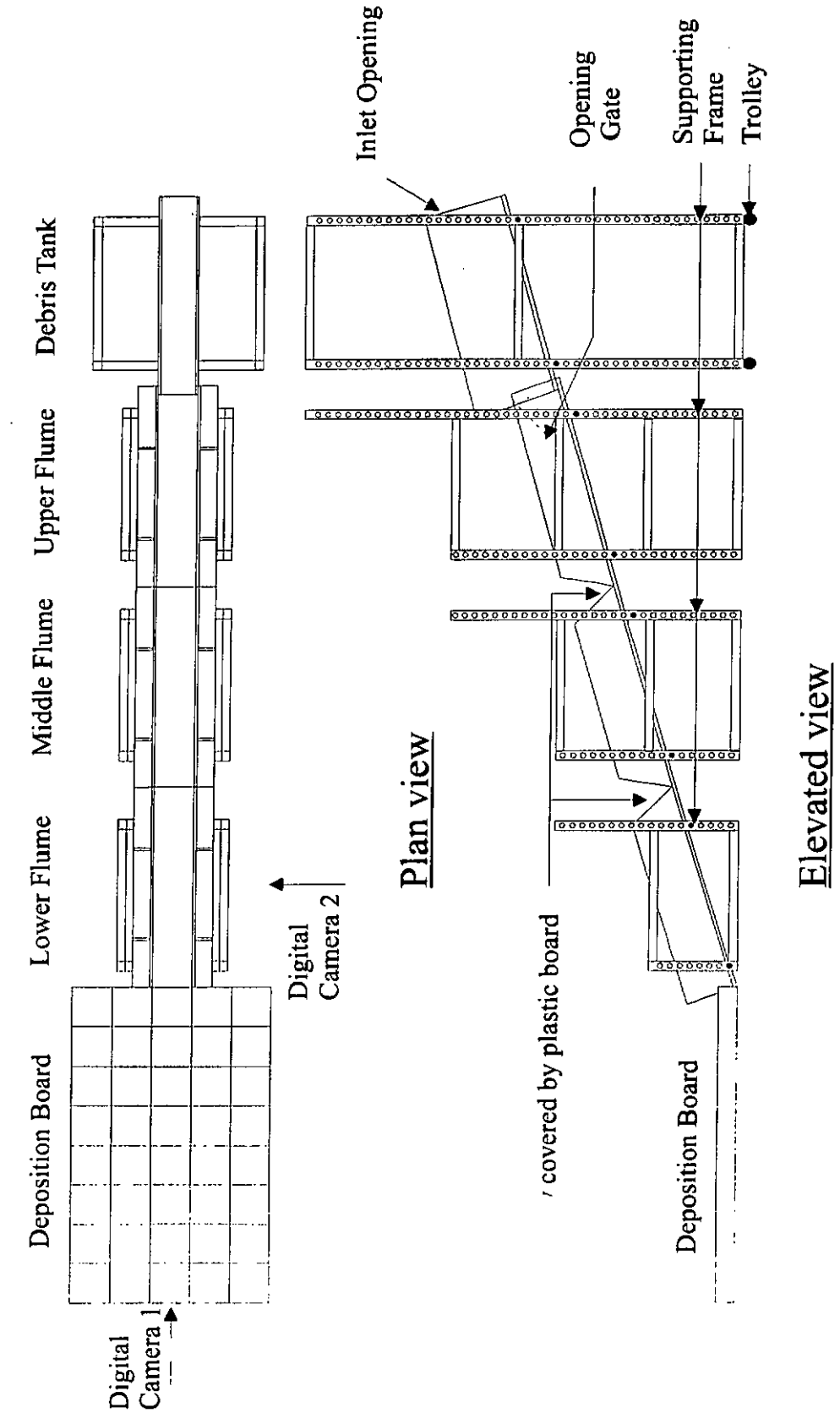

Figure3.10 A sketch for the set-up of the debris flow flume

3.4.2 Flume Comparison

A comparison of the features of the new flume with those of some previous flumes is shown in Table 3.4, and indicates that the present design is more versatile. The new flume can model debris flows with different cross section and flume topography. The size of the flume was designed by a dimensionless analysis, rather than in an arbitrary manner. Such flume design is used to scale up the experimental simulations and to yield debris flow phenomena that are comparable with the real debris flows of size similar to that of the Tsing Shan event.

Author	Debris volume	Flume gradient (degree)	Cross Section of flume	Deposition Board gradient (degree)	Flume flexibility	Flume length (m)	Flume width (cm)	Flume Bed
New Flume	60,000 cm^3	10 – 40 10 – 40 10 – 40	Rectangular and triangular	0 – 10	3 adjustable sub-channels	3	20	Rigid
Iverson and LaHusen (1993)	20 m^3	31	rectangular	2.5	fixed	95	200	Rigid
King (1996a)	27000 cm^3	15	rectangular	0	fixed	2	12	Rigid
Liu (1996)	97336 cm^3	10 - 34	rectangular	0 – 10	fixed	1.5	16	Rigid
Mainali and Rajaratnam (1994)	N.I.	28.6	rectangular	N.A.	fixed	4.25	5.1	Rigid
Steijn and Coutard (1989)	0.15 m^3	10 - 30	inclined surface	N.I.	fixed	2 - 3.5	N.A.	Rigid
Takahashi et al. (1992)	N.I.	18	rectangular	5	fixed	1 - 4	10	Erodible

N.A.= Not applicable, N.I. = No information

Table 3.4 Comparison of previous designs of experimental flumes with the present new flume

3.4.3 Experimental Procedures

One of the most important factors that can affect the rheological behavior of debris materials is temperature. Consideration of the temperature effect on viscosity is essential in the experimental simulation of debris flow. It is because the shear stress is a function of temperature. All experiments were conducted in laboratory under well-controlled conditions and the debris materials were kept at 19°C before each test.

Owing to the fact that the amount of debris materials provided by the Geotechnical Engineering Office was limited, the debris materials used in each experiment had to be reused. The debris materials used were oven dried after each usage. After oven drying, the debris materials stuck together. It is important that under no circumstance should the oven-dried debris materials be applied by mechanical crushing because this would normally lead to breakage of the coarse debris particles and hence change the particle size distribution. Instead, the oven-dried debris material should be soaked in water with water content equal to that required in the next experiment.

A total of 10,000cm^3 debris material of water content 0.2545 was poured into the supply tank. In order to reduce segregation of the coarse particle during pouring, the debris material was mixed in the supply tank for one minute continuously before the debris was allowed to slide down the flume. To avoid the undesirable loss of water content during the flow, we sprayed 300cm^3 water onto the flume surface before each experiment. Two digital video cameras were set up to capture the motion of the debris flow along the flume and on the deposition board. The shape of the debris fan

was recorded after its development was completed. Various depths of the debris fan were measured at 10cm x 10cm grid points by a digital calliper to an accuracy of 0.01mm.

Chapter 4 Experimental Results

A series of experiments were conducted by using debris materials with different granular content and by varying the flume slope (α) and deposition board slope (β). The cross-section used was either rectangular or triangular in shape. As discussed in the last chapter, the water content of the debris samples was fixed at 0.2545 unless otherwise specified and the temperature of debris material was kept at 19 °C at all times because the viscosity of debris material is highly dependent on the temperature variation. To avoid loss of water, the channel bed was wetted and sprinkled with 300ml of tap water. In order to reduce segregation of coarse granular materials in debris samples, the debris was mixed thoroughly and steadily for 1 minute after pouring into the supply tank. The experiments were conducted within 1 minute after mixing. To capture the transient motions of the flow at the lower part of the channel and deposition board, two digital video cameras were used in this study. In the following sections, the effects of flume slope, deposition board slope, granular content and flume cross section are summarised separately.

4.1 Effect of Flume Slope

In order to study the runout distance of debris flow travelling on different flume slopes, experiments A11-A13, in which the flume angle was set to be 26 - 38°,

were conducted for material m1. The experimental results are tabulated in Table 4.1 and the shapes of deposition fans are reported in Figure 4.1(A).

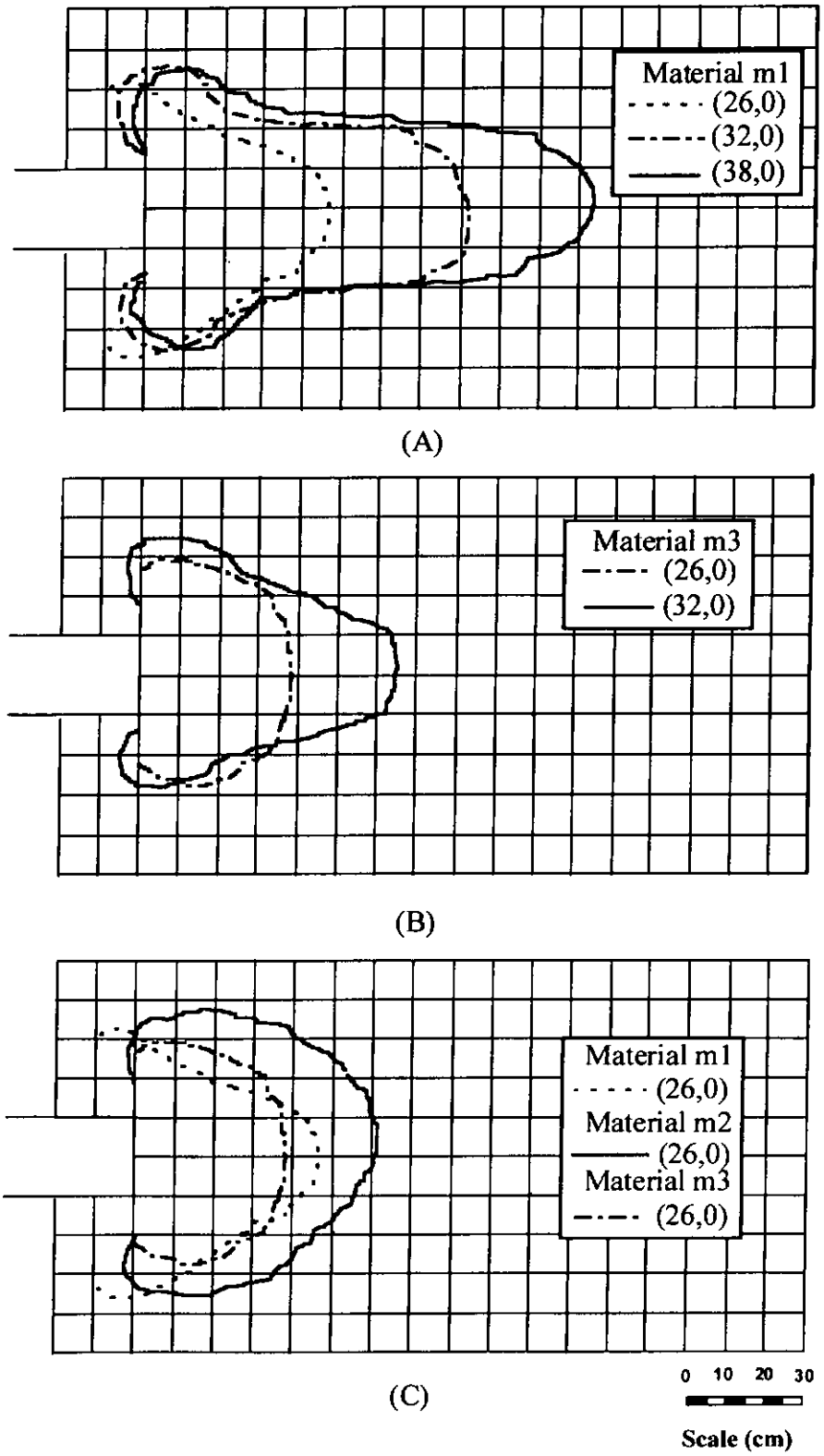

Figure 4.1 Shape and spreading of deposition fans for different materials and flume slope

No.	Material	Water content	Cross Section	Flume Slope (degree)	Deposition Board Slope (degree)	Runout Distance (cm)	Average Runout Distance (cm)	Max. Fan Width (cm)	Average Fan Width (cm)	Fan Area (cm^2)	Average Fan Area (cm^2)
A1	m3	0.2545	R	26	0	38	38	56	56	1838	1838
A2	m3	0.2545	R	32	0	65	65	57	57	2819	2819
A3	m2	0.2545	R	26	0	62	63.5	70	71	3713	3775
A4	m2	0.2545	R	26	0	65		72		3838	
A5	m2	0.2545	R	26	5	139	135.5	50	49.5	5769	5600
A6	m2	0.2545	R	26	5	132		49		5431	
A7	m2	0.2545	T	26	0	72	77	72.5	70.8	4419	4588
A8	m2	0.2545	T	26	0	82		69		4756	
A9	m2	0.2545	T	26	5	146	138.5	60	58.5	7063	6538
A10	m2	0.2545	T	26	5	131		57		6013	
A11	m1	0.2545	R	38	0	115	115	70.5	70.5	5200	5200
A12	m1	0.2545	R	32	0	81	81	71	71	3844	3844
A13	m1	0.2545	R	26	0	38	44	66	69.5	2431	2672
A14	m1	0.2545	R	26	0	50		73		2913	
A15	m1	0.2545	R	26	5	109.0	126	43.0	44	4013	4491
A16	m1	0.2545	R	26	5	143.0		45.0		4969	
A17	m1	0.2545	T	26	0	87	86.5	66.5	63.8	4775	4581
A18	m1	0.2545	T	26	0	86		61		4388	
A19	m1	0.2545	T	26	5	132	137.5	48	48	5206	5397
A20	m1	0.2545	T	26	5	143		48		5588	
A21	m1	0.2545	R	26	2	69	69	57	57	3194	3194
A22	m1	0.2545	R	26	0	102	102	78	78	5419	5419
A23	m3	0.2763	R	26	0	86	86	67	67	3775	3775
A24	m3	0.3123	R	26	0	170	170	68	68	6750	6750

Note: (1) R = Rectangular, T = Triangular
(2) All initial volume of debris materials are 10,000 cm^3 except A22 (15,000 cm^3)

Table 4.1 Parameters used in our experiments and the observed Runout of debris fan

For experiment A13 with the flume angle of 26°, the lateral spread was larger than the longitudinal runout, forming a semi-elliptic fan. While for experiments A11 and A12 with a steeper flume angle at 38 and 32° respectively, the longitudinal runout increased more rapidly than the lateral spread and lead to a pear-shape deposition fan. These results were quantitatively the same for both material m1 and m3 (see Figure 4.1 (A) and (B)). As expected intuitively, the runout distance increased with the flume slope. It is interesting to note that when the flume slope increased from 26 to 32° for material m1, the runout distance increased by 84%, while it increased by 42% only for flume slope increasing from 32 to 38°. It is because the debris runout distance depends on the flume slope nonlinearly. The runout distance no longer increased at the same rate if the flume slope became steeper.

4.2 Effect of Granular Content

In order to study the effect of the runout distance of debris flow with different granular materials, experiments A1, A3 and A13 were conducted for flume slope of 26° for materials m3, m2 and m1 respectively (Figure 4.1C). It is noted that the runout distance for material m2 with richer sand content (20% gravel and 80% sand) was 31% longer than that for material m1 with richer gravel content (50% gravel and 50% sand). While the runout distances for materials m1 and m3 were about the same owing to their richness in gravel content. According to the experimental results, it appears that debris with richer sand content can produce a longer runout distance compared to that with lesser sand content but richer gravel content. Thus, it is concluded that empirical data fitting of runout distance to slope angle irrespective to local soil conditions is not appropriate.

4.3 Effect of Volume and Water Content

In addition, comparing the results of experiments A13 and A22, Table 4.1 shows that the runout distance of experiment A13 increased by 132% as the initial volume of debris material increased from 10,000 cm^3 to 15,000 cm^3. The effect of water content on the runout distance of debris flow was also studied. Results of experiments A13 and A23 in Figure 4.2 show that the runout distance increased by 95% when the water content of material m3 changed from 0.2545 to 0.2763. It should be noted that in experiment A24 debris flow ran all the way down to the end of the deposition board (i.e. 170cm). The runout distance of experiment A24 should be longer than 170cm. It is noted that the runout distance of debris flow was very sensitive to an increase in water content. As a result, it is concluded that apart from the topography and channel gradient the permeability of local soil may also be a critical factor to the runout predictions of debris flows.

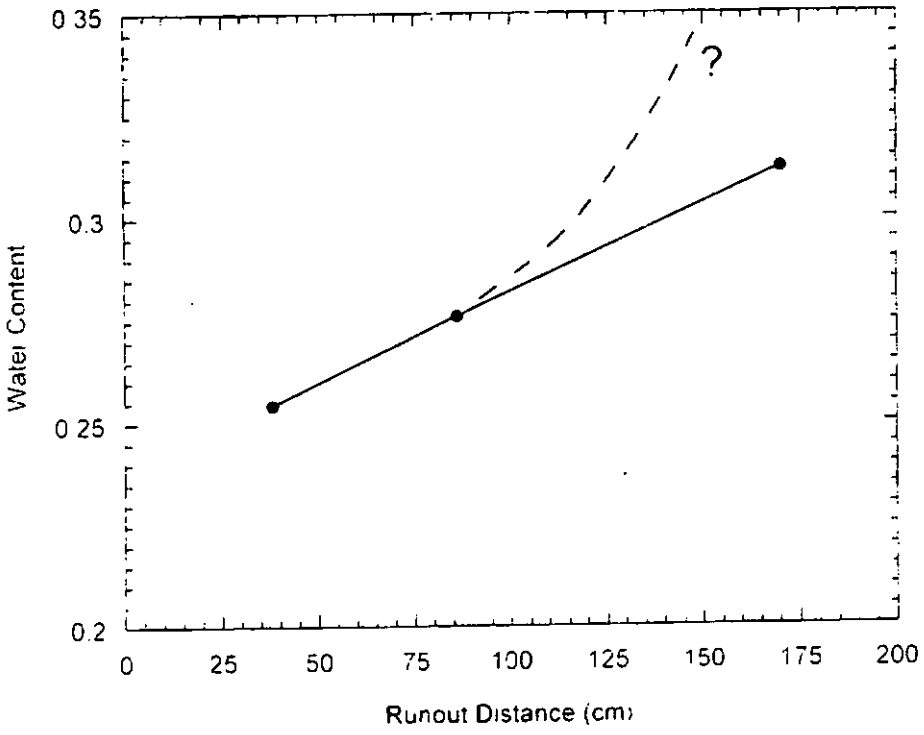

Figure 4.2 Relationship between runout distance and water content (experiments A1, A23 and A24)

4.4 Effect of Deposition Board Slope

In order to study the effect of runout distance of debris flow with different deposition board slope, experiments A3-A10 and A13-A21 in which the deposition board slope was varied from 0° to 5° for materials m2 and m1 respectively were conducted.

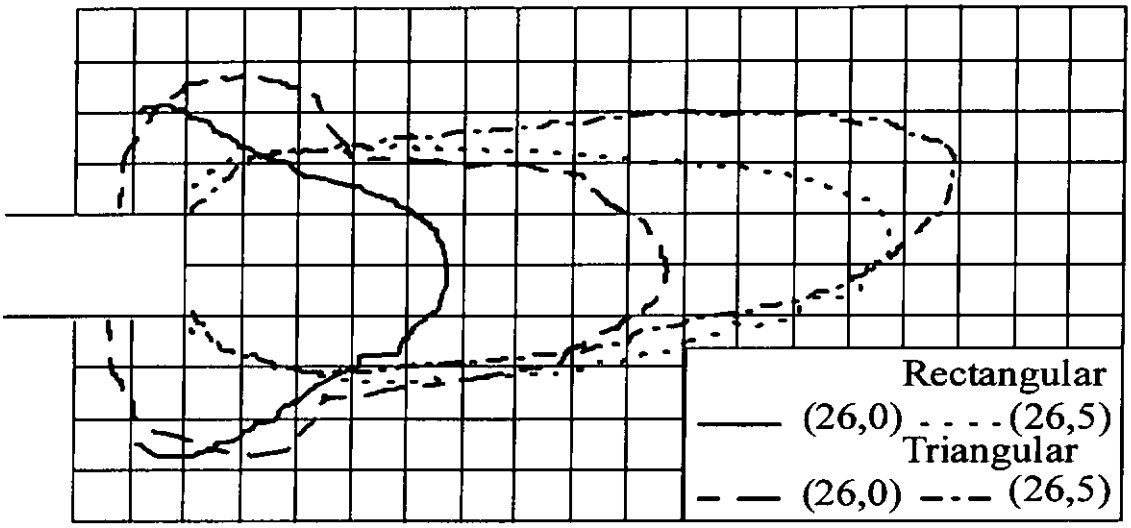

(A) Material m1

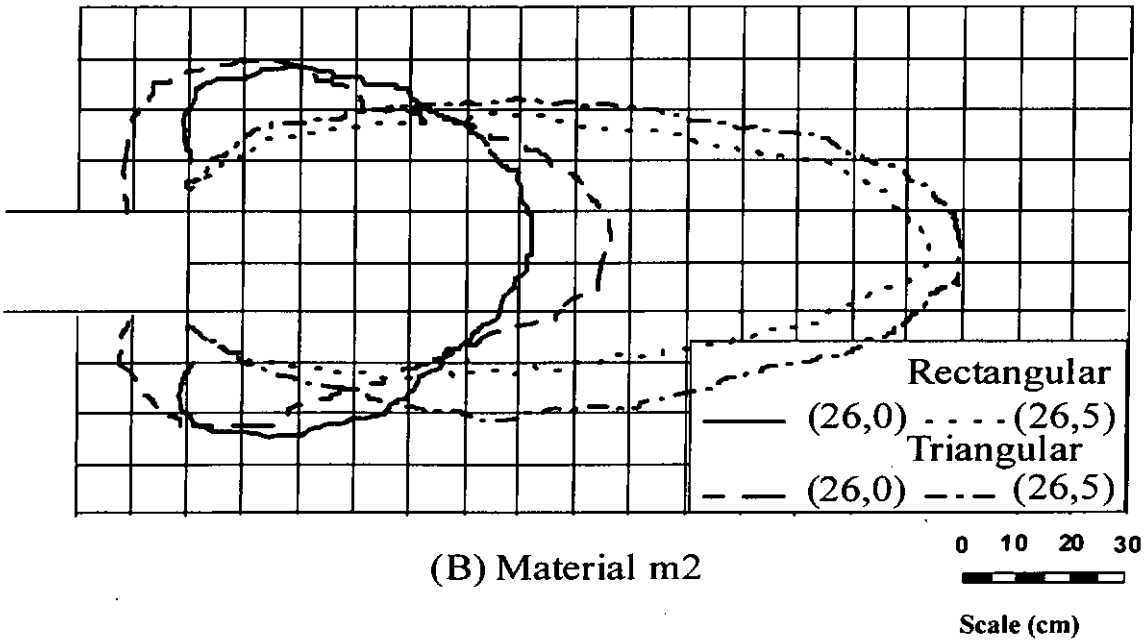

(B) Material m2

Figure 4.3 Shape and spreading of deposition fan for different deposition board slope and flume cross section

For rectangular channels, Figure 4.3 shows that the runout of material m1 increased by 186 % from 44 cm to 126 cm while that of material m2 increased 113 % from 63.5 cm to 135.5 cm when the deposition board slope increased from 0° to 5°. Figure 4.4 shows that the runout distance of debris flow tended to increase at a faster rate when the deposition board slope increased. Conversely, the maximum widths of debris fans decreased 37% for rectangular cross-section of flume and 25% for triangular cross-section of flume for material m1 when the deposition board slope increased from 0° to 5°. The average fan area of debris flow for material m1 increased 43% when deposition slope increased from 0° to 5°. As expected gentler deposition ground can greatly reduce the runout distance and, thus reduces the potential hazards of debris flow.

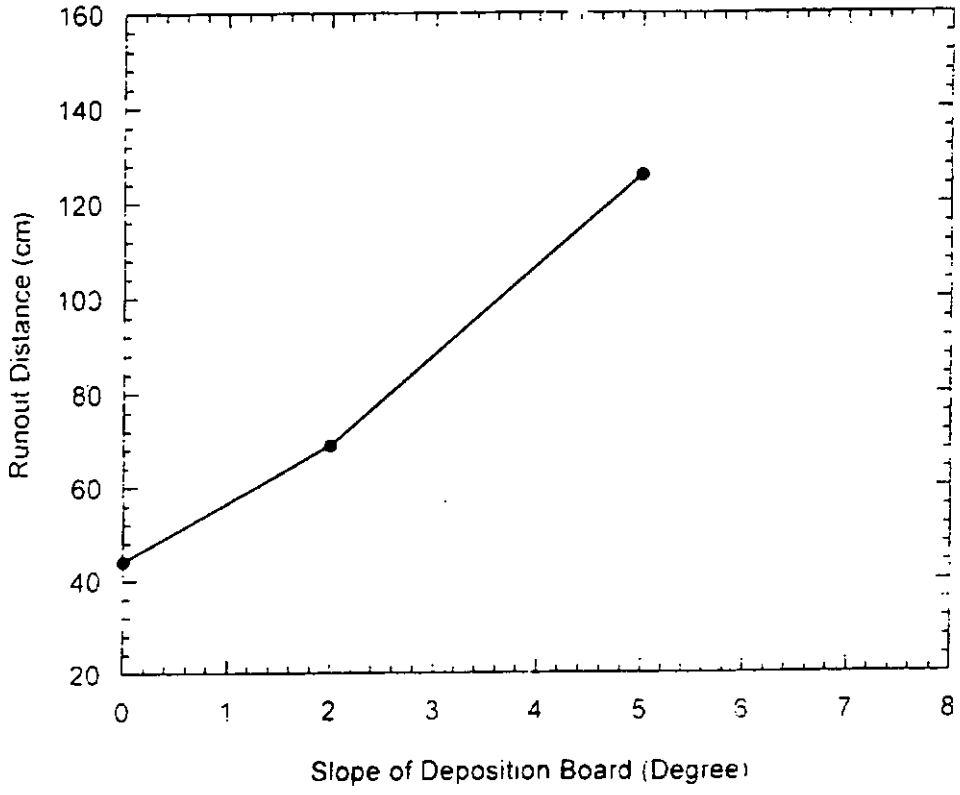

Figure 4.4 Relationship between runout distance and deposition board slope (experiments A13, A15 and A21)

4.5 Effect of Flume Cross Section

In Figure 4.3, it is observed that the runout for triangular cross-section was farther than the rectangular one. It is interesting to note that when deposition board slope increased from 0 to 5°, the runout distance increased on average for materials m1 and m2 by 150% for the rectangular channel and 70% only for the triangular channel. In general, the runout distance increased up to 100% as the rectangular cross-section changed to triangular (see material m1 and zero deposition slope in (A) of Figure 4.3). However, this increment can also be as little as 20% if the debris material m2 was used (see (B) of Figure 4.3). Therefore, for actual catchment basin design, we have to know the cross-section of the gully and the material of debris that is going to run down the gully. Hence, a detailed site investigation is needed if a reliable design is needed. This also suggests that empirical formulas for runout distance, which have been widely used for design, should not be used indiscriminately to Hong Kong. Empirical formulas must be obtained from areas with similar geological conditions, and its use should not be generalized to other situations.

4.6 Debris Fan Development

The temporal process of a typical debris fan in the experimental simulation (experiment A12) is shown in Figure 4.5. As the flow reached downstream at the mouth of the lower channel, it began to spread out and to deposit. When time T = 0.12 sec, the fan shape resembled to a half circle. The fan length quickly developed and reached 75% of its maximum runout distance at this stage after 0.6 sec. The other 25% of fan length was developed gradually in the following 2.96 sec. When the flow no longer proceeded downstream and increased its fan length, the fan width began to spread out to the debris fan sides. At the same time, the debris fan thickness developed and the fan became stable after 6.56 sec. It is also noted that coarser particles were found to be more concentrated at the debris fan boundary. This result suggested that the flow carried large particles at the surge when flowing along the channel. This result matched the physical phenomena of real debris flow that is capable of carrying large boulders at the surge (Takahashi, 1991; Johnson and Rodine, 1984). For the case of the deposition board slope $\beta = 5^{\circ}$ in experiment A5 (see Figure 4.6), the temporal formation of debris fan was basically similar to that in Figure 4.5, except that the lateral spread did not develop at the last stage. In Figure 4.7, an apparent surge at the lower channel is observed. Its shape remains basically constant as the surge progresses. This indicates that the change in velocity of the surge is small along the lower channel, although the velocity of surge is decreasing gradually along the lower channel. A typical three dimensional view of the deposition fan of debris flow in experiment A19 is shown in Figure 4.8.

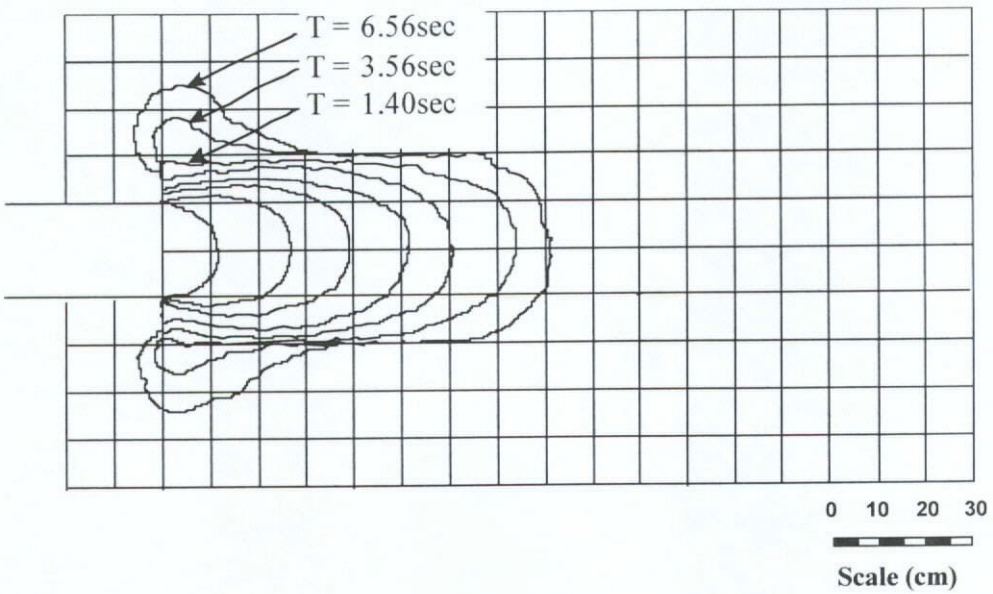

Note: (1)Time step between each developing fan is 0.12 sec, unless otherwise specified. The developing fan starts at t = 0 sec.
(2)It is from experiment A12.

Figure 4.5 Temporal formation of debris fan for the case of $\beta = 0^o$

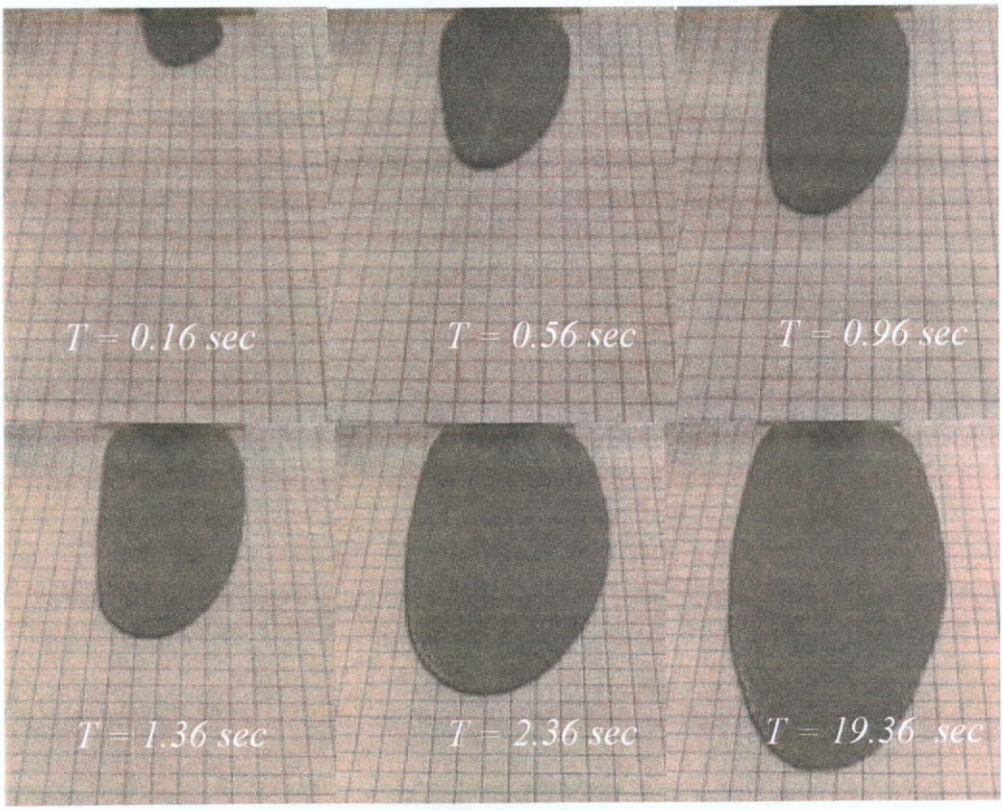

Figure 4.6 Temporal formation of debris fan for the case of $\beta = 5^o$ (experiment A5)

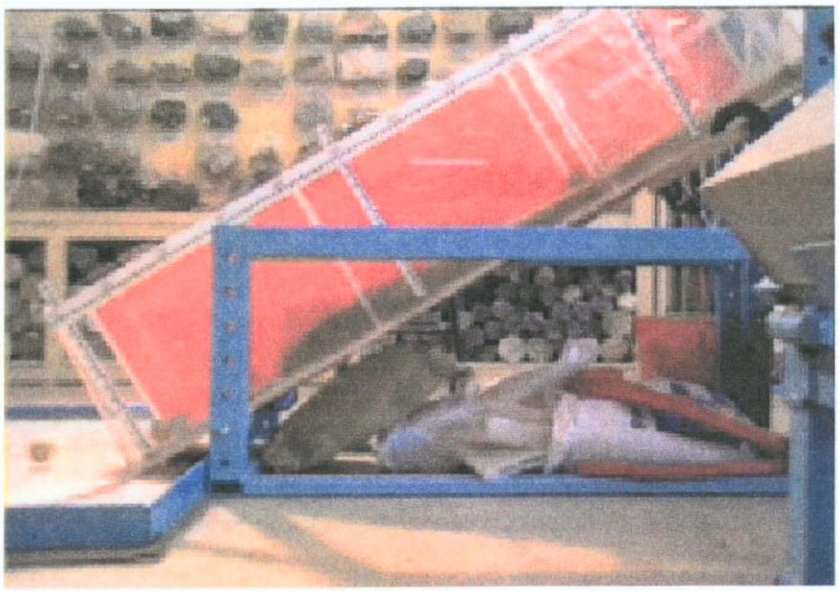

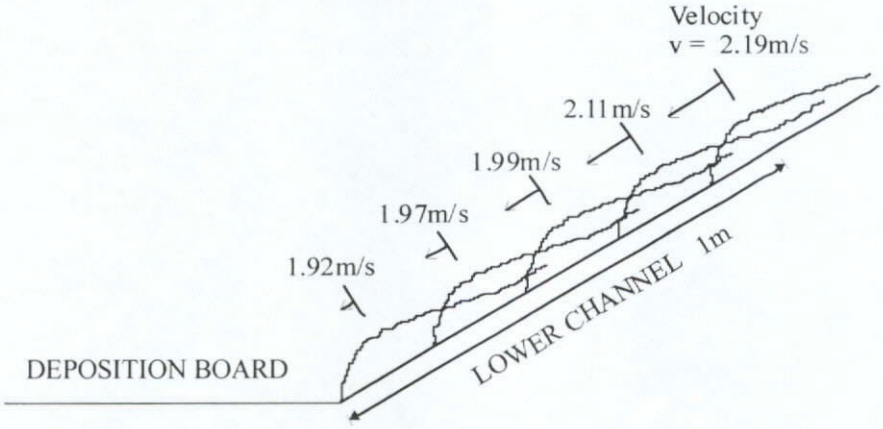

Figure 4.7 Schematic representation of a debris flow surge.
Note: vertical scale is exaggerated.

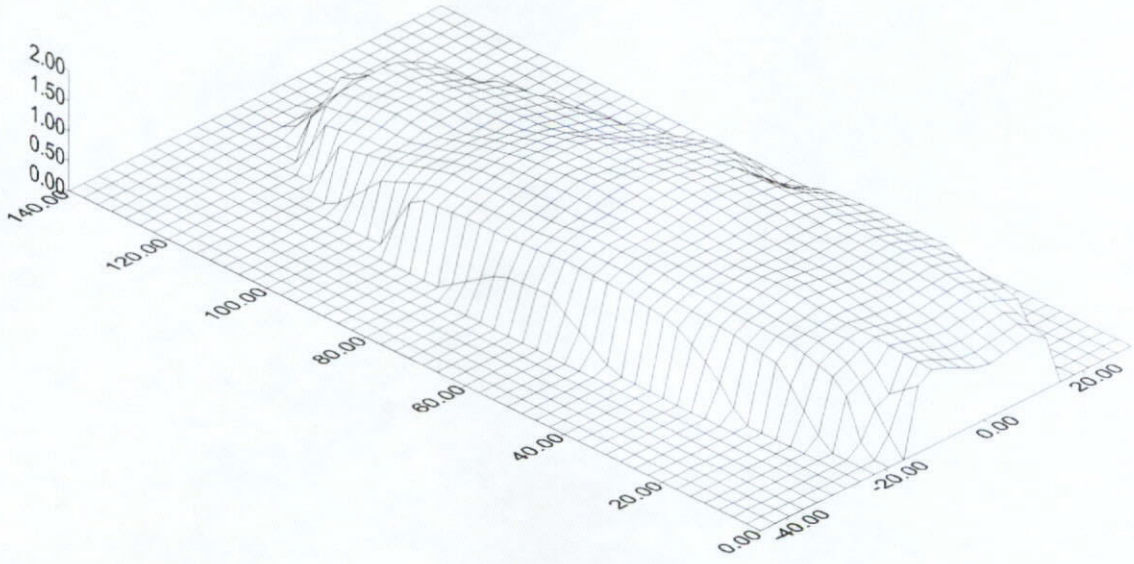

Figure 4.8 A three dimensional view of the debris fan (experiment A19)

4.7 Prototype Results by Dimensionless Analysis

As shown in Table 4.2, the three constitutive scaling parameters and the four geometric scaling factors of the corresponding prototype are comparable with those of the Tsing Shan Debris Flow. Therefore, the present design should yield meaningful results that can be used to study debris flow of a size comparable to the Tsing Shan event. In additional to providing insight on the debris flow mechanism under various conditions, the experimental results can also be used to assess the validity of various theoretical models. This will be considered in Chapter 5.

Parameters / Dimensionless numbers	Parameters of Modeling (flume)	Corresponding Parameters of prototype (flume)	Parameters of TheTsing Shan Debris Flow
L = Flume Length (m)	3	330	330
W = Flume Width (m)	0.2	20	20
H = Flow Depth (m)	0.02 - 0.04	2.2-4.4	3 - 5
Q = Flow Rate (m^3/s)	$6.50x10^{-3}$ - $1.53x10^{-2}$	825 - 1945	838.58
V = Velocity (m/s)	0.88 - 2.19	9.18 - 22.97	12.5
T = Shear Strength (N/m^2)	10.99 - 45.02	1263 - 4947	4171
μ = Viscosity (Ns/m^2)	1.53 - 1.80	1849 - 2072	1877
γ' = Shear Strain Rate (s^{-1})	21.88 - 81.25	2.09 - 10.44	2.50 - 4.17
υ = mean volume fraction of granular phase	0.6	0.6	0.56
λ = Linear Grain Concentration	9.67 - 10.03	10	10
δ = Typical Grain Diameter (I.e. d_{50}, mm)	1.35 - 1.90	200	200
ρ = Density of Reconstituted Debris (kg/m^3)	1796 - 1879	1877	1877
B = Bagnold Number	0.1239 - 1.1384	0.23902 – 1.34081	0.3163 - 0.5271
S = Savage Number	$3.70x10^{-3}$ - $2.02x10^{-1}$	$6.72x10^{-3}$ – $3.37x10^{-1}$	$9.10x10^{-3}$ - $4.21x10^{-2}$
F = Friction Number	1.4475 - 13.1896	1.12369 – 12.607	3.9551 - 10.9864

Table 4.2 Comparison of parameters of experimental model with that of the Tsing Shan Debris Flow

Chapter 5 Numerical Simulations and Comparison

5.1 Selection of Mathematical Models for Comparison

As suggested by Ayotte and Hungr (1998) in a study on the debris flows of Hong Kong, the Voellmy model is the most capable for predicting the observed runout of debris flows in Hong Kong. In Figure 5.1, the runout predictions by the dispersive model (Takahashi and Yoshida, 1979), the constant friction slope model (Hungr et al., 1984), the sled model (Heim, 1932), and the DAN model (Hungr, 1995) were plotted against experimental observations. The parameters used for these models are based upon the experimental measurements and those used by Ayotte and Hungr (1998). All input values used for the above models are tabulated in detail in Table 5.1 and their selections are explained in the following paragraphs.

According to Bagnold's experiment (Bagnold, 1954), the kinematic friction factor $\tan\alpha$ is taken as 0.75 when the Bagnold number B < 40. Because the Bagnold number of the experiments (see Table 4.2) is less than 40, the kinematic friction factor is taken as 0.75 for the dispersive model. The density of interstitial fluid is taken as the same as the density of water 1000 kg/m^3. The density of soil particle is taken as 2620 kg/m^3 (King, 1996a). The active earth pressure coefficient of soil is assumed to be 0.3. The surge velocity is measured at the middle of the lower channel (i.e. 0.5m from the mouth of the lower flume). The debris layer thickness is taken as the

maximum depth of the flowing mass or the surge height at the lower channel. All these parameters are used for the dispersive model in equation (50). Similarly, the parameters above are also adopted for the constant friction slope model in equation (58) whereas the friction slope S_f is assumed to be $\tan 10^\circ$ (Hungr et al.,1984).

The parameters for the sled model in equation (10) are the same as those given above. The apparent friction angle ϕ used in the sled model was measured in each experiment as gradient of the energy line connecting the centers of gravity of the initial debris mass and the deposited debris mass.

As shown in Figure 5.1, the prediction by the DAN program appears to be superior to other models, whereas most of these models underestimate the runout distance except the for constant friction slope model.

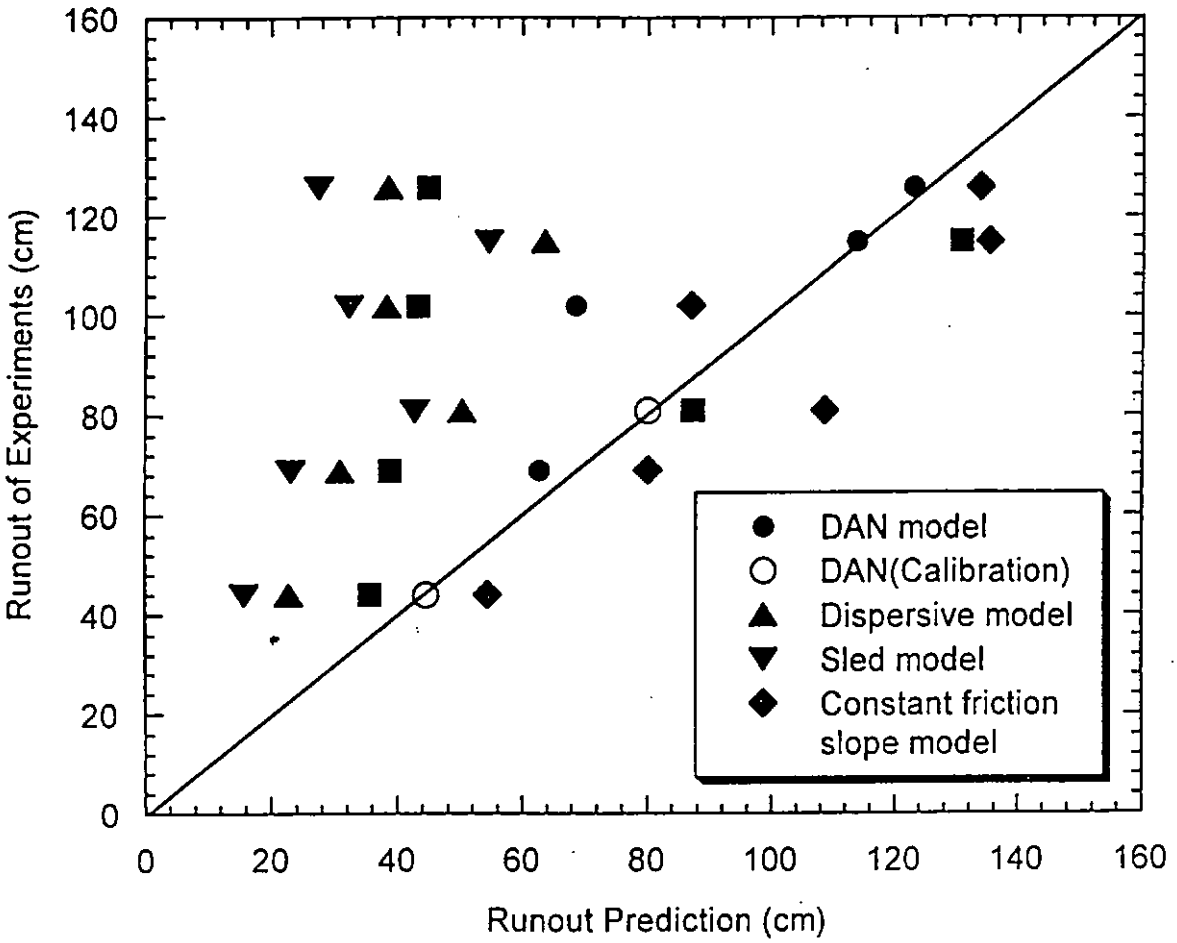

Figure 5.1 Comparison of runout predicted by the DAN model, the dispersive model, the sled model and the constant friction slope mode with the experimental observations. The open circles are data for calibrating the Voellmy model in DAN.

Input values for runout prediction of various models						
Input values \ Experiment number	Dispersive model (Takahashi and Yoshida, 1979)					
	A11	A12	A13	A21	A15	A22
Gradient of channel (degree), α	38	32	26	26	26	26
Gradient of deposition board (degree), β	0	0	0	2	5	0
Upstream velocity (m/s), u_u	1.90	1.55	0.88	1.00	1.00	1.20
Maximum flow depth (m), h_u	0.020	0.025	0.040	0.035	0.035	0.045
Volume concentration of solid phase, c_u	0.6	0.6	0.6	0.6	0.6	0.6
Density of interstitial fluid (kg/m^3), ρ	1000	1000	1000	1000	1000	1000
Active pressure coefficient, k_a	0.3	0.3	0.3	0.3	0.3	0.3
Density of particle (kg/m^3), σ	2620	2620	2620	2620	2620	2620
Kinematic friction factor, $\tan\alpha$	0.75	0.75	0.75	0.75	0.75	0.75
Gravitational acceleration (m/s^2), g	9.81	9.81	9.81	9.81	9.81	9.81
Input values \ Experiment number	Constant friction slope model (Hungr et al.,1984)					
	A11	A12	A13	A21	A15	A22
Friction slope, S_f	0.1763	0.1763	0.1763	0.1763	0.1763	0.1763
Input values \ Experiment number	Sled model (Heim, 1932)					
	A11	A12	A13	A21	A15	A22
Apparent friction angle (degree), ϕ	34.04	29.83	26.60	25.50	24.82	24.50

Table 5.1 Input values for various models

5.2 Calibration of the Voellmy Model in DAN Program

In this section, adoption of the program DAN to simulate the experimental modelling of debris flows is discussed. Instead of directly adopting the constitutive parameters used in the study of debris flows in Hong Kong (Ayotte and Hungr, 1998), an independent calibration using the experimental data for material m1 (experiments A12 and A13) through back analyses has been done. As expected in the experiment, the basal resistance of the flume surface is larger than that of the deposition board. Different combinations of the model parameters (the turbulence coefficient K and the friction coefficient F) are assumed for the flume surface (Region II) and the surface of deposition board (Region III) then (see Figure 5.2 and Figure 5.3). As a first input, we adopted the typical model parameters (K_I = 300 m/s^2, F_I = 0.3) used in Ayotte and Hungr (1998) for the initial slide mass (Region I), where the subscript of the model parameters represents the region name in the model. The lateral pressure coefficients (k_a and k_p) and coefficient at rest k_o are taken as 0.8, 2.5 and 1 respectively. These coefficients were adopted from the back analysis of twenty debris flows in Hong Kong (Ayotte and Hungr, 1998). Details of the input data for the DAN program are shown in Figures 5.2 and 5.3.

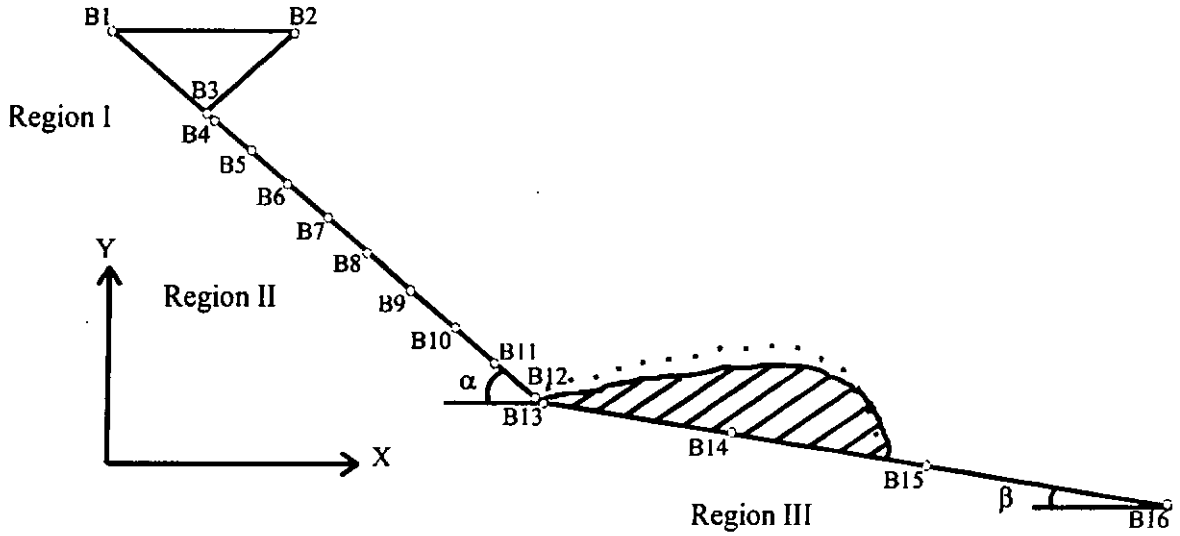

	Input Data for DAN program					
	$\alpha = 26^\circ$ $\beta = 0^\circ$		$\alpha = 26^\circ$ $\beta = 2^\circ$		$\alpha = 26^\circ$ $\beta = 5^\circ$	
	X-coord.	Y-coord.	X-coord.	Y-coord.	X-coord.	Y-coord.
B1	-28.3	182.8	-28.3	182.8	-28.3	182.8
B2	19.3	182.8	19.3	182.8	19.3	182.8
B3	0.0	159.0	0.0	159.0	0.0	159.0
B4	4.0	157.0	4.0	157.0	4.0	157.0
B5	23.0	147.7	23.0	147.7	23.0	147.7
B6	48.0	135.4	48.0	135.4	48.0	135.4
B7	67.5	125.8	67.5	125.8	67.5	125.8
B8	85.0	117.2	85.0	117.2	85.0	117.2
B9	135.0	92.5	135.0	92.5	135.0	92.5
B10	202.5	59.2	202.5	59.2	202.5	59.2
B11	232.5	44.6	232.5	44.6	232.5	44.6
B12	265.0	26.5	265.0	26.5	265.0	26.5
B13	270.0	26.0	270.0	26.0	270.0	26.0
B14	360.0	26.0	360.0	22.86	360.0	18.13
B15	440.0	26.0	440.0	20.06	440.0	11.13
B16	560.0	26.0	560.0	15.87	560.0	0.63

Figure 5.2 Input data for DAN program
(Region I, B1 – B3; Region II, B4 – B12; Region III, B13 – B16)

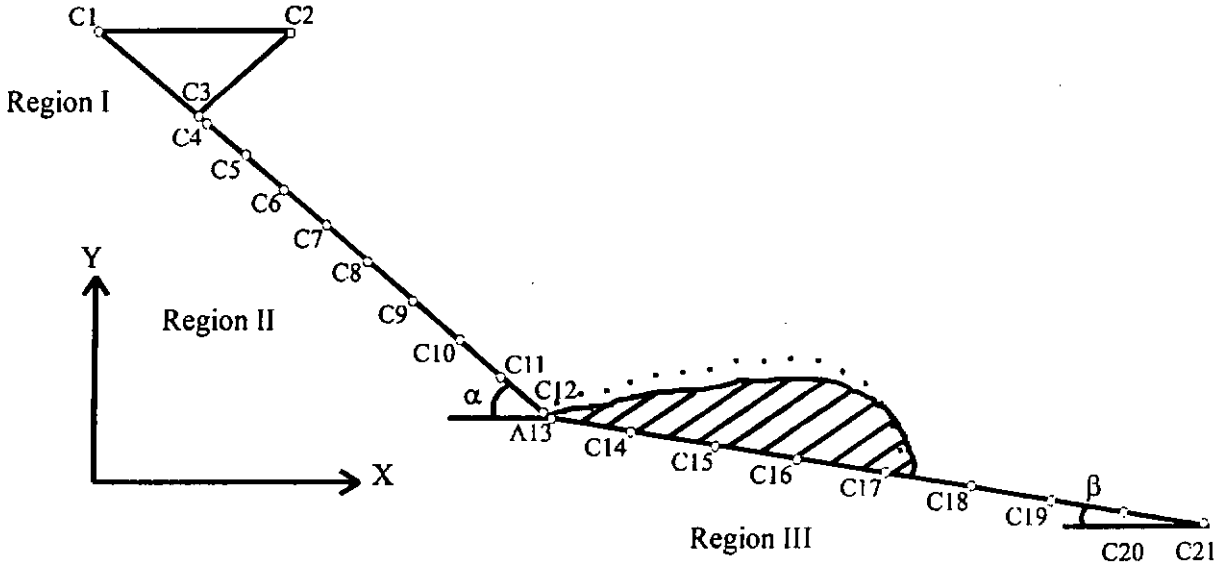

	Input Data for DAN program			
	$\alpha = 32^\circ \quad \beta = 0^\circ$		$\alpha = 38^\circ \quad \beta = 0^\circ$	
	X-coord.	Y-coord.	X-coord.	Y-coord.
C1	-28.3	182.8	-28.3	182.8
C2	19.3	182.0	19.3	182.8
C3	0.0	159.0	0.0	159.0
C4	8.0	156.0	7.88	152.84
C5	36.5	137.65	31.52	134.37
C6	65.0	119.3	63.04	109.74
C7	97.5	99.4	94.56	85.11
C8	130.0	79.5	126.08	60.48
C9	162.5	59.65	157.60	35.85
C10	195.0	39.8	189.12	11.22
C11	224.7	19.91	220.64	-13.41
C12	254.4	0.01	228.52	-19.57
C13	260.0	0	236.60	-25.73
C14	250.0	0	250.0	-25.73
C15	260.0	0	260.0	-25.73
C16	270.0	0	270.0	-25.73
C17	280.0	0	280.0	-25.73
C18	320.0	0	320.0	-25.73
C19	400.0	0	400.0	-25.73
C20	480.0	0	480.0	-25.73
C21	560.0	0	560.0	-25.73

Figure 5.3 Input data for DAN program
(Region I, C1 – C3; Region II, C4 – C12; Region III, C13 – C21)

A number of combinations of the model parameters (the turbulence coefficient K and the friction coefficient F) were found to be capable of matching the observed runout distance of 44 cm observed in the experiment A13 (see Figure 5.4). In order to select the most probable pair of parameters, the predictions by each probable pair with those observed in another experiment A12 were examined. The results obtained by using the best-fitted parameters of the Voellmy model compare extremely well with experiments as shown in Figure 5.1. That is the two parameters K and F that can be found by two observations made in experiments A12 and A13. The friction coefficients and turbulence coefficients used in Figure 5.1 for the path of flume and deposition board are 0.506 and 900m/s^2, and 0.1 and 700m/s^2 respectively. It should be noted that because the channel width abruptly widens at the mouth of the lower channel, the width input for the deposition board (Region III) is assumed as the maximum width of the debris fan observed in experimental simulations. All these parameters are comparable to those calibrated by Hungr (1995) for field events.

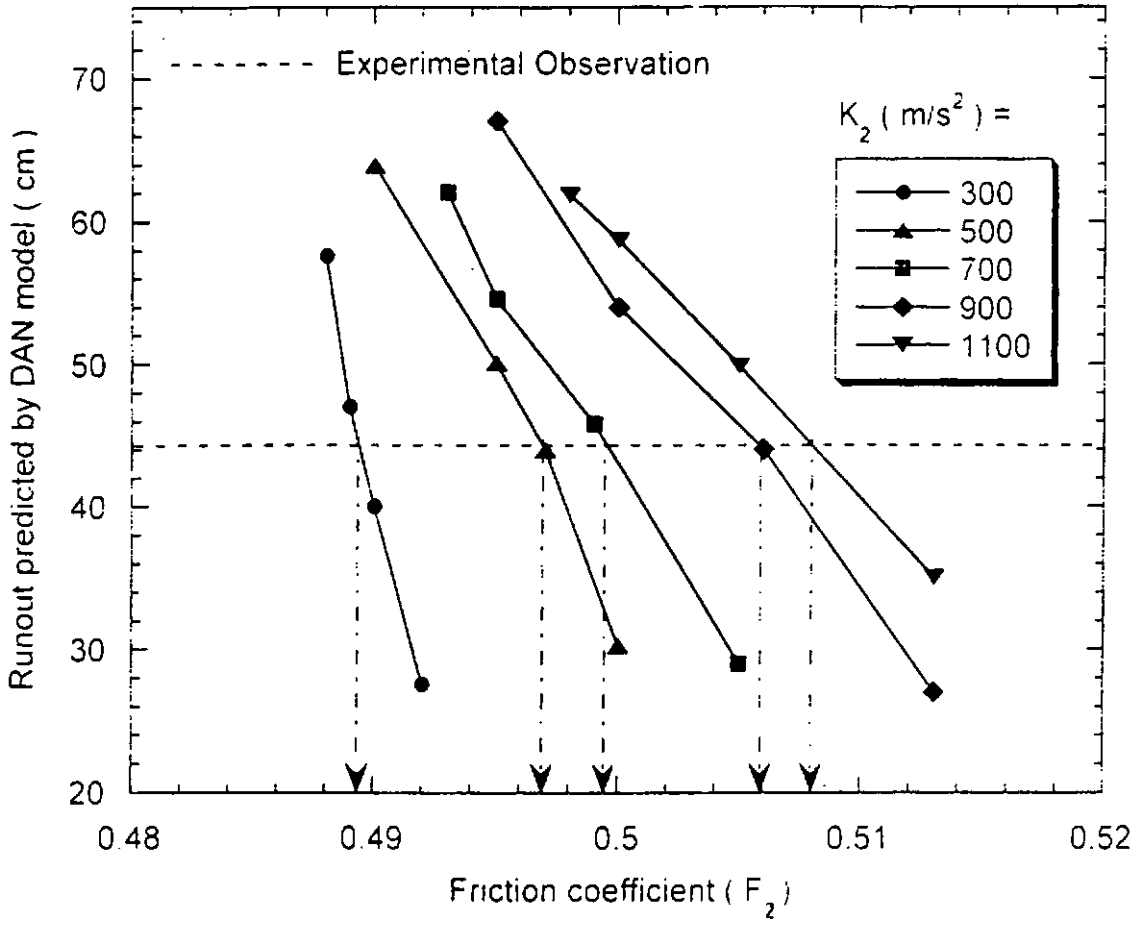

Note : (1) K is the turbulence coefficient
(2) F_3 = 0.1 and K_3 = 700

Figure 5.4 Calibration of the friction and turbulence coefficients of material m1 using the runout of experiment A13

5.3 Deposition Depth Profiles

In addition to the maximum runout, valuable data can be obtained by examining the prediction of the deposition fan thickness along the distance measured from the toe of the flume. Figures 5.5 and 5.6 plot the experimental observations (in dotted lines) with the theoretical prediction by the DAN model (in solid line) for the variation of flume slope (from 26° to 38°) and of deposition board slope (from 0° to 5°). The experimental observations shown in Figures 5.5 and 5.6 are obtained along the centrelines of the deposition fans; whereas those predictions by the DAN model are only two-dimensional equivalent predictions because the DAN model is not truly a three-dimensional model. Nevertheless, the longitudinal profile of the deposition fan can be predicted better for the case of deposition board slope $\beta = 0°$ than that for $\beta = 5°$.

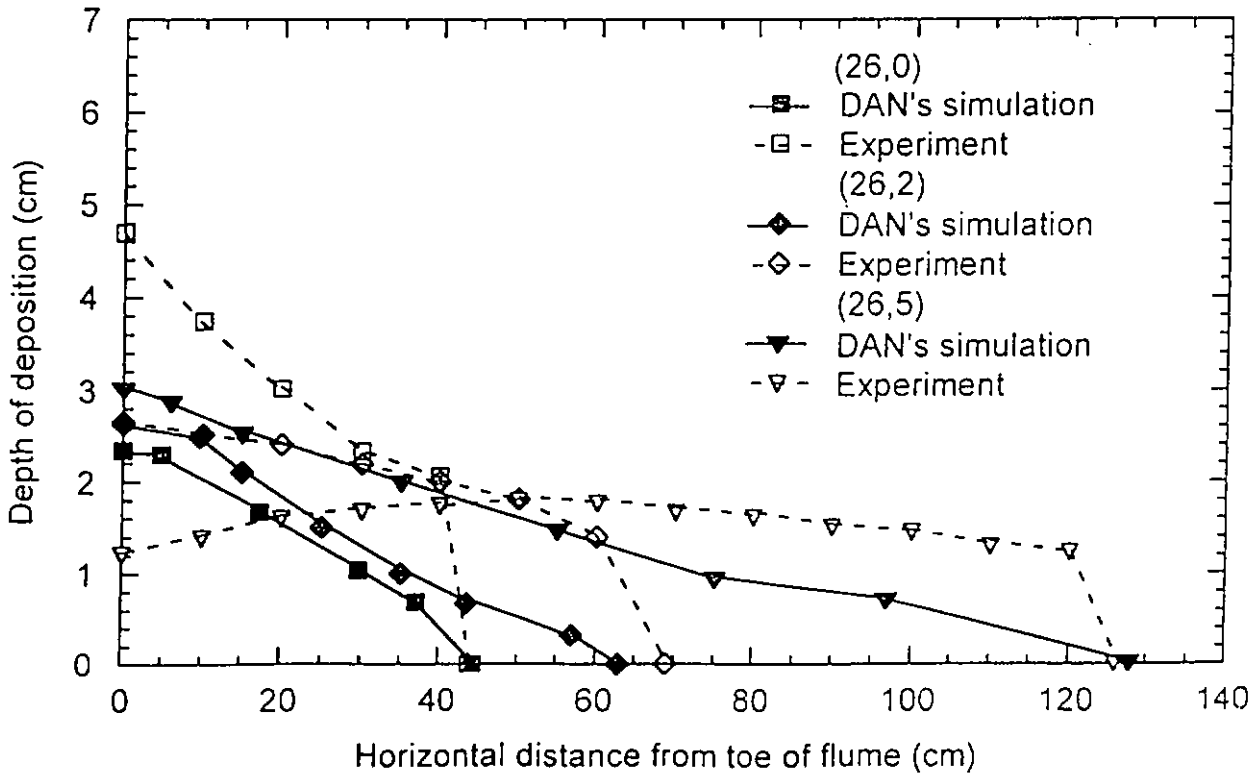

Figure 5.5 A comparison of the deposition fan depth of material m1 predicted by DAN model and that observed in experiments with different deposition board slope ($F_2 = 0.506$, $K_2 = 900$ m/s^2; $F_3 = 0.1$, $K_3 = 700$ m/s^2)

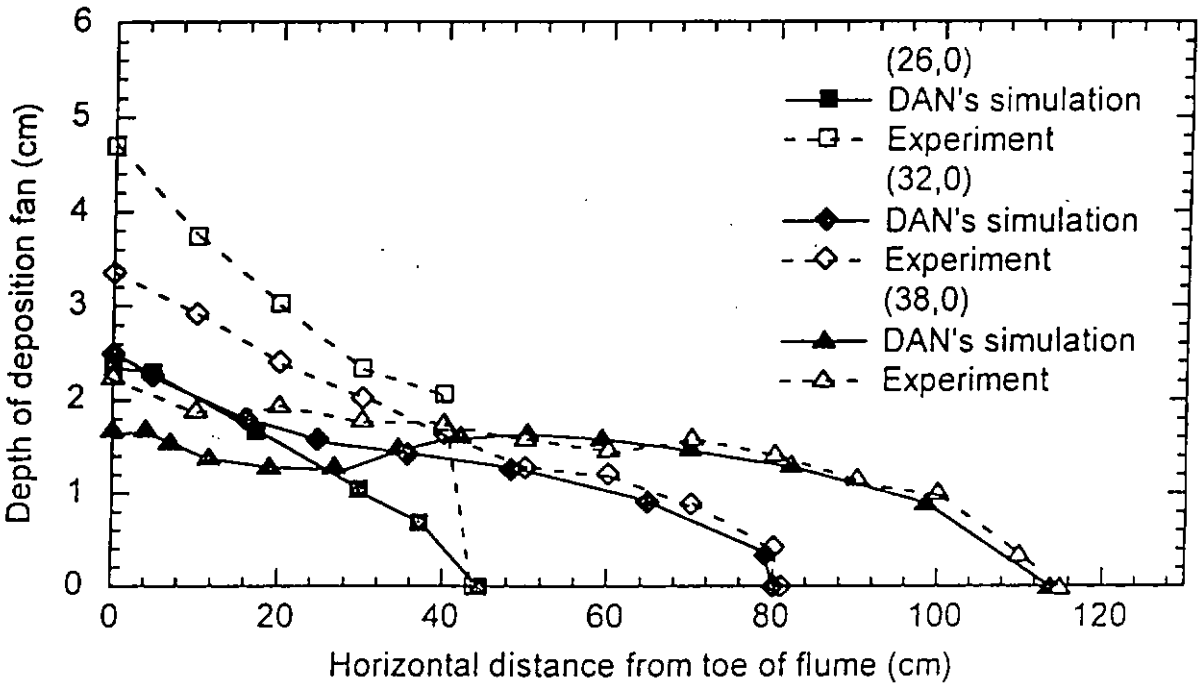

Figure 5.6 A comparison of deposition fan depth of material m1 predicted by DAN model and that observed in experiments with different flume slope
(F_2 = 0.506, K_2 = 900 m/s^2; F_3 = 0.1, K_3 = 700 m/s^2)

5.4 Discussion and Concluding Remarks

A comparison of the applicability of models for the runout prediction of debris flow is made. Apart from the DAN and the constant friction slope model, most of the other models underestimate the runout distance of debris flows. However, the DAN model can closely predict the runout distance of debris flow except for the result of experiment A22. This discrepancy may be due to the increase of initial volume of debris material. As a result, it is concluded that the Voellmy model of the DAN program is capable of predicting the maximum runout distance of debris flow in the laboratory if the model parameters are properly calibrated against the experimental observations. This model can provide a good and reasonable prediction to the runout

distance of debris flow provided that the maximum width of deposited material can be estimated in a ravine. However, the prediction for the longitudinal profile of debris fan by the DAN model needs to be further refined.

Chapter 6 Conclusions

A dimensionless analysis has been used for the design of a debris flow flume is proposed. The designed flume is used to model the real scale debris flows by ensuring the equivalence of the three constitutive scaling parameters (Bagnold number, Savage number and friction number) and the four geometric scaling factors (velocity factor, flow factor, yield stress factor and viscosity factor) between the model tests and real events. The first three parameters reflect the relative importance of the dispersive, friction and viscous forces at the microscopic level, while the latter four factors ensure that the same macroscopic governing equations are applicable to both the model and prototype. It has been shown that the corresponding parameters of the prototype are comparable to those of the Tsing Shan Debris Flow. Thus, the experiments should be capable of simulating debris flow mechanisms of scales comparable to those of the Tsing Shan Debris Flow. This flume design is able to scale up the experimental simulations and to yield debris flow phenomena that are similar to the real debris flows. More specifically, the debris flow runout was reported as functions of the flume slope, deposition board slope, granular content and flume cross section. In addition, the experimental observations are compared with the dispersive model (Takahashi and Yoshida, 1979), the constant friction slope model (Hungr et al., 1984), the sled model (Heim, 1932), and the DAN model (Hungr, 1995).

As expected intuitively, the runout distance increased with the flume slope. For material m1 (50% sand and 50% gravel), when the flume slope increased from 26° to 32°, the runout distance increased by 84%; while it increased by only 42% when the flume slope increased from 32° to 38°. This is because the debris runout distance depends nonlinearly on the flume slope. It is also interesting to note that the lateral spread of debris fan on a flat deposition ground was larger than the longitudinal runout for a flume angle at 26° (forming a semi-elliptic deposition fan). While the lateral spreads of debris fan on a flat deposition board were smaller than the longitudinal runouts for flume angle at 32° and 38° (forming a pear-shape deposition fan).

It is observed that when the deposition board slope increased from 0° to 2° the runout of debris flow for material m1 can increase by 57 % from 44 cm to 69 cm for a rectangular cross-section of flume. While a further 3° increase to the deposition board slope (i.e. deposition board slope is 5°) can lead to 83 % increase in the runout distance. As a result, it is concluded that the runout distance of debris flow tends to increase at a faster rate when the deposition board slope increases. As expected, a gentler deposition ground slope will lead to a shorter runout distance.

For experiment with flume slope at 26° and deposition board slope at 0°, the runout distance for material with richer sand content (20% gravel and 80% sand) was 31% longer than that for material with richer gravel content (50% gravel and 50% sand). While the runout distances for materials with similar gravel content were comparable. Thus, it is concluded that empirical data fitting of runout distance to slope angle irrespective to local soil conditions is not appropriate.

In general, the runout distance of debris flow on a flat deposition ground may increase by 100% when the cross-section changed from rectangular to triangular. However, this increment can be as little as 20% if other debris material was used. Therefore, the granular content of debris flow must be considered for the runout prediction and thus a detailed site investigation is needed if a reliable design of a catchment basin is desirable.

Simple analytical formulas of the dispersive model, the constant friction slope model, the sled model, and the numerical program DAN developed by Hungr (1995) were used to yield runout predictions for comparison with the experimental results. The dispersive model, the constant friction slope model and the sled model are unable to fit the data adequately. Whereas the prediction by the DAN model is found to be comparable if the Voellmy constitutive model was used. As suggested by Ayotte and Hungr (1998) in a study on the debris flows of Hong Kong, the Voellmy model of DAN program is capable of predicting the observed runout of debris flows in Hong Kong. Thus, it is plausible that our experimental observations are indeed comparable to the real phenomena of debris flows because both can be modelled adequately by the Voellmy model of DAN program. However, more studies are needed for verification.

Chapter 7 Further Work and Recommendations

Some recommendations on the experimental simulations of debris flows with regard to superelevation of curved channel, impact pressure of debris flow, and vertical run-up distance can be made for further study.

As most natural debris flows move on curved paths, the curvature of channel and bed morphology plays an important role in the flowing mechanism. In addition, studies on superelevation of debris flow in channel bends can provide information both for the barrier design at the outside of the channel bends and for the estimation of velocity of past events. Thus, both the effect of course meandering and bed morphology on the runout distance needs to be examined experimentally.

In general, barriers are commonly used for alleviating hazards induced by debris flows. The barrier design needs a thorough understanding of the impact pressure of debris flow as a function of velocity and discharge. However, field data are rarely measured in the field and are usually obtained by back-calculation. Thus, in general, the design of barriers is primarily done empirically or analytically. An alternative is to study impact pressure of debris flow by experimental simulation, provided there is appropriate scaling in the experimental design.

However, on some occasions debris flows deposit materials in front of the barrier at which subsequent debris flow could climb up against the maximum barrier height. Whether analytical prediction of run-up distance is applicable to the run-up in actual events is questionable (Lo and Ho, 1998). Again, an alternative to study the run-up distance against barrier is by experiments.

The above recommendations offer further directions for experimental studies.

References:

Ayotte, D. and Hungr, O. (1998). *Runout Analysis of Debris Flows and Debris Avanlanches in Hong Kong.* A Report for the Geotechnical Engineering Office, Hong Kong. University of British Columbia, Canada.

Bagnold, R.A. (1954) Experiments on a Gravity-Free Dispersion of Large Solid Spheres in a Newtonian Fluid under Shear. *Proceedings of the Royal Society of London*, A, Vol. 225, pp.49-63.

Benda, L.E. and Cundy, T.W. (1990). Predicting Deposition of Debris Flow in Mountain Channels. *Canadian Geotechnical Journal*, Vol.27, pp.409-417.

B.S. 1377 (1990). *British Standard Methods of Test for Soils for Civil Engineering Purposes (part 2), Classification Tests*, British Standards Institution.

B.S. 1377 (1990). *British Standard Methods of Test for Soils for Civil Engineering Purposes (part 4), Compaction-Related Tests*, British Standards Institution.

Campbell, R.H. (1974). Debris Flows Originating From Soil Slips During Rainstorms in Southern California. *Quarterly Journal of Engineering Geology*, Vol.7, pp339-349.

Cannon, S.H. (1989). An Evaluation of the Travel-Distance Potential of Debris Flows. *Utah Geological and Mineral Survey Miscellaneous Publication*, Vol.89, No.2, pp1-35.

Cannon, S.H. (1993). An Empirical Model for the Volume-Change Behaviour of Debris Flow. *Proceedings of ASCE National Conference on Hydraulic Engineering*, San Francisco, California, July 25-30, pp.1768-1773.

Cannon, S.H. and Savage, W.Z. (1988). A Mass-Change Model for the Estimation of Debris- Flow Runout. *Journal of Geology*, Vol.96, No.2, pp221-227.

Chen, C.L. (1987). Comprehensive Review of Debris Flow Modelling Concepts in Japan, Geological Society of America, *Reviews in Engineering Geology*, Vol.7, pp.13-29.

Chen, C.L. (1988). General Solutions for Viscoplastic Debris Flow. *Journal of Hydraulic Engineering*, Vol.114, No.3, pp.259-282.

Chen, H. and Lee, C.F. (1998). Debris Flow Modelling With Three-Dimensional Lagrangian Finite Elements. *Proceedings of the One Day Seminar on Planning, Design and Implementation of Debris Flow and Rockfall Hazards Mitigation Measures*, The Association of Geotechnical Specialists (HK) Limited and The

Hong Kong Institution of Engineers (Geotechnical Division), October 27, Hong Kong, pp.29-45.

Chen, K.Q., Wang, Q.K. and Wang, L.H. (1983) *Debris Flow Prevention.* Chinese Railway Publish. Co., Beijing, China (in Chinese)

Corominas, J. (1996). The Angle of Reach as a Mobility Index for Small and Large Landslides. *Canadian Geotechncial Journal*, Vol.33, pp.260-271.

Day, R.W. (1994). Case Study of Debris Flow. *Journal of Performance of Constructed Facilities*, Vol.8, No.3, pp192-200.

DeGraff, J.V. (1994). The Geomorphology of Some Debris Flows in the Southern Sierra Nevada, California. *Geomorphology*, Vol.10, pp231-252.

Erlichson, H. (1991). A Mass Change Model for the Estimation of Debris Flow Runout: A Second Discussion: Conditions for the Application of the Rocket Equation. *Journal of Geology*, Vol.99, pp.633-634.

Fei, X. and Yang, M. (1985). The Physical Properties of Flow with Hyperconcentration of Sediment. *Proceedings of International Workshop on Flow at Hyperconcentrations of Sediment*, IRTCES, Beijing, China, Paper I2, pp.1-22.

Garcia, J.A. and Savage, S.B. (1993). Kinetic-Theory Approach to the Nevado del Ruiz 1985 debris flow. *Hydraulic Engineering'93.* Vol.2, pp.1408 -1413, ASCE, New York.

Heim, A. (1932). Bergsturz und Menschenleben. Naturforsch. Gesell. Zurich, *Vierteljahrsschr*, 77(20), 218pp.

Hsu, K.J. (1975). Catastrophic Debris Streams (sturzstroms). *Geological Society of America Bulletin,* Vol.86, pp.129-140.

Hua, G. (1989). Classifications of Bingham Debris Flow and Similarity Rules. *In Collected Papers of the 2nd National Conference on Debris Flow,* pp.1-9, Science Press, Beijing (in Chinese).

Hungr, O. (1990a). Momentum Transfer and Friction in the Debris of Rock Avalanches: Discussion. *Canadian Geotechnical Journal*, Vol.27, pp.697.

Hungr, O. (1990b). A Mass Change Model for the Estimation of Debris Flow Runout: A Discussion. *Journal of Geology*, Vol.98, pp.791.

Hungr, O. (1995). A Model for the Runout Analysis of Rapid Flow Slide, Debris Flows, and Avalanches. *Canadian Geotechnical Journal*, Vol.32, pp.610-623.

Hungr, O., Morgan, G.C and Kellerhals, R. (1984). Quantitative Analysis of Debris Torrent Hazards for Design of Remedial Measures. *Canadian Geotechnical Journal*, Vol.21, pp.663-677.

Hutchinson, J.N. (1986). A Sliding-Consolidation Model for Flow Slides. *Canadian Geotechncial Journal*, Vol.23, pp.115-126.

IGGAS (1982). Debris flow in GanSu Province. *Institute of Glaciology and Geocryology Academia Sincia (IGGAS)*. (in Chinese)

Iverson, R.M. (1997). The Physics of Debris Flow. *Review in Geophysics*, Vol. 35, pp.245-296.

Iverson, R.M., Costa, J.E. and LaHusen, R.G. (1992). Debris-Flow Flume at H.J. Andrews Experimental Forest. Oregon. *U.S. Geological Survey, Open-File Report* 92-483.

Iverson, R.M. and Denlinger, R.P. (1987). The Physics of Debris Flows – a Conceptual Assessment. Erosion and Sedimentation in the Pacific Rim. *Proceeding of International Symposium*, pp.155-165.

Iverson, R.M. and LaHusen, R.G. (1993). Friction in Debris Flows: Inferences from Large-Scale Flume Experiments. *Hydraulic Engineering'93*. Vol. 2, pp. 1604-1609, ASCE, New York.

Jan, C.D. (1997). A Study on the Numerical Modelling of Debris Flows. *Proceeding of the 1st International Conference on Debris-Flow Hazards Mitigation: Mechanics, Prediction and Assessment*, ASCE, pp.717-726.

Johnson, A.M. (1965). A Model for Debris Flow, Pennsylvania State University, *PhD. Dissertation*, State College, Pennsylvania.

Johnson, A.M. and Rodine, J.R. (1984). *Debris flow. In Slope Instability* (ed. D. Brunsden and D.B. Prior), Wiley, New York.

Johnson, R.W. (1998). The Handbook of Fluid Dynamics. CRC Press. Boca Raton.

Kang, Z. (1997) Kinetic Analysis on the Deceleration and Deposition Processes of Viscous Debris Flows. *Proceeding of the 1st International Conference on Debris-Flow Hazards Mitigation: Mechanics, Prediction, and Assessment.* ASCE, pp.153-157.

King, J.P. (1996a). *The Tsing Shan Debris Flow.* Vol. 1-3, *GEO Special Project Report*, SPR 6/96, GEO. Hong Kong

King, J.P. (1996b). Tsing Shan Debris Flood of June 1992. *GEO Special Project Report*, SPR 7/96, GEO.

Laigle, D. (1997). A Two-Dimensional Model for the Study of Debris Flow Spreading on a Torrent Debris Fan. *Proceeding of the 1st International Conference on Debris-Flow Hazards Mitigation: Mechanics, Prediction, and Assessment*. ASCE , New York, pp.123-132.

Lambe, W. and Whitman, R. (1979). *Soil Mechanics*, S.I. version, John Wiley & Sons.

Lau, K.C. and Woods, N.W. (1997). Review of Methods for Predicting the Travel Distance of Debris from Landslides on Natural Terrain. *Technical Note TN 7/97*, Planning Division, Geotechnical Engineering Office, Hong Kong.

Liu, X. (1996). Size of a Debris Flow Deposition: Model Experiment Approach. *Environmental Geology*, Vol.28, pp.70-77.

Lo, D.O.K and Ho, K.K.S. (1998). Some Salient Aspects of the Design of Barriers for Natural Terrain Landslides. *Proceeding of 1-Day Seminar on Planning, Design and Implementation of Debris Flow and Rockfall Hazards Mitigation Measures.* The Association of Geotechnical Specialists (Hong Kong) Limited and The Hong Kong Institution of Engineers (Geotechnical Division), pp.141-175.

Mainali, A. and Rajaratnam, N. (1994). Experimental Study of Debris Flows. *Journal of Hydraulic Engineering*, Vol.120, No.1, pp.104-123.

Major, J.J. (1997). Depositional Processes in Large-Scale Debris Flow Experiments. *Journal of Geology*, Vol.105, pp.345-366.

Middelton, G.V. and Hampton, M.A.(1976). Subaqueous Sediment Transport and Deposition by Sediment Gravity Flows. *Marine Sediment Transport and Environmental Management*, New York, (Edited by D.J. Stanley and D.J.P.Swift). pp197-218.

Mizuyama, T. and Uehara, S. (1983) Experimental Study of the Depositional Process of Debris Flows. *Transaction, Japanese Geomorphological Union*, Vol.4, No.1, pp.49-64.

Moore, D.P. and Mathews, W.H. (1978). The Rubble Creek Landslide, Southwestern British Columbia. *Canadian Journal of Earth Science*, Vol.15, pp.1039-1053.

O'Brien, J.S., Julien, P.Y., and Fullerton, W.T. (1993). Two-Dimensional Water Flood and Mudflow Simulation. *Journal of the Hydraulics Division*, ASCE, Vol.119 (HY2), pp.244-261.

Okuda, S., Suwa, H., Okunishi, K., Yokoyama, K. and Ogawa, K. (1981). *Synthetic Observation on Debris Flow*, Part 7, *Annual Disaster Preventive Research Institution of Kyoto University*, No. 24B-1, 411-488 (in Japanese).

Phien-Wei, N., Nutalaya, P., Zin, A. and Tang, Z.B. (1993). Catastrophic Landslides and Debris Flows in Thailand. *Bulletin, International Association of Engineering Geology*, Vol.48, no.10, pp.93-100.

Pierson, T.C. (1995). Flow Characteristics of Large Eruption-Triggered Debris Flows at Snow-Clad Volcanoes: Constraints for Debris Flow Models. *Journal of Volcanology Geothermal Research,* Vol.66, pp.283-294.

Sassa, K. (1984). The Mechanism Starting Liquefied Landslides and Debris Flows. *Proceedings of 4th ISL*, Toronto.Vol.2, pp.349-354.

Sassa, K. (1988). Special Lecture: Geotechnical Model for the Motion of Landslides. *Proceedings of the 5th International Symposium on Landslides*, pp.37-55.

Sassa, K. (1996). Prediction of Earthquake Induced Landslides. *Proceedings of the Seventh International Symposium on Landslides*, Trondheim, pp.115-132.

Sassa, K., Kaibori, M. and Kitera, N. (1985). Liquefaction and Undrained Shear of Torrent Deposits as the Cause of Debris Flows. *Proceedings of International Symposium on Erosion*, Debris Flows and Disaster Prevention, Tsukuba, pp.231-236.

Savage, S.B. (1984). The Mechanics of Rapid Granular Flows, *Advanced Applied Mechanic*, Vol.24, pp.289-366.

Savage, S.B. and Hutter, K. (1989). The Motion of a Finite Mass of Granular Material Down a Rough Incline, *Journal of Fluid Mechanic*, Vol.199, pp.177-215.

Savage, S.B. amd Hutter, K. (1991). The Dynamics of Avalanches of Granular Materials from Initiation to Runout. Part 1: Analysis, *Acta Mechanica*, Vol.86, pp.201-223.

Scheidegger, A.E. (1973). On the Prediction of the Reach & Velocity of Catastrophic Landslides. *Rock Mechanics*, Vol.5, pp231-236.

Shen, S. and Xie, S. (1985). Structure Mode and Rheologic Property of Mud Debris Flow. *Proceedings of International Workshop on Flow at Hyperconcentrations of Sediment*, IRTCES, Beijing, China, Paper IV4, pp.1-15.

Shieh, C.L. and Tsai, Y.F. (1997). Experimental Studies on the Configuration of Debris-flow Fan. *Proceeding of the 1st International Conference on Debris-Flow Hazards Mitigation: Mechanics, Prediction, and Assessment.* ASCE, pp.133-142.

Shreve, R.L. (1968). The Blackhawk Landslide. *Geological Society of America*, Special paper 108.

Skempton, A.W. (1954) The Pore-Pressure Coefficients A and B. *Geotechnique*, Vol.4, pp.143-147.

Steijin, H.V. and Coutard, J.P. (1989). Laboratory Experiments with Small Debris Flows: Physical Properties Related to Sedimentary Characteristics. *Earth Surface Processes and Landforms*, Vol.14, pp.587-596.

Takahashi, T. (1978). Mechanical Characteristics of Debris Flow. *Journal of the Hydraulics Division*, Vol.104, No.HY8, pp.1153-1169.

Takahashi, T. (1981). Debris Flow. *Annual Review in Fluid Mech*anic, Vol.13, pp.57-77.

Takahashi, T. (1991) *Debris Flow. IAHR-AIRH Monograph Series*, A.A. Balkema, Rotterdam.

Takahashi, T., Nakagawa, H., Harada, T. and Yamashiki, Y. (1992). Routine Debris Flows with Particle Segregation. *Journal of Hydraulic Engineering*, Vol.118, No.11, pp1490-1507.

Takahashi, T and Yoshida, H. (1979). Study on the Deposition of Debris Flows (1) – Deposition Due to Abrupt Change of Bed Slope. *Annuals*, Disaster Prevention (in Japanese)

Turner, A.K. (1996). Landslides, Investigation and Mitigation. *Special Report 247.* Transportation Research Board, National Research Council. pp525-549.

VanGassen, W. and Cruden, D.M. (1989). Momentum Transfer and Friction in the Debris of Rock Avalanches. *Canadian Geotechnical Journal*, Vol.26, pp.623-628.

Voellmy, A. (1955). Uber Die Zerstorungskraft Von Lawinen, *Schweizerische Bauzeitung*, Vol.73, pp.212-285.

Voight, B. (1978). Lower Gros Ventre Slide, Wyoming, U.S.A. *Rockslides and Avalanches*, Elsevier Scientific Publish. Co., New York. pp.113-166.

Wan, Z.H. and Wang, Z.Y. (1994). *Hyperconcentrated Flow.* IAHR-AIRH Monograph Series, A.A. Balkema, Rotterdam.

Wang, Z.Y. (1999). Landslides and Debris Flow. *Proceedings of a 1-Day Workshop on Landslide Slide and Debris Flow*, Department of Civil and Structural Engineering, The Hong Kong Polytechnic University on September 1, 1999.

Wang, G., Shao, S., and Fei, X. (1997). Particle Model for Alluvial Fan Formation. *Proceeding of the 1st International Conference on Debris-Flow Hazards Mitigation: Mechanics, Prediction and Assessment.* ASCE, pp.143-152.

Wong, H.N., Chen, Y.M. and Lam, K.C. (1996). *Factual Report on the November 1993 Natural Terrain Landslides in Three Study Areas on Lantau Island*, (3Volumes), Special Project Report No. SPR 10/96, GEO, Hong Kong.

Wong, H.N. and Ho, K.K.S. (1996). Travel Distance of Landslide Debris. *Proceeding of the Seventh International Symposium on Landslides*, Vol.1, pp.417-422.

Wu, J., Kang, Z., Tian, L. and Zhuang, S. (1990). *Observation and Study of Debris Flow in Jiangjia Gully,* Yunnan. Science Press, Beijing. (in Chinese)

Yano, K. and Daido, A. (1965) Fundamental Study on Mud-Flow. *Bulletin of the Disaster Prevention Research Institute* Vol.14, part 2, February, pp.69-83.

Zhang, S. (1993). A Comprehensive Approach to the Observation and Prevention of Debris Flows in China. *Natural Hazards*, Vol.7, pp.1-23.

Appendix 1
Shear Stress and Shear Strain Rate in the Viscosity Test

The Brookfield DV-II+ viscometer which is capable of measuring viscosity ranging from 15cp to $6x10^6$cp is used. The viscometer can rotate from 0.1 to 200 revolution per minute (RPM). In the viscosity test, the following equations are used to determine the shear stress and shear strain rate in terms of the rotational speed of the viscometer and the rotating torque:

Shear stress: $$\tau = \frac{M}{2\pi R_b^2 L} \quad \text{(B1)}$$

Shear strain rate: $$\dot{\gamma} = \frac{2\varpi R_c^2 R_b^2}{x^2(R_c^2 - R_b^2)} \quad \text{(B2)}$$

Where ϖ = angular velocity of spindle (rad/sec)

$$= \left(\frac{2\pi}{60}\right) N$$

N = revolution per minute

R_c = radius of container = 4.8cm for a 600ml beaker

R_b = radius of spindle (cm) = 0.16cm

x = radius at which shear strain rate is being calculated

M = torque input by instrument = torque x 673.7/100 (dyne/cm^2)

L = effective length of spindle = 3.1cm

A sketch showing the viscometer and the spindle dimensions is shown in Figure A2.1.

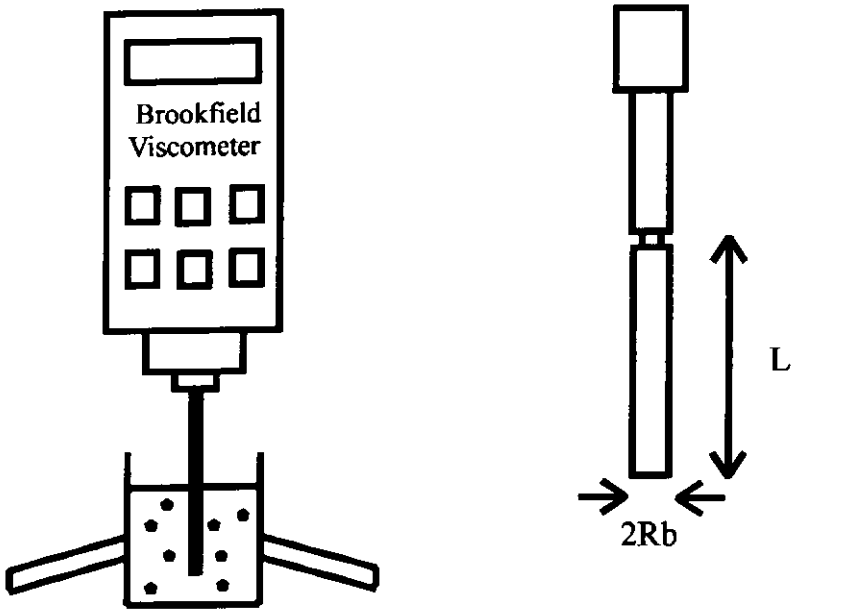

Rotational Viscometer (A)

Details of spindle (B)

Figure A2.1 A sketch of the rotational viscometer

Appendix 2
Derivation of Scaling Factors

For the derivation of the geometric scaling factors for modeling debris flows in experimental simulation, Hua (1989) assumed that the flow mechanism of debris flow can be described by the equations of motion in fluid mechanics (Equation A1).

$$\frac{\partial V_x}{\partial t}+V_x\frac{\partial V_x}{\partial x}+V_y\frac{\partial V_x}{\partial y}+V_z\frac{\partial V_x}{\partial z}=g_x-\frac{1}{\rho}\left(\frac{\partial P_{xx}}{\partial x}+\frac{\partial \tau_{yx}}{\partial y}+\frac{\partial \tau_{zx}}{\partial z}\right)$$

$$\frac{\partial V_y}{\partial t}+V_x\frac{\partial V_y}{\partial x}+V_y\frac{\partial V_y}{\partial y}+V_z\frac{\partial V_y}{\partial z}=g_y-\frac{1}{\rho}\left(\frac{\partial P_{yy}}{\partial y}+\frac{\partial \tau_{xy}}{\partial x}+\frac{\partial \tau_{zy}}{\partial z}\right) \qquad \text{(A1)}$$

$$\frac{\partial V_z}{\partial t}+V_x\frac{\partial V_z}{\partial x}+V_y\frac{\partial V_z}{\partial y}+V_z\frac{\partial V_z}{\partial z}=g_z-\frac{1}{\rho}\left(\frac{\partial P_{zz}}{\partial z}+\frac{\partial \tau_{xz}}{\partial x}+\frac{\partial \tau_{yz}}{\partial y}\right)$$

where ρ is density, V_x, V_y, V_z are velocities in x, y and z directions, g is gravitational acceleration, P and τ are the normal stress and shear stress respectively.

For simplicity, the equation in x direction is considered here. The parameter λ is a characteristic scale and is used here to denote the ratio of the same kind variable of prototype and model. In particular, the following ratios are defined:

$$\lambda_L=\frac{L_p}{L_M} \qquad \lambda_V=\frac{V_p}{V_M} \qquad \lambda_\rho=\frac{\rho_p}{\rho_M}$$

$$\lambda_\tau=\frac{\tau_p}{\tau_M} \qquad \lambda_P=\frac{P_p}{P_M} \qquad \lambda_t=\frac{t_p}{t_M}$$

$$\frac{g_{x,P}}{g_{x,M}}=\frac{g_{y,P}}{g_{y,M}}=\frac{g_{z,P}}{g_{z,M}}=\lambda_g$$

where L is length, V is velocity, ρ is density, τ is shear stress, P is pressure, t is time and subscript "p" is used for prototype, and those for model are denoted by subscript "m". Along the x direction, substituting all these characteristic scales into equation (A1), we have

$$\lambda_g g_{x,M} - \frac{1}{\lambda_\rho \rho_M}\left[\frac{\lambda_P}{\lambda_L}\frac{\partial P_M}{\partial x_M} + \frac{\lambda_\tau}{\lambda_L}\frac{\partial \tau_{yx,M}}{\partial y_M} + \frac{\lambda_\tau}{\lambda_L}\frac{\partial \tau_{zx,M}}{\partial z_M}\right]$$
$$= \frac{\lambda_V}{\lambda_t}\frac{\partial V_{x,M}}{\partial t_M} + \lambda_V V_{x,M}\frac{\lambda_V}{\lambda_L}\frac{\partial V_{x,M}}{\partial x_M} + \lambda_V V_{y,M}\frac{\lambda_V}{\lambda_L}\frac{\partial V_{x,M}}{\partial y_M} + \lambda_V V_{z,M}\frac{\lambda_V}{\lambda_L}\frac{\partial V_{x,M}}{\partial z_M} \quad \text{(A2)}$$

Comparing coefficients of equation (A2), we obtain,

$$\lambda_g = \frac{\lambda_P}{\lambda_\rho \lambda_L} = \frac{\lambda_\tau}{\lambda_\rho \lambda_L} = \frac{\lambda_V}{\lambda_t} = \frac{\lambda_V^2}{\lambda_L} \quad \text{(A3)}$$

and $\lambda_P = \lambda_\tau$

Normalize equation (A3) using $\frac{\lambda_V^2}{\lambda_L}$, we obtain

$$\frac{\lambda_V^2}{\lambda_g \lambda_L} = 1 \quad \text{(A4)}$$

$$\frac{\lambda_P}{\lambda_\rho \lambda_V^2} = 1 \quad \text{(A5)}$$

$$\frac{\lambda_\tau}{\lambda_\rho \lambda_V^2} = 1 \quad \text{(A6)}$$

$$\frac{\lambda_t \lambda_V}{\lambda_L} = 1 \quad \text{(A7)}$$

As shown above, equations (A5) and (A6) are identical. For steady flow, Hua (1989) remarked that equation (A7) can be neglected. Therefore, equations (A4) and (A5) must be satisfied for ensuring the similarity of the prototype and the model.

Considering the Bingham fluid, it is given that

$$\tau = \tau_B + \mu \frac{dV}{dh} \tag{A8}$$

where τ_b = *Bingham yield stress*, μ = Bingham viscosity, $\frac{dV}{dh}$ = shear strain rate.

The shear stress is controlled by two components (yield strength and viscosity), and all of their characteristic shear stress scale should be satisfied. That is,

$$\lambda_\tau = \lambda_{\tau_B} = \lambda_\mu \lambda_{\frac{dV}{dy}} \tag{A9}$$

Substituting equations (A9) into (A6), we obtain two conditions:

(a) Condition 1

$$\frac{\lambda_{\tau_B}}{\lambda_\rho \lambda_V{}^2} = \frac{\lambda_{\tau_B}}{\frac{\lambda_V{}^2 \lambda_L{}^2 \lambda_\rho{}^2}{\lambda_\mu{}^2} \frac{\lambda_\mu{}^2}{\lambda_\rho \lambda_L{}^2}} = \frac{\lambda_{\tau_B} \lambda_\rho \lambda_L{}^2}{\lambda_\mu{}^2} \frac{1}{\lambda_{\mathrm{Re}}{}^2} = \frac{\lambda_{He}}{\lambda_{\mathrm{Re}}{}^2} = 1 \tag{A10}$$

where $\lambda_{\mathrm{Re}} = \frac{\lambda_V \lambda_L \lambda_\rho}{\lambda_\mu}$ (characteristic Reynold number scale), Reynold number $\mathrm{Re} = \frac{VL\rho}{\mu}$ and Hedstrom-1 number $He = \frac{\tau_B \rho L^2}{\mu^2}$ (Johnson, 1998)

(b) Condition 2

$$\frac{\lambda_\mu \lambda_{\frac{dV}{dy}}}{\lambda_\rho \lambda_V{}^2} = \frac{\lambda_\mu \lambda_V}{\lambda_\rho \lambda_V{}^2 \lambda_L} = \frac{1}{\frac{\lambda_\rho \lambda_V \lambda_L}{\lambda_\mu}} = \frac{1}{\lambda_{\mathrm{Re}}} = 1 \tag{A11}$$

or $\lambda_{\mathrm{Re}} = 1$

By using equation (A4), we obtain $\frac{\lambda_V{}^2}{\lambda_g \lambda_L} = 1$ *or* $\lambda_{Fr} = 1$ (where Froude number $Fr = \frac{V}{\sqrt{gL}}$). The geometrical scaling factors for velocity and flow rate are:

Velocity: $\lambda_V = \lambda_g \lambda_L^{1/2} = \lambda_L^{1/2}$ (A12)

Flow rate: $\lambda_Q = \lambda_V \lambda_L^{2} = \lambda_L^{1/2} \lambda_L^{2} = \lambda_L^{5/2}$ (A13)

By using equation (A11), the following viscosity factor is obtained:

$$\lambda_{\mathrm{Re}} = \frac{\lambda_\rho \lambda_V \lambda_L}{\lambda_\mu} = 1,$$

Viscosity: $\lambda_\mu = \lambda_\rho \lambda_V \lambda_L = \lambda_\rho \lambda_L^{3/2}$ (A14)

By using equation (A10), the following yield stress factors is obtained:

$$\frac{\lambda_{He}}{\lambda_{\mathrm{Re}}^{2}} = \frac{\lambda_{\tau_B} \lambda_\rho \lambda_L^{2}}{\lambda_\mu^{2}} \frac{\lambda_\mu^{2}}{\lambda_\rho^{2} \lambda_V^{2} \lambda_L^{2}} = \frac{\lambda_{\tau_B}}{\lambda_\rho \lambda_V^{2}} = 1$$

Yield stress: $\lambda_{\tau_B} = \lambda_\rho \lambda_V^2 = \lambda_\rho \lambda_L$ (A15)

Therefore, the four geometric scaling factors can be derived. A summary table for these four geometric scaling factors are tabulated as follows:

Geometric scaling factors	
Velocity factor, τ_V	$\lambda_V = \lambda_L^{1/2}$
Flow rate factor, τ_Q	$\lambda_Q = \lambda_L^{5/2}$
Yield strength factor, τ_{τ_B}	$\lambda_{\tau_B} = \lambda_\rho \lambda_L$
Viscosity factor, τ_μ	$\lambda_\mu = \lambda_\rho \lambda_L^{3/2}$

Table A1.1 Geometric scaling factors (Hua, 1989)